Final Report

DEVELOPMENT OF A STATE-OF-THE-ART ACID DEPOSITION MODEL FOR THE SOUTH COAST AIR BASIN OF CALIFORNIA

by

Spyros N. Pandis and John H. Seinfeld

Final Report

DEVELOPMENT OF A STATE-OF-THE-ART ACID DEPOSITION MODEL FOR THE SOUTH COAST AIR BASIN OF CALIFORNIA

by

Environmental Quality Laboratory
California Institute of Technology
Pasadena, CA 91125
John H. Seinfeld, Principal Investigator

submitted to

State of California Air Resources Board

under

Agreement A732-043

March 25, 1989

DISCLAIMER

The statements and conclusions in this report are those of the contractor and not necessarily those of the California Air Resources Board. The mention of commercial products, their source or their use in connection with material reported herein is not to be construed as either an actual or implied endorsement of such products.

ABSTRACT

Three different aqueous-phase modules have been developed to describe the physicochemical processes associated with the aqueous-phase in the atmosphere. These modules constitute the central core of an urban-scale acid deposition model and can be incorporated into an Eulerian three dimensional grid-based system. The fog model (Module 2) has been implemented in a trajectory framework and has been employed to predict the temperature profile, fog development, liquid water content, gas and aqueous phase concentrations of pollutants, and wet deposition rates of main ionic species during the radiation fog episode in Bakersfield in the San Joaquin Valley of California over the period January 4-5, 1985.

TABLE OF CONTENTS

CHAPTER 1	SUMMARY AND INTRODUCTION	1
	References	9
CHAPTER 2	SENSITIVITY ANALYSIS OF A CHEMICAL MECHANISM FOR AQUEOUS-PHASE ATMOSPHERIC CHEMISTRY	11
	Abstract	12
	Introduction	12
	Aqueous-Phase Chemical Mechanism Formulation	14
	Aqueous-Phase Chemistry	14
	Mathematical Description	27
	Sensitivity Analysis Method	29
	S(IV) to S(VI) Transformation and Sulfur Chemistry	33
	SO_5^-, SO_4^{2-}, and HSO_5^- Chemistry	40
	$HOCH_2SO_3^-$ Chemistry	45
	Nitrite and Nitrate Chemistry	45
	Formaldehyde and Formic Acid Chemistry	49
	Other Organic Species	53
	Oxygen and Hydrogen Chemistry	54
	Chlorine Chemistry	54
	Importance of Initial Gas and Aqueous-Phase Concentrations	58
	Effects on the S(IV) to S(VI) Conversion	58
	Nitrogen Chemistry	60
	Formic Acid and Formaldehyde Chemistry	60
	HSO_5^-	62
	Liquid Water Content w_L	62

Accomodation Coefficient and Droplet Radius 64

Temperature Effects 66

Condensed Mechanism 68

Comparison of the DDM with the Indirect Method 68

Conclusions 71

Acknowledgment 72

References 72

CHAPTER 3 MATHEMATICAL MODELING OF ACID DEPOSITION DUE TO RADIATION FOG 83

Abstract 84

Introduction 85

Radiation Fog and Acid Deposition 87

Model Description 89

1. Gas-phase Model 91

2. Radiation Fog Model 92

Boundary Conditions 95

3. Aqueous-Phase Model 97

Full Model Description 97

Application of the Model to the San Joaquin Valley of California on 4-5 January 1985 100

Input Data for the Model 101

Fog Development 102

Species Concentrations in the Aqueous and Gas Phase 107

Effect of the Fog Development on the Aerosol Mass 110

Wet Deposition Rates 114

Sulfate Production 118

Sensitivity to Deposition 122

Conclusions 124

Acknowledgments 125

References 126

CHAPTER 4 ON THE RELATION BETWEEN THE SIZE AND COMPOSITION OF FOG AND CLOUD DROPLETS AND THE SIZE AND COMPOSITION OF ATMOSPHERIC AEROSOL 131

Chemical Composition Differences in Fog and Cloud Droplets of Different Sizes 132

Abstract 132

Introduction 133

Model Description 135

1. Conditioning Period 136

Gas-Phase Chemistry Operator 137

Aerosol Operators 137

2. Rapid Growth Period 138

Aqueous-Phase Chemistry and Droplet Microphysics Operator 139

3. Dissipation Period 140

Representative Cases for Evaluation 141

Case 1 (base case) 141

Case 2 144

Case 3 144

Case 4 144

Results and Discussion 149

Size/Composition Distribution of Fog and Cloud Droplets (Base Case) 146

Influence of Gas- and Aqueous-Phase Chemistry 152

Influence of Cooling Rate 156

Influence of Initial Aerosol Distribution 161

Conclusions 161

Acknowledgments 165

References 165

APPENDIX BRIEF DOCUMENTATION OF ACID DEPOSITION MODULES 1-3 169

Module 1 172

Module 2 174

Module 3 177

CHAPTER 1

SUMMARY AND INTRODUCTION

Summary and Introduction

Since the early 1980s, scientists and the public have focused increasing attention on the expanding phenomena of soil and lake acidification, forest decline, and deterioration of cultural monuments. Many of these effects are attributed to what is commonly identified as acid rain or acid deposition.

Acid deposition consists of the delivery of acidic substances, principally sulfuric acid and nitric acid, from the atmosphere to the earth's surface. Upon emission to the atmosphere SO_2 and NO_x are photochemically oxidized, yielding sulfuric and nitric acid vapors. Sulfuric acid is rapidly incorporated into aerosol particles, while nitric acid may be scavenged by particles or droplets or remain in the gas-phase. Even in the absence of an aqueous phase (no clouds or fog), the acidic gases and dry particles can be transported to and deposited at ground level; this process is called dry deposition. When an aqueous phase is present (inside a cloud or a fog), gas phase species like SO_2, HNO_3, NH_3 and aerosol particles are scavenged by water droplets resulting in a solution that can be significantly acidic. Additional cloudwater or fogwater acidity beyond that attained purely from scavenging of gases and particles results from aqueous-phase chemistry, most notably oxidation of dissolved SO_2 to sulfuric acid. These acidic water droplets can reach the earth's surface either as precipitation or as impacted cloud and fog drops, in the process termed wet deposition. If they are not rained or deposited out the aqueous droplets can evaporate leaving as residue fresh aerosol particles that may themselves undergo dry deposition to the earth's surface. The atmospheric paths leading to wet and dry acidic deposition are depicted in Figure 1.

Deposition in forms other than rain is relatively more important in California than in other parts of the country [1]. Ambient concentrations of nitric acid in California are roughly twice those in the eastern U.S., resulting in high rates of dry acid deposition [1]. At the same time Hoffmann and co-workers have reported highly acidic fogs in

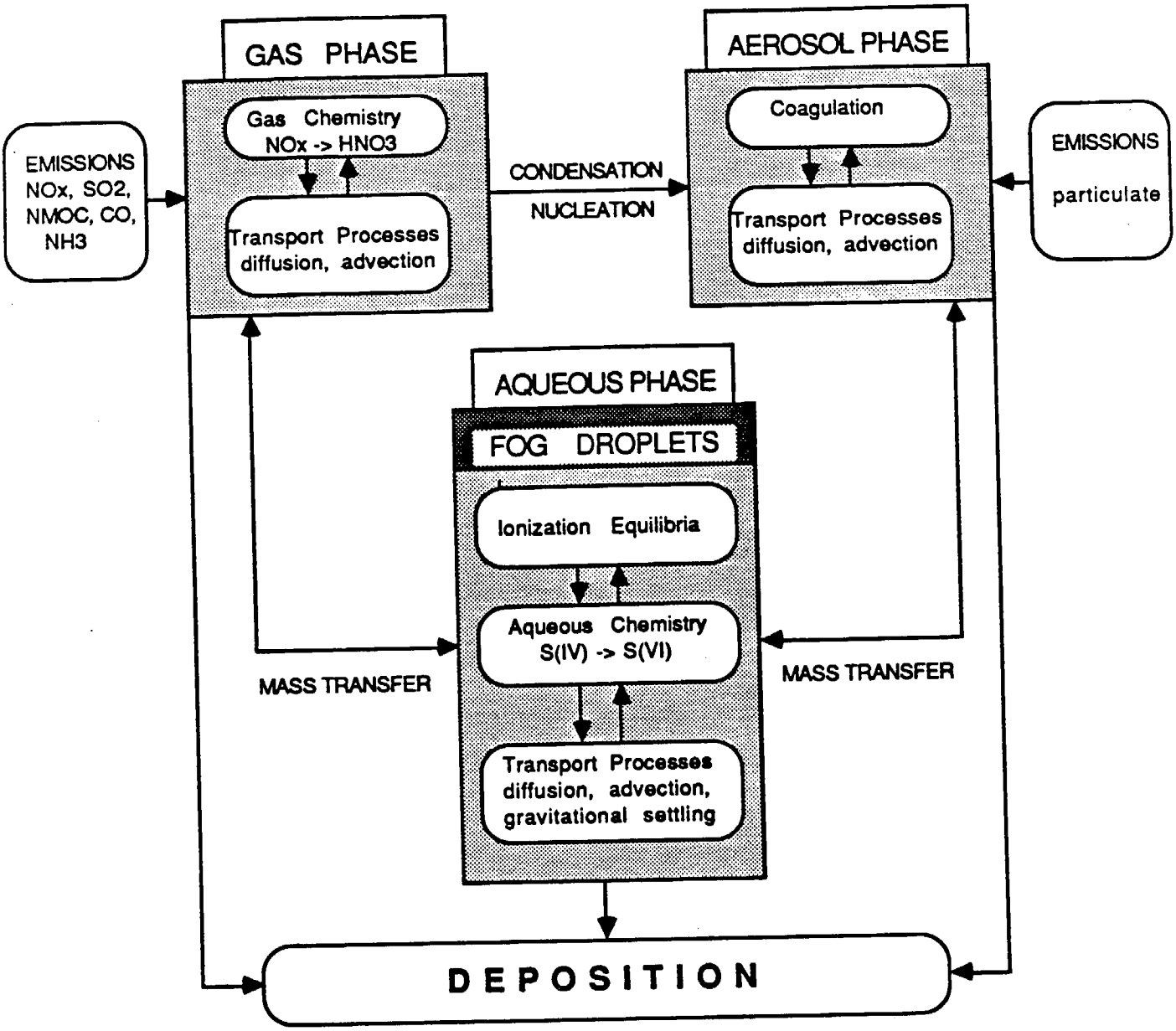

Figure 1 Atmospheric processes leading to acid deposition.

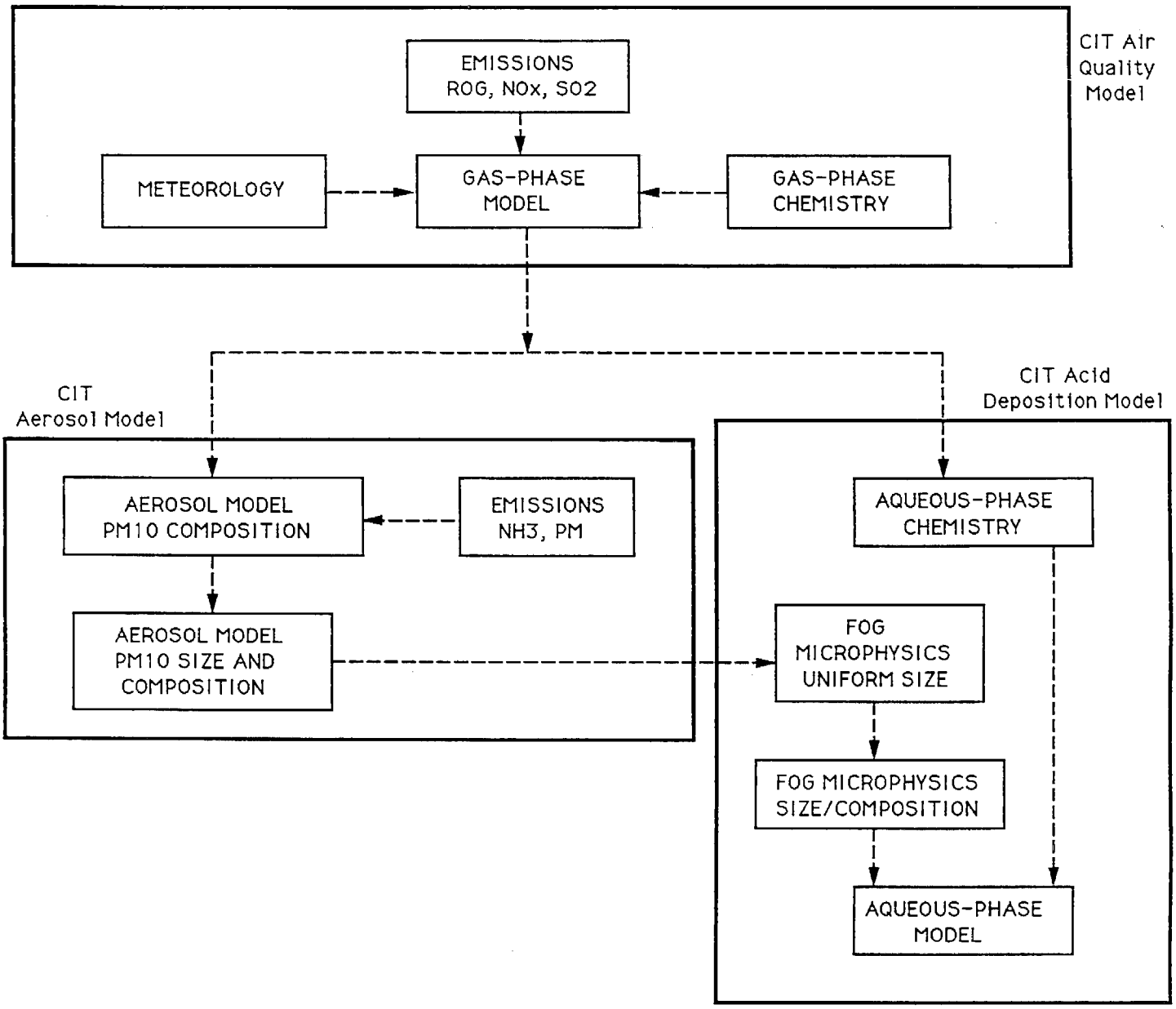

Figure 2. Elements of a mathematical model for relating pollutant emissions to ambient air quality and acid deposition.

California, with pH values as low as 1.69 [2]. In these fogs concentrations of anions and cations such as SO_4^{2-}, NO_3^-, and NH_4^+ were higher by one to two orders of magnitude than in precipitation in the same areas.

Mathematical models will eventually be a major tool in our effort to understand and ultimately to control acid deposition. The development of such a mathematical model represents a major challenge as it requires the ability to describe the entire range of atmospheric physicochemical phenomena depicted in Figure 1. A complete acid deposition model should include descriptions of:

- emissions of pollutants like NO_x, SO_2, organics, and primary aerosol particles,
- gas-phase chemistry to produce an array of species including nitric and sulfuric acid vapors,
- aerosol formation,
- formation of cloud or fog droplets by condensation of water vapor on the aerosol particles that serve as condensation nuclei, and evaporation of droplets to leave an aerosol residue,
- scavenging of gaseous species by the water droplets, followed by ionization,
- aqueous-phase reactions and,
- dry and wet deposition mechanisms as the ultimate modes of delivery of acidity to the earth's surface.

A detailed three-dimensional description of all the physicochemical processes shown in Figure 1 would produce a complicated model whose main elements are depicted in Figure 2. Past experience has shown that the best way to proceed in such a demanding task is to develop, test, and evaluate the component submodels before assembling them into a full three-dimensional model. This was done succesfully in the past in the development of the Caltech Air Quality Model with the development of the gas-phase chemistry and meteorology submodels, and with the Caltech Aerosol Model

and the aerosol thermodynamics and dynamics submodels correspondingly (Figure 2). Therefore before attempting to address the full problem over a three-dimensional modeling region, it is necessary to develop the individual components of the aqueous-phase model.

The main emphasis of this project has been the development of a state-of-the-art acid deposition model for California. In the original proposal the following four tasks were outlined:

1. Update the gas-phase chemistry module in the Caltech air quality model to incorporate the new ERT/SAPRC surrogate species mechanism.
2. Develop an aqueous-phase chemistry module for cloud and fog water chemistry.
3. Integrate the aqueous-phase chemistry module into the Caltech grid-based air quality model.
4. Perform selected preliminary sensitivity tests.

In the course of our work it became apparent that the amount of liquid water present in the atmosphere is a parameter of major importance for acidic deposition and that a state-of-the-art aqueous-phase chemistry module should include a description of the variations of liquid water content inside a fog or cloud. Hence we decided it was necessary to devote more attention than had previously been envisioned to the development of the aqueous-phase chemistry module (Task 2) than to the integration of this module into the Caltech grid-based airshed model (Task 3). The development of the aqueous-phase chemistry module is the single most important and most difficult step involved in the development of the full Eulerian acid deposition model and required the predominant fraction of our effort. A short summary of the work performed for each one of the proposed tasks is given below:

Task 1. The gas-phase chemistry module in the Caltech air quality model has been updated to reflect the most current understanding in that area. The detailed

SAPRC/ERT gas-phase chemical reaction mechanism with the recent modifications and extensions of Carter and Atkinson has replaced the previously used mechanism. The code for the Caltech air quality model has been made compatible with the photochemical mechanism preparation and emissions processing software of Carter and Atkinson. This enables the user of the model to update or change the gas-phase mechanism relatively readily and without the need of extensive re-programming.

Task 2. Three different modules have been developed describing the physicochemical processes associated with the aqueous-phase in the atmosphere.

Module 1: The first module treats the chemistry of the aqueous-phase and the dynamic exchange of species between the gas and aqueous phases in a homogeneous parcel of air containing water droplets. This module consists of 109 aqueous-phase reactions together with 17 aqueous-phase ionic equilibria. The amount of the aqueous-phase (liquid water content) is an input to this module.

Module 2: The second module describes the physics of the development and dissipation of radiation fog by solving the fundamental energy, water vapor and liquid water balance equations. The liquid water content is predicted in the module using the saturation assumption, in which the appropriate amount of liquid water forms to maintain the relative humidity at 100%. The atmospheric cooling or heating rates and the vertical temperature profile are also among the variables predicted by the module.

Module 3: The next level of treatment beyond assuming that all the water droplets have the same size and chemical composition is to explicitly model the size-composition distribution of droplets as a result of nucleation on aerosol particles. The temperature is the main input to the model. The development of the full aerosol size/composition spectrum is followed using the sectional approach, including the growth of the aerosol particles to fog or cloud droplets, the aqueous-phase chemical reactions inside the droplets and the scavenging of gas-phase species. Under appropriate conditions the fog or cloud

evaporates resulting in aerosol particles of a different size and chemical composition than that originally served as condensation nuclei.

Task 3. Modules 1 and 2 have been integrated into a Lagrangian trajectory framework and several preliminary computations have been performed. We feel it is desirable to complete the development of all three of the above aqueous-modules before incorporating them into the Caltech grid-based airshed model. The decision on which module to employ in any particular application should be based on factors such as the availability of necessary data, the computing requirements of each module and the degree of detail desired in describing the acid deposition phenomenon.

Task 4. Several sensitivity studies have been performed using the above modules. A detailed sensitivity study of the aqueous-phase chemical mechanism has been done using the Direct Decoupled Method and the Module 1. Module 2 has been evaluated against extensive data for a radiation fog episode in Bakersfield in the San Joaquin Valley. A preliminary sensitivity analysis for Module 2 and Module 3 has also been performed.

Our goal is to integrate Modules 1-3 into the Caltech grid-based airshed model. We plan to pursue this objective after the present project ends at no cost to the ARB. Since we are planning to analyze the SCAQS data from the viewpoint of aerosol processes acid deposition, it is necessary for us to carry out this integration in order to perform this analysis.

Each of the three modules developed in this project can serve as a base for a comprehensive grid-based model. The aqueous-phase chemistry module (module 1) has computational requirements roughly comparable to those of a gas-phase chemistry module and requires as input the amount of liquid water in every computational cell at each time step. The amount of liquid water is more difficult to measure compared to other necessary meteorological information like the wind field or ambient temperature

and therefore is not routinely available for episodes to be modeled. The amount of wet acid deposition is obtained approximately from the results of module 1 by parametrizing the gravitational settling of the fog droplets. The radiation fog module (module 2) calculates the liquid water content ab initio and therefore does not require that as input information, at the expense of more computing time. It also is based on a parametrization of the droplet gravitational settling. Module 3 employs no major assumptions as it is based entirely on first principles and is expected to be the most accurate module but in return it requires a significant amount of computing time.

Depending on the available computing resources, on the desired level of basic prediction and on the available input information from field measurements any one of the above three approaches can be adopted to simulate dry and wet acid deposition over a region. Evaluation of the corresponding model would require collection of a data base including the necessary initial and boundary conditions as well as measurements of the variables predicted by the models such as gas- and aqueous-phase concentrations, liquid water content, depositional fluxes etc.

The remainder of this report deals with each of the developed aqueous-phase modules. The approach used is to describe each module independently and therefore each Chapter has its own Summary and Conclusions.

References

1. ARB, "The Fifth Annual Report to the Governor and the Legislature on the Air Resources Board's Acid Deposition Research and Monitoring Program", California Air Resources Board, Sacramento, CA, 1988.
2. J. M. Waldman, J. W. Munger, D. J. Jacob, R. C. Flagan, J.J. Morgan, and M. R. Hoffmann, "Chemical composition of acid fog", Science, 218, 677-680, 1982.

CHAPTER 2

SENSITIVITY ANALYSIS OF A CHEMICAL MECHANISM FOR AQUEOUS-PHASE ATMOSPHERIC CHEMISTRY

(Published in *Journal of Geophysical Research*, 94, 1105-1126, 1989)

Sensitivity Analysis of a Chemical Mechanism for Aqueous-Phase Atmospheric Chemistry

Spyros N. Pandis and John H. Seinfeld

Department of Chemical Engineering, California Institute of Technology,

Pasadena, CA 91125, U.S.A.

Abstract

The sensitivity analysis of a comprehensive chemical mechanism for aqueous-phase atmospheric chemistry is performed. The main aqueous-phase reaction pathways for the system are the oxidation of S(IV) by H_2O_2, OH, O_2 (catalysed by Fe^{3+} and Mn^{2+}), O_3 and HSO_5^-. The HO_2(aq) and OH(aq)radicals contribute indirectly to this process by producing and consuming H_2O_2(aq) respectively. The dominant pathway for HNO_3(aq) acidity is scavenging of nitric acid from the gas phase. HCOOH is produced because of the reaction of HCHO(aq)with OH(aq). The gas phase concentrations of SO_2, H_2O_2, HO_2, OH, O_3, HCHO, NH_3, HNO_3 and HCl are of primary importance. Increase of the liquid water content of the cloud results to a decrease of the sulfate concentration but increase of the total sulfate amount in the aqueous-phase. A condensed mechanism is derived from the analysis.

Introduction

Acid precipitation may be causing significant damage to various ecosystems, for example acidification of lakes, tree damage etc [Havas et al., 1984 ; Schofield, 1982]. To identify and describe the physicochemical pathways leading to acid deposition several models have been developed describing the gas- and aqueous- phase chemistry as well as the mass transport processes coupling the two phases [Graedel et al. 1981, 1983;

Chameides et al. 1982, 1984; Jacob and Hoffmann, 1983; Seigneur and Saxena, 1984; Young and Lurmann, 1984; Hoffmann and Jacob, 1984; Jacob, 1986]. In these models the treatment of the aqueous-phase chemistry has been continously evolving as more and more experimental kinetic information becomes available. Some of the recent improvements have been the recognition of the potential importance of the metal (Fe^{3+} and Mn^{2+}) catalysed oxidation of SO_2 by O_2 [Hoffmann and Jacob, 1984], the aqueous-phase free radical chemistry [Chameides and Davis, 1982; Schwartz, 1984] and the chemistry of formic acid and formaldehyde [Chameides, 1984; Jacob 1986].

As atmospheric aqueous-phase reaction mechanisms increase in size and complexity, identification of the important and unimportant kinetic pathways has become an increasingly difficult task. Although the qualitative features of the aqueous-phase reaction system appear to be reasonably well understood, there are questions that still remain partially or completely unanswered. They concern the relative importance of the pathways included in the latest mechanisms, the role of every species in the entire reaction system and the influence of the mechanism's parameters such as the liquid water content, the sticking coefficient, the droplet radius, the temperature, etc. on the behavior of the reaction system.

Our goal in this paper is to address quantitatively the above questions through a sensitivity analysis. To accomplish this goal we have developed an aqueous-phase mechanism that represents the current understanding of the physicochemical processes taking place in cloudwater.

This work begins with a presentation of the aqueous-phase chemical mechanism. Next a brief description of the sensitivity analysis method [Decoupled Direct Method (DDM)] employed here is given; details are available in the cited references. The sensitivity analysis results are then presented and discussed, leading to a ranking of the most important reaction pathways for the various species. Additionally the influence

of the gas-phase concentrations and the mechanism's parameters on the aqueous-phase species concentrations is addressed. Based on these results a condensed mechanism can be proposed and tested for the base scenario. Finally we briefly summarize the sensitivity methods available and actually compare the DDM with the indirect or brute force method.

Aqueous-Phase Chemical Mechanism Formulation

The aqueous-phase model treats the chemistry of the aqueous-phase (no gas-phase reactions are included), and the dynamic exchange of species between the two phases, in a homogeneous parcel of air in a cloud. At $t = 0$ an air parcel containing an initial gas mixture with high water vapor concentration and aerosol particles consisting of SO_4^{2-}, NO_3^-, Cl^-, NH_4^+, Na^+, Fe^{3+} and Mn^{2+} is assumed to be suddenly cooled by an isobaric process. The cloud droplets that are formed then are assumed to be chemically homogeneous and to attain instantaneously the same radius α that remains constant. Transport processes such as entrainment and mixing of outside air into the cloud are neglected as are the effects of temporal variations in temperature and liquid water content.

Aqueous-Phase Chemistry

The chemical mechanism that we have developed is based on the work of Graedel et al. [1981,1983], Chameides [1982,1984], Schwartz [1984], Seigneur and Saxena [1984], Hoffman and Calvert [1985], Jacob [1986], and Systems Applications, Inc. [1987]. The mechanism includes 49 individual aqueous-phase species and 20 gas-phase species (Table 1), 17 aqueous-phase ionic equilibria (Table 2), 20 gas-phase aqueous-phase reversible reactions (Table 2) and 109 aqueous-phase reactions (Table 3). The proposed mechanism combines most of the aqueous-phase reactions that have been used

TABLE 1

Chemical Species, Initial Concentrations and Model Parameters

Aqueous – Phase Species	*Initial Concentration* μM	*Gas – Phase Species*	*Initial Concentration ppb*
$SO_2 \cdot H_2O, HSO_3^-, SO_3^{2-}$	0	SO_2(g)	0.98
$H_2SO_4, HSO_4^-, SO_4^{2-}$	8.0		
HNO_2, NO_2^-	0	HNO_2(g)	4×10^{-4}
HNO_3, NO_3^-	2.0	HNO_3(g)	0.55
$CO_2 \cdot H_2O, HCO_3^-, CO_3^{2-}$	11.9	CO_2(g)	340×10^3
H_2O_2, HO_2^-	0	H_2O_2(g)	0.95
$HCHO, H_2C(OH)_2$	0	HCHO(g)	0.29
$HCOOH, HCOO^-$	0	HCOOH(g)	0.007
NO	0	NO(g)	0.016
NO_2	0	NO_2(g)	0.039
O_3	0	O_3(g)	53.2
$CH_3C(O)O_2NO_2$	0	$CH_3C(O)O_2NO_2$(g)	0.6
$CH_3C(O)OOH$	0	$CH_3C(O)OOH$(g)	1×10^{-4}
CH_3OOH	0	CH_3OOH(g)	1.0
HCl, Cl^-	8.0	HCl(g)	0.5
OH	0	OH(g)	3×10^{-4}
HO_2, O_2^-	0	HO_2(g)	0.04
NO_3	0	NO_3(g)	4×10^{-6}
NH_4OH, NH_4^+	2.0	NH_3(g)	0.6
CH_3O_2	0	CH_3O_2(g)	0.02
CH_3OH	0	CH_3OH(g)	0.8
H^+	14.74		
OH^-	6.78×10^{-4}		
Fe^{3+}	0.4		
Mn^{2+}	0.2		
Na^+	0.8		
"Aqueous Phase Only" Species With Zero Initial Concentrations			
$Cl_2^-, Cl, ClOH^-$			
SO_4^-, SO_5^-, HSO_5^-			
$HOCH_2SO_3^-, {}^-OCH_2SO_3^-$			
CO_3^-			
Fixed Model Parameters	*Value*		
Temperature, T	298K		
Liquid Water Content, w_L	4×10^{-7}(l water/l air)		
Droplet Radius, α	10 μm		
Zenith Angle, θ	30°		
Cloud Transmissivity	0.5		

in previous studies. It includes detailed aqueous-phase free radical chemistry, chlorine chemistry, chemistry of formaldehyde and formic acid as well as a complete description of sulfur chemistry. The reactions of the mechanism have been divided into the following six groups:

(a) Oxygen-Hydrogen Chemistry

(b) Carbonate Chemistry

(c) Chlorine Chemistry

(d) Nitrite and Nitrate Chemistry

(e) Methane oxidation Chemistry

(f) Sulfur Chemistry

It is convenient to consider the sum of each reactant species in a particular class that is in rapid equilibrium, because of dissociation or hydration, as a single entity [Schwartz, 1984]. Therefore the 49 aqueous-phase species can actually be represented by 29 different groups, like:

$$[\mathrm{S(IV)}] = [\mathrm{SO_2 \cdot H_2O}] + [\mathrm{HSO_3^-}] + [\mathrm{SO_3^{2-}}]$$

$$[\mathrm{S(VI)}] = [\mathrm{H_2SO_4(aq)}] + [\mathrm{HSO_4^-}] + [\mathrm{SO_4^{2-}}]$$

$$[\mathrm{N(V)}] = [\mathrm{HNO_3(aq)}] + [\mathrm{NO_3^-}]$$

$$[{\mathrm{HO_2}}^T] = [\mathrm{HO_2(aq)}] + [\mathrm{O_2^-}]$$

where [I] denotes the concentration of aqueous-phase species I in (mol/l of water).

Some of the products of reactions 51, 53, 62, 86, 99, 100 and 105 are not included in the chemical mechanism because they have no known significant reactions and would only increase the size of our species matrix.

TABLE 2

Equilibrium Reactions

Equilibrium Reaction	K_{298} (M or M/atm)[a]	$\frac{-\Delta H}{R}$(K)	*Reference*
$SO_2(g) \rightleftharpoons SO_2 \cdot H_2O$	1.23	3120	Smith and Martell (1976)
$SO_2 \cdot H_2O \rightleftharpoons HSO_3^- + H^+$	1.23×10^{-2}	1960	Smith and Martell (1976)
$HSO_3^- \rightleftharpoons SO_3^{2-} + H^+$	6.61×10^{-8}	1500	Smith and Martell (1976)
$H_2SO_4(aq) \rightleftharpoons HSO_4^- + H^+$	1000		Perrin(1982)
$HSO_4^- \rightleftharpoons SO_4^{2-} + H^+$	1.02×10^{-2}	2720	Smith and Martell (1976)
$H_2O_2(g) \rightleftharpoons H_2O_2(aq)$	7.45×10^4	6620	Lind and Kok (1986)
$H_2O_2(aq) \rightleftharpoons HO_2^- + H^+$	2.2×10^{-12}	−3730	Smith and Martell (1976)
$HNO_3(g) \rightleftharpoons HNO_3(aq)$	2.1×10^5		Schwartz (1984)
$HNO_3(aq) \rightleftharpoons NO_3^- + H^+$	15.4	8700[b]	Schwartz (1984)
$HNO_2(g) \rightleftharpoons HNO_2(aq)$	49.	4780	Schwartz and White (1981)
$HNO_2(aq) \rightleftharpoons NO_2^- + H^+$	5.1×10^{-4}	−1260	Schwartz and White (1981)
$O_3(g) \rightleftharpoons O_3(aq)$	1.13×10^{-2}	2300	Kozac and Heltz (1983)
$NO_2(g) \rightleftharpoons NO_2(aq)$	1.00×10^{-2}	2500	Schwartz (1984)
$NO(g) \rightleftharpoons NO(aq)$	1.9×10^{-3}	1480	Schwartz and White (1981)
$CH_3O_2(g) \rightleftharpoons CH_3O_2(aq)$	6.0	5600	Jacob (1986)
$CH_3OH(g) \rightleftharpoons CH_3OH(aq)$	2.2×10^2	4900	Snider and Dawson (1985)
$CO_2(g) \rightleftharpoons CO_2 \cdot H_2O$	3.40×10^{-2}	2420	Smith and Martell (1976)
$CO_2 \cdot H_2O \rightleftharpoons HCO_3^- + H^+$	4.46×10^{-7}	−1000	Smith and Martell (1976)
$HCO_3^- \rightleftharpoons CO_3^{2-} + H^+$	4.68×10^{-11}	−1760	Smith and Martell (1976)
$NH_3(g) \rightleftharpoons NH_4OH$	75	3400	Hales and Drewes (1979)
$NH_4OH \rightleftharpoons NH_4^+ + OH^-$	1.75×10^{-5}	−450	Smith and Martell (1976)
$H_2O \rightleftharpoons H^+ + OH^-$	1.0×10^{-14}	−6710	Smith and Martell (1976)

TABLE 2 - continuation

Equilibrium Reactions

Equilibrium Reaction	K_{298} (M or M/atm)	$\frac{-\Delta H}{R}$ (K)	*Reference*
$CH_3C(O)O_2NO_2(g) \rightleftharpoons CH_3C(O)O_2NO_2(aq)$	2.9	5910	Lee (1984*b*)
$HCHO(g) \rightleftharpoons HCHO(aq)$	6.30×10^3	6460	Ledbury and Blair (1925)
$HCHO(aq) \overset{H_2O}{\rightleftharpoons} H_2C(OH)_2(aq)$	1.82×10^3	4020	Le Hanaf (1968)
$HCOOH(g) \rightleftharpoons HCOOH(aq)$	3.5×10^3	5740	Latimer (1953)
$HCOOH(aq) \rightleftharpoons HCOO^- + H^+$	1.78×10^{-4}	-20	Martell and Smith (1977)
$HCl(g) \rightleftharpoons HCl(aq)$	7.27×10^2	2020	Marsh and McElroy (1985)
$HCl(aq) \rightleftharpoons H^+ + Cl^-$	1.74×10^6	6900	Marsh and McElroy (1985)
$Cl_2^- \rightleftharpoons Cl + Cl^-$	5.26×10^{-6}		Jayson et al. (1973)
$CH_3OOH(g) \rightleftharpoons CH_3OOH(aq)$	2.27×10^2	5610	Lind and Kok (1986)
$CH_3C(O)OOH(g) \rightleftharpoons CH_3C(O)OOH(aq)$	4.73×10^2	6170	Lind and Kok (1986)
$NO_3(g) \rightleftharpoons NO_3(aq)$	2.1×10^5	8700	Jacob (1986)
$OH(g) \rightleftharpoons OH(aq)$	25	5280	Jacob (1986)
$HO_2(g) \rightleftharpoons HO_2(aq)$	2.0×10^3	6640	Jacob (1986)
$HO_2(aq) \rightleftharpoons H^+ + O_2^-$	3.50×10^{-5}		Perrin (1982)
$HOCH_2SO_3^- \rightleftharpoons {}^-OCH_2SO_3^- + H^+$	2.00×10^{-12}		Sorensen et al. (1970)

[a] The temperature dependence is represented by:

$$K = K_{298} \exp\left[\frac{-\Delta H}{R}\left(\frac{1}{T} - \frac{1}{298}\right)\right]$$

where K is the equilibrium constant at temperature T (in K).

[b] Value for equilibrium:

$$HNO_3(g) \rightleftharpoons NO_3^- + H^+$$

TABLE 3(a)

Oxygen-Hydrogen Chemistry

	Reaction	*Rate Expression*		
		M^n $(\text{sec})^{-1}$	$-E/R$	Reference
1.	$H_2O_2 \xrightarrow{h\nu} 2OH$			Graedel and Weschler (1981)
2.	$O_3 \xrightarrow{h\nu, H_2O} H_2O_2 + O_2$			Graedel and Weschler (1981)
3.	$OH + HO_2 \longrightarrow H_2O + O_2$	7.0×10^9	-1500	Sehested et al. (1968)
4.	$OH + O_2^- \longrightarrow OH^- + O_2$	1.0×10^{10}	-1500	Sehested et al. (1968)
5.	$OH + H_2O_2 \longrightarrow H_2O + HO_2$	2.7×10^7	-1700	Christensen et al. (1982)
6.	$HO_2 + HO_2 \longrightarrow H_2O_2 + O_2$	8.6×10^5	-2365	Bielski (1978)
7.	$HO_2 + O_2^- \xrightarrow{H_2O} H_2O_2 + O_2 + OH^-$	1.0×10^8	-1500	Bielski (1978)
8.	$O_2^- + O_2^- \xrightarrow{2H_2O} H_2O_2 + O_2 + 2OH^-$	< 0.3	0	Bielski (1978)
9.	$HO_2 + H_2O_2 \longrightarrow OH + O_2 + H_2O$	0.5	0	Weinstein and Bielski (1979)
10.	$O_2^- + H_2O_2 \longrightarrow OH + O_2 + OH^-$	0.13	0	Weinstein and Bielski (1979)
11.	$OH + O_3 \longrightarrow HO_2 + O_2$	2×10^9	0	Staehelin et al. (1984)
12.	$HO_2 + O_3 \longrightarrow OH + 2O_2$	$< 1 \times 10^4$	0	Sehested et al. (1984)
13.	$O_2^- + O_3 \xrightarrow{H_2O} OH + 2O_2 + OH^-$	1.5×10^9	-1500	Sehested et al. (1983)
14.	$OH^- + O_3 \xrightarrow{H_2O} O_2^- + HO_2$	70	0	Staehelin and Hoigne (1982)
15.	$HO_2^- + O_3 \longrightarrow OH + O_2^- + O_2$	2.8×10^6	0	Staehelin and Hoigne (1982)
16.	$H_2O_2 + O_3 \longrightarrow H_2O + 2O_2$	$7.8 \times 10^{-3}[O_3]^{-0.5}$	0	Martin et al. (1983)

TABLE 3(b)

Carbonate Chemistry

	Reaction	*Rate Expression*		
		$M^n\ (\text{sec})^{-1}$	$-E/R$	Reference
17.	$HCO_3^- + OH \longrightarrow H_2O + CO_3^-$	1.5×10^7	-1910	Weeks and Rabani (1966)
18.	$HCO_3^- + O_2^- \longrightarrow HO_2^- + CO_3^-$	1.5×10^6	0	Schmidt (1972)
19.	$CO_3^- + O_2^- \xrightarrow{H_2O} HCO_3^- + O_2 + OH^-$	4.0×10^8	-1500	Behar (1970)
20.	$CO_3^- + H_2O_2 \longrightarrow HO_2 + HCO_3^-$	8.0×10^5	-2820	Behar (1970)

TABLE 3(c)

Chlorine Chemistry

	Reaction	*Rate Expression*		
		M^n $(\text{sec})^{-1}$	$-E/R$	Reference
21.	$Cl^- + OH \longrightarrow ClOH^-$	4.3×10^9	-1500	Jayson et al. (1973)
22.	$ClOH^- \longrightarrow Cl^- + OH$	6.1×10^9	0	Jayson et al. (1973)
23.	$ClOH^- \xrightarrow{H^+} Cl + H_2O$	$2.1 \times 10^{10}\,[H^+]$	0	Jayson et al. (1973)
24.	$Cl \xrightarrow{H_2O} ClOH^- + H^+$	1.3×10^3	0	Jayson et al. (1973)
25.	$HO_2 + Cl_2^- \longrightarrow 2Cl^- + O_2 + H^+$	4.5×10^9	-1500	Ross and Neta (1979)
26.	$O_2^- + Cl_2^- \longrightarrow 2Cl^- + O_2$	1.0×10^9	-1500	Ross and Neta (1979)
27.	$HO_2 + Cl \longrightarrow Cl^- + O_2 + H^+$	3.1×10^9	-1500	Graedel and Goldberg (1983)
28.	$H_2O_2 + Cl_2^- \longrightarrow 2Cl^- + HO_2 + H^+$	1.4×10^5	-3370	Hagesawa and Neta (1978)
29.	$H_2O_2 + Cl \longrightarrow Cl^- + HO_2 + H^+$	4.5×10^7	0	Graedel and Goldberg (1983)
30.	$OH^- + Cl_2^- \longrightarrow 2Cl^- + OH$	7.3×10^6	-2160	Hagesawa and Neta (1978)

TABLE 3(d)

Nitrite and Nitrate Chemistry

	Reaction	*Rate Expression*		
		M^n $(\text{sec})^{-1}$	$-E/R$	Reference
31 .	$NO + NO_2 \xrightarrow{H_2O} 2NO_2^- + 2H^+$	2.0×10^8	-1500	Lee (1984a)
32 .	$NO_2 + NO_2 \xrightarrow{H_2O} NO_2^- + NO_3^- + 2H^+$	1.0×10^8	-1500	Lee (1984a)
33 .	$NO + OH \longrightarrow NO_2^- + H^+$	2.0×10^{10}	-1500	Strehlow and Wagner (1982)
34 .	$NO_2 + OH \longrightarrow NO_3^- + H^+$	1.3×10^9	-1500	Gratzel et al. (1970)
35 .	$HNO_2 \xrightarrow{h\nu} NO + OH$			Rettich (1970)
36 .	$NO_2^- \xrightarrow{h\nu, H_2O} NO + OH + OH^-$			Graedel and Weschler (1981)
37 .	$HNO_2 + OH \longrightarrow NO_2 + H_2O$	1.0×10^9	-1500	Rettich (1978)
38 .	$NO_2^- + OH \longrightarrow NO_2 + OH^-$	1.0×10^{10}	-1500	Treinin and Hayon (1978)
39 .	$HNO_2 + H_2O_2 \xrightarrow{H^+} NO_3^- + 2H^+ + H_2O$	$6.3 \times 10^3\,[H^+]$	-6693	Lee and Lind (1986)
40 .	$NO_2^- + O_3 \longrightarrow NO_3^- + O_2$	5.0×10^5	-6950	Damschen and Martin (1983)
41 .	$NO_2^- + CO_3^- \longrightarrow NO_2 + CO_3^{2-}$	4.0×10^5	0	Lilie et al. (1978)
42 .	$NO_2^- + Cl_2^- \longrightarrow NO_2 + 2Cl^-$	2.5×10^8	-1500	Hagesawa and Neta (1978)
43 .	$NO_2^- + NO_3 \longrightarrow NO_2 + NO_3^-$	1.2×10^9	-1500	Ross and Neta (1979)
44 .	$NO_3^- \xrightarrow{h\nu, H_2O} NO_2 + OH + OH^-$			Graedel and Wescler (1981)
45 .	$NO_3 \xrightarrow{h\nu} NO + O_2$			Graedel and Wescler (1981)
46 .	$NO_3 + HO_2 \longrightarrow NO_3^- + H^+ + O_2$	4.5×10^9	-1500	Jacob (1986)
47 .	$NO_3 + O_2^- \longrightarrow NO_3^- + O_2$	1.0×10^9	-1500	Jacob (1986)
48 .	$NO_3 + H_2O_2 \longrightarrow NO_3^- + H^+ + HO_2$	1.0×10^6	-2800	Chameides (1984)
49 .	$NO_3 + Cl^- \longrightarrow NO_3^- + Cl$	1.0×10^8	-1500	Ross and Neta (1979)

TABLE 3(e)

CH_4 Oxidation Chain

	Reaction	*Rate Expression*		
		M^n $(\text{sec})^{-1}$	$-E/R$	Reference
50.	$H_2C(OH)_2 + OH \xrightarrow{O_2} HCOOH + HO_2 + H_2O$	2.0×10^9	-1500	Bothe et al. (1980)
51.	$H_2C(OH)_2 + O_3 \longrightarrow$ products	0.1	0	Hoigne and Bader (1983a)
52.	$HCOOH + OH \xrightarrow{O_2} CO_2 + HO_2 + H_2O$	1.6×10^8	-1500	Scoles and Willson (1967)
53.	$HCOOH + H_2O_2 \longrightarrow$ product $+ H_2O$	4.6×10^{-6}	-5180	Shapilov et al. (1974)
54.	$HCOOH + NO_3 \xrightarrow{O_2} NO_3^- + H^+ + CO_2 + HO_2$	2.1×10^5	-3200	Dogliotti and Hayon (1967)
55.	$HCOOH + O_3 \longrightarrow CO_2 + HO_2 + OH$	5.0	0	Hoigne and Bader (1983b)
56.	$HCOOH + Cl_2^- \xrightarrow{O_2} CO_2 + HO_2 + 2Cl^- + H^+$	6.7×10^3	-4300	Hagesawa and Neta (1978)
57.	$HCOO^- + OH \xrightarrow{O_2} CO_2 + HO_2 + OH^-$	2.5×10^9	-1500	Anbar and Neta (1967)
58.	$HCOO^- + O_3 \longrightarrow CO_2 + OH + O_2^-$	100.0	0	Hoigne and Bader (1983b)
59.	$HCOO^- + NO_3 \xrightarrow{O_2} NO_3^- + CO_2 + HO_2$	6.0×10^7	-1500	Jacob (1986)
60.	$HCOO^- + CO_3^- \xrightarrow{O_2,H_2O} CO_2 + HCO_3^- +$ $+HO_2 + OH^-$	1.1×10^5	-3400	Chen et al. (1973)
61.	$HCOO^- + Cl_2^- \xrightarrow{O_2} CO_2 + HO_2 + 2Cl^-$	1.9×10^6	-2600	Hagasawa and Neta (1978)
62.	$CH_3C(O)O_2NO_2 \longrightarrow NO_3^-$ + products	4.0×10^{-4}	0	Lee (1984b)
63.	$CH_3O_2 + HO_2 \longrightarrow CH_3OOH + O_2$	4.3×10^5	-3000	Jacob (1986)
64.	$CH_3O_2 + O_2^- \xrightarrow{H_2O} CH_3OOH + O_2 + OH^-$	5.0×10^7	-1600	Jacob (1986)
65.	$CH_3OOH + h\nu \xrightarrow{O_2} HCHO + OH + HO_2$			Graedel and Wechsler (1981)
66.	$CH_3OOH + OH \longrightarrow CH_3O_2 + H_2O$	2.7×10^7	-1700	Jacob (1986)
67.	$CH_3OH + OH \longrightarrow HCHO + HO_2 + H_2O$	4.5×10^8	-1500	Anbar and Neta (1967)
68.	$CH_3OH + CO_3^- \xrightarrow{O_2} HCHO + HO_2 + HCO_3^-$	2.6×10^3	-4500	Chen et al. (1973)
69.	$CH_3OH + Cl_2^- \xrightarrow{O_2} HCHO + HO_2 + H^+ + 2Cl^-$	3.5×10^3	-4400	Hagesawa and Neta (1978)
70.	$CH_3OOH + OH \longrightarrow HCHO + OH + H_2O$	1.9×10^7	-1800	Jacob (1986)
71.	$CH_3OH + NO_3 \xrightarrow{O_2} NO_3^- + H^+ + HCHO + HO_2$	1.0×10^6	-2800	Dogliotti and Hayon (1967)

TABLE 3(f)

Sulfur Chemistry

	Reaction	*Rate Expression*		
		M^n $(\text{sec})^{-1}$	$-E/R$	Reference
72.[a]	$S(IV) + O_3 \longrightarrow S(VI) + O_2$	2.4×10^4		
		3.7×10^5	-5530	
		1.5×10^9	-5280	Hoffmann and Calvert (1985)
73.[a]	$S(IV) + H_2O_2 \longrightarrow S(VI) + H_2O$	1.3×10^6	-4430	McArdle and Hoffmann (1983)
74.[a]	$S(IV) + \frac{1}{2}O_2 \xrightarrow{Mn^{2+},Fe^{3+}} S(VI)$	4.7	$-13,700$	
		0.82	$-11,000$	
		5.0×10^3	$-13,700$	
		1.0×10^7	$-11,000$	Martin (1984)
75.	$SO_3^{2-} + OH \xrightarrow{O_2} SO_5^- + OH^-$	4.6×10^9	-1500	Huie and Neta (1987)
76.	$HSO_3^- + OH \xrightarrow{O_2} SO_5^- + H_2O$	4.2×10^9	-1500	Huie and Neta (1987)
77.	$SO_5^- + HSO_3^- \xrightarrow{O_2} HSO_5^- + SO_5^-$	3.0×10^5	-3100	Huie and Neta (1987)
	$SO_5^- + SO_3^{2-} \xrightarrow{O_2} HSO_5^- + SO_5^-$	1.3×10^7	-2000	Huie and Neta (1987)
78.	$SO_5^- + O_2^- \xrightarrow{H_2O} HSO_5^- + OH^- + O_2$	1.0×10^8	-1500	Jacob (1986)
79.	$SO_5^- + HCOOH \xrightarrow{O_2} HSO_5^- + CO_2 + HO_2$	200	-5300	Jacob (1986)
80.	$SO_5^- + HCOO^- \xrightarrow{O_2} HSO_5^- + CO_2 + O_2^-$	1.4×10^4	-4000	Jacob (1986)
81.	$SO_5^- + SO_5^- \longrightarrow 2SO_4^- + O_2$	2.0×10^8	-1500	Jacob (1986)
82.	$HSO_5^- + HSO_3^- \xrightarrow{H^+} 2SO_4^{2-} + 3H^+$	7.5×10^7	-4755	Jacob (1986)
83.	$HSO_5^- + OH \longrightarrow SO_5^- + H_2O$	1.7×10^7	-1900	Jacob (1986)
84.	$HSO_5^- + SO_4^- \longrightarrow SO_5^- + SO_4^{2-} + H^+$	$< 1.0 \times 10^5$	0	Jacob (1986)
85.	$HSO_5^- + NO_2^- \longrightarrow HSO_4^- + NO_3^-$	0.31	-6650	Jacob (1986)
86.	$HSO_5^- + Cl^- \longrightarrow SO_4^{2-} + \text{product}$	1.8×10^{-3}	-7050	Jacob (1986)

TABLE 3(f) - continuation

Sulfur Chemistry

	Reaction	*Rate Expression*		
		M^n $(\text{sec})^{-1}$	$-E/R$	Reference
87.	$SO_4^- + HSO_3^- \xrightarrow{O_2} SO_4^{2-} + H^+ + SO_5^-$	1.3×10^9	-1500	Jacob (1986)
88.	$SO_4^- + SO_3^{2-} \xrightarrow{O_2} SO_4^{2-} + SO_5^-$	5.3×10^8	-1500	Jacob (1986)
89.	$SO_4^- + HO_2 \longrightarrow SO_4^{2-} + H^+ + O_2$	5.0×10^9	-1500	Jacob (1986)
90.	$SO_4^- + O_2^- \longrightarrow SO_4^{2-} + O_2$	5.0×10^9	-1500	Jacob (1986)
91.	$SO_4^- + OH^- \longrightarrow SO_4^{2-} + OH$	8.0×10^7	-1500	Jacob (1986)
92.	$SO_4^- + H_2O_2 \longrightarrow SO_4^{2-} + H^+ + HO_2$	1.2×10^7	-2000	Ross and Neta (1979)
93.	$SO_4^- + NO_2^- \longrightarrow SO_4^{2-} + NO_2$	8.8×10^8	-1500	Jacob (1986)
94.	$SO_4^- + HCO_3^- \longrightarrow SO_4^{2-} + H^+ + CO_3^-$	9.1×10^6	-2100	Ross and Neta (1979)
95.	$SO_4^- + HCOO^- \xrightarrow{O_2} SO_4^{2-} + CO_2 + HO_2$	1.7×10^8	-1500	Jacob (1986)
96.	$SO_4^- + Cl^- \longrightarrow SO_4^{2-} + Cl$	2.0×10^8	-1500	Ross and Neta (1979)
97.	$SO_4^- + HCOOH \xrightarrow{O_2} SO_4^{2-} + H^+ + CO_2 + HO_2$	1.4×10^6	-2700	Jacob (1986)
98.[a]	$S(IV) + CH_3C(O)O_2NO_2 \longrightarrow S(VI)$	6.7×10^{-3}	0	Lee (1984)
99.	$HSO_3^- + CH_3OOH \xrightarrow{H^+} SO_4^{2-} + 2H^+ + \text{prd}$	1.9×10^7	-3800	Hoffmann and Calvert (1985)
100.[a]	$HSO_3^- + CH_3C(O)OOH \longrightarrow SO_4^{2-} + H^+ + \text{prd}$	5.0×10^7	-4000	
		6.0×10^2		Hoffmann and Calvert (1985)
101.	$S(IV) + HO_2 \longrightarrow S(VI) + OH$	1.0×10^6	0	Hoffmann and Calvert (1985)
	$S(IV) + O_2^- \xrightarrow{H_2O} S(VI) + OH + OH^-$	1.0×10^5	0	Hoffmann and Calvert (1985)
102.	$SO_4^- + CH_3OH \xrightarrow{O_2} SO_4^{2-} + HCHO$			
	$+H^+ + HO_2$	2.5×10^7	-1800	Dogliotti and Hayon (1967)

TABLE 3(f) - continuation

Sulfur Chemistry

	Reaction	*Rate Expression*		
		M^n $(\text{sec})^{-1}$	$-E/R$	Reference
103.	$2HSO_3^- + NO_3 \xrightarrow{O_2} NO_3^- + 2H^+ + SO_4^{2-} + SO_4^-$	1.0×10^8	0	Chameides (1984)
104.	$2NO_2 + HSO_3^- \xrightarrow{H_2O} SO_4^{2-} + 3H^+ + 2NO_2^-$	2.0×10^6	0	Lee and Schwartz (1983)
105a.[b]	$S(IV) + N(III) \longrightarrow S(VI) + \text{product}$	1.4×10^2	0	Martin (1984)
105b.[c]	$2HSO_3^- + NO_2^- \longrightarrow OH^- + \text{product}$	4.8×10^3	−6100	Oblath et al. (1981)
106.	$HCHO + HSO_3^- \longrightarrow HOCH_2SO_3^-$	2.9×10^2	−4900	Boyce and Hoffmann (1984)
	$HCHO + SO_3^{2-} \xrightarrow{H_2O} HOCH_2SO_3^- + OH^-$	2.5×10^7	−1800	Boyce and Hoffmann (1984)
107.	$HOCH_2SO_3^- + OH^- \longrightarrow SO_3^{2-} + HCHO + H_2O$	3.6×10^3	−4500	Munger et al. (1986)
108.	$HOCH_2SO_3^- + OH \xrightarrow{O_2} SO_5^- + HCHO + H_2O$	1.4×10^9	−1500	Jacob (1986)
109.	$HSO_3^- + Cl_2^- \xrightarrow{O_2} SO_5^- + 2Cl^- + H^+$	3.4×10^8	−1500	Huie and Neta (1987)
	$SO_3^{2-} + Cl_2^- \xrightarrow{O_2} SO_5^- + 2Cl^-$	1.6×10^8	−1500	Huie and Neta (1987)

[a] Reaction with "non-elementary" rate expression.

[b] For pH $\leq$ 3.

[c] For pH $>$ 3.

Mathematical Description

The dynamics of the aqueous-phase and gas-phase species are described by a set of mass balance differential equations, the general form of which, for an aqueous-phase species with concentration $c_i(aq)$ (moles/l of water), is given by

$$\frac{dc_i(aq)}{dt} = k_{mt}c_i(g) - k_{mt}\frac{1}{K_{Hi}RT}c_i(aq) + R_i \tag{1.1}$$

where k_{mt} is a combined rate coefficient for gas-phase plus interfacial mass transport,

$$k_{mt} = \frac{3\eta D_{g,i}}{\alpha^2} \tag{1.2}$$

and where $c_i(g)$ (moles/l of gas) is the concentration of species i in the gas phase, K_{Hi} is the effective Henry's law constant of species i, R is the ideal gas constant(0.082058 l atm/ mole K), T is the temperature (K), R_i (moles/ l of water s) is the reaction rate of i in the aqueous-phase, $D_{g,i}$ is the diffusivity of species i in air, α is the cloud droplet radius and finally η is a coefficient correcting for free molecular effects. This coefficient can be approximated by [Fuchs and Sutugin, 1971]:

$$\eta = \left\{1 + \left[\frac{1.33 + 0.71Kn^{-1}}{1 + Kn^{-1}} + \frac{4(1 - a_w)}{3a_w}\right]Kn\right\}^{-1} \tag{1.3}$$

here Kn is the Knudsen number, that is the ratio of the mean free path of air to the droplet radius and a_w is the sticking coefficient. The sticking coefficient represents the probability that a gas molecule reaching the droplet surface will adhere to it. For cloud droplets Kn is much smaller than unity so as a_w approaches unity, η approaches 1. As a_w decreases approaching zero, η also decreases. For example, for a cloud droplet of radius 10 μm and a species with $a_w = 10^{-4}$, $\eta = 0.01$.

The sticking coefficient a_w for gaseous species on small droplets has been an elusive quantity. In recent measurements of the sticking coefficients of SO_2 [Gardner et al.,1987]

and HO_2 [Mozurkewich et al.,1987] onto aqueous solutions it has been found that the corresponding values of a_w are slightly larger than 0.01. Such values of a_w would imply that interfacial mass-transport does not substantially inhibit the rate of aqueous-phase reactions of these species under representative conditions [Schwartz, 1986]. In the absence of other data a value of $a_w = 0.01$ has been used in our base case simulation for all species.

The effective (or modified) Henry's law coefficient K_{Hi} for a species i that undergoes ionic dissociation differs from the Henry's law coefficient H_i as it contains all the ionic forms of the dissolved gas. For example,

$$K_{H,S(IV)} = H_{S(IV)}\left[1 + \frac{K_1}{[\mathrm{H^+}]} + \frac{K_1 K_2}{[\mathrm{H^+}]^2}\right] \tag{1.4}$$

where K_1 and K_2 the first and the second ionic dissociation constants for $SO_2 \cdot H_2O$ (Table 2).

Finally the temporal variations in the concentrations of the gas-phase species $c_i(g)$ (Table 1) are given by equations of the general form :

$$\frac{dc_i(g)}{dt} = -k_{mt} w_L c_i(g) + k_{mt} w_L \frac{1}{K_{Hi} RT} c_i(aq) \tag{1.5}$$

where w_L is the water liquid content (l water/l air) of the cloud.

In our description of the process we assume that aqueous equilibrium and electroneutrality are continously maintained [Seinfeld, 1986], so that the electroneutrality equation can be expressed in the form:

$$f\Big([\mathrm{H^+}]; [\mathrm{S(IV)}], [\mathrm{S(VI)}], [\mathrm{N(III)}], ..., [\mathrm{CO_3^-}], [\mathrm{Fe^{3+}}], [\mathrm{Mg^{2+}}], [\mathrm{Na^+}]\Big) = 0 \tag{1.6}$$

and as all the lumped concentrations (S(IV), S(VI) etc.) are known at any time equation (1.6) reduces to one nonlinear equation with one unknown, $[\mathrm{H^+}]$.

The initial conditions for the base case (Table 1) have been chosen to be representative of a day-time cloud environment in the northeastern United States region

[Systems Applications Inc., 1987; Jacob, 1986; Chameides, 1982]. Some of the results of the base case simulation are shown in figures 1 and 2. The pH changes from an initial value of 4.9 to 3.6 after two hours. Both $SO_2(g)$ and $H_2O_2(g)$ concentrations decrease significantly as both species are transported to the aqueous-phase where they react rapidly to produce S(VI). The scavenging of $HNO_3(g)$ appears to be the only source of nitrate acidity in the cloud. The presence of the cloud results in a net production of formic acid and a small decrease in the amount of formaldehyde. Peroxymonosulfate concentration reaches a maximum and then decreases.

Sensitivity Analysis Method

The sensitivity analysis can provide a direct means for determining the important reactions in a chemical mechanism, the effects of uncertainties in the input parameters on the mechanism's predictions and generally provide considerable insight into the entire system. Sensitivity analysis has been used for the identification of the most important reactions, initial and boundary conditions in atmospheric and combustion mechanisms [Falls et al. 1979; Dickinson and Gelinas, 1976; Dougherty et al. 1979, 1980; Dunker 1980,1984].

Two classes of methods have been used for sensitivity analysis. The local or deterministic methods produce information on how the uncertainty to one parameter, for example, k_i, affects one of the dependent variables, for example, y_j [Oran and Boris, 1987]. The global or stochastic methods consider the effects of simultaneously varying parameters over a range of values [Cukier et al.,1978 ; Koda et al. 1979 ; Stolarski et al.,1978].

Since our main goal is the determination of the relative importance of the 109 reactions in the mechanism local sensitivity analysis methods are sufficient, of which there are four main canditates :

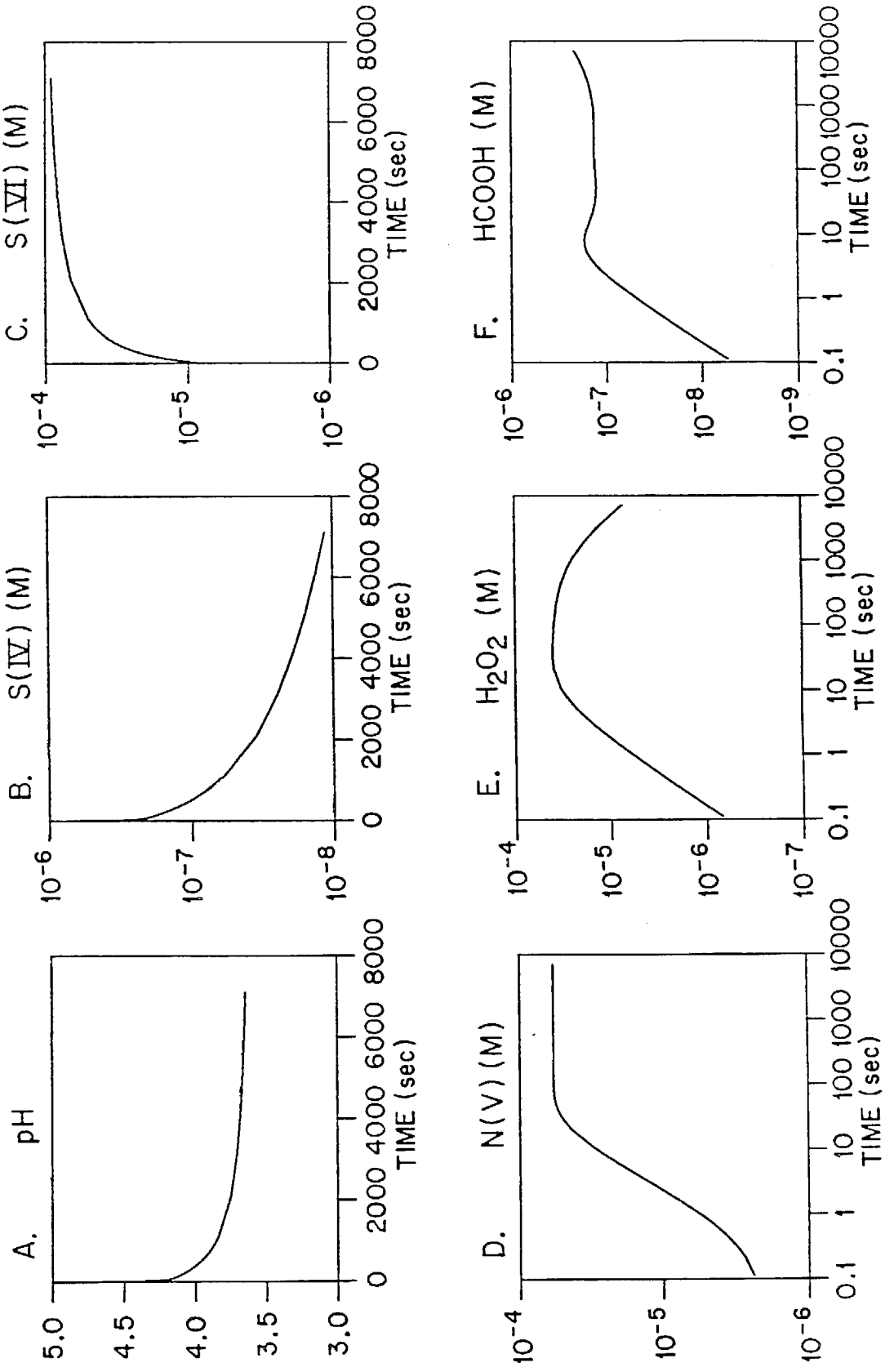

Figure 1. Calculated aqueous-phase concentrations in (mol / l of water) for the base scenario.

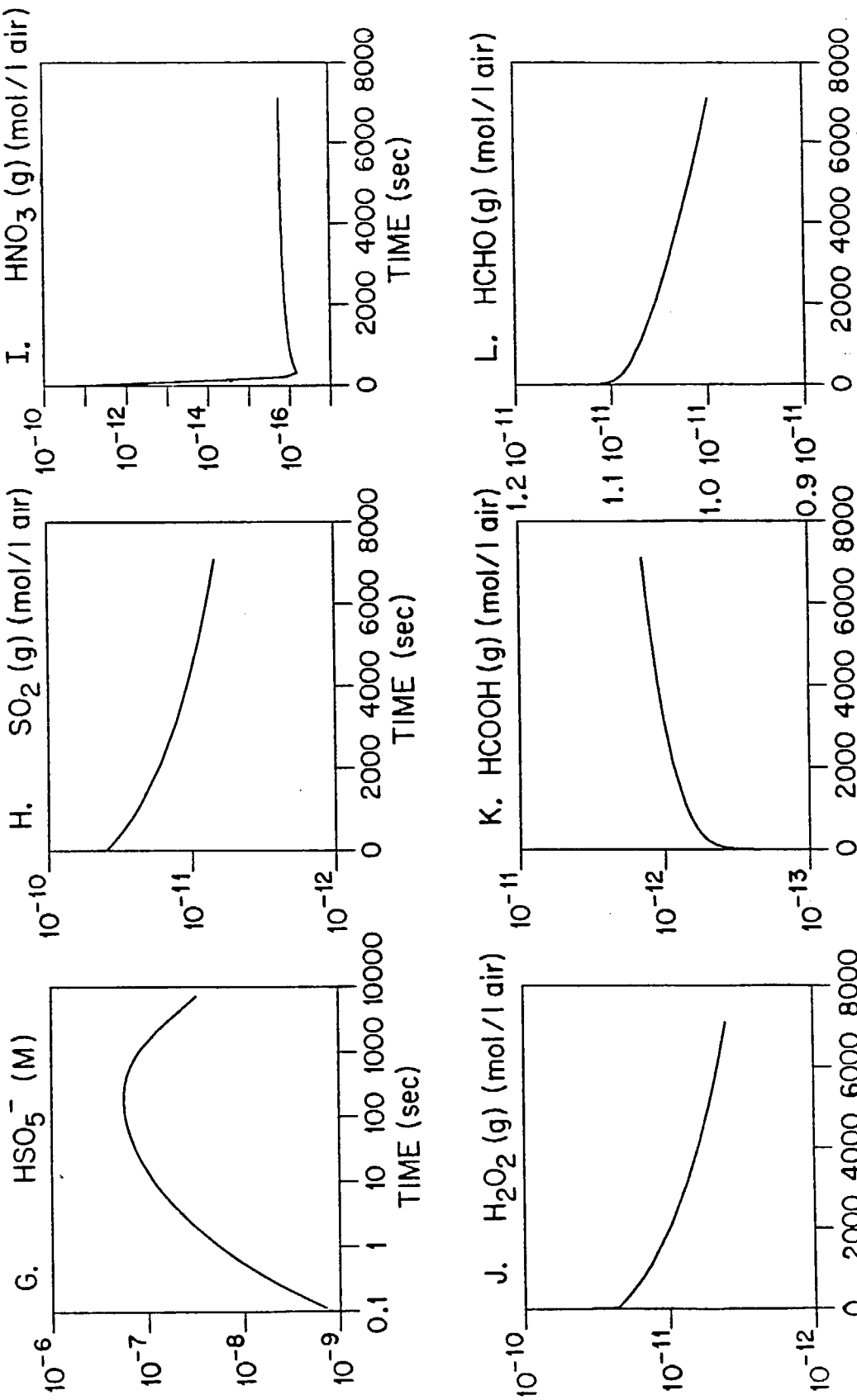

Figure 2. Calculated aqueous-phase concentrations in (mol / l of water) and gas-phase concentrations in (mol / l of air) for the base scenario

(a) The indirect or brute force method [Dunker, 1980]

(b) The coupled direct method [Dickinson et al., 1976; Frank, 1978]

(c) The Green's function method [Dougherty et al., 1979]

(d) The decoupled direct method [Dunker, 1984]

Most appropriate for the current problem is the decoupled direct method (DDM) because of its efficiency in the calculation of large numbers of sensitivity coefficients, its simplicity, accuracy and stability.

The system of ordinary differential equations for the aqueous and gas-phase concentrations can be written in the form :

$$\frac{d\mathbf{y}}{dt} = \mathbf{f}(\mathbf{y}, t; \lambda), \qquad \mathbf{y}(t_o) = \mathbf{y_o} \tag{2.1}$$

where $\mathbf{y}$ is the N-dimensional vector of concentrations, λ is the M-dimensional time-independent vector of input parameters, and $\mathbf{y_o}$ is the initial condition on $\mathbf{y}$. The first-order sensitivity coefficients are defined as:

$$s_{kl} = \frac{\partial y_k}{\partial \lambda_l} \tag{2.2}$$

The N-dimensional vector $\mathbf{s_i}$, consisting of the sensitivity coefficients s_{ji} of the N species concentrations to the parameter λ_i, satisfies the differential equation :

$$\frac{d\mathbf{s_i}}{dt} = \mathbf{J}(\mathbf{y}, t; \lambda)\ \mathbf{s}_i + \mathbf{f}_i(\mathbf{y}, t; \lambda), \qquad \mathbf{s}_i(t_o) = \frac{\partial \mathbf{y_o}}{\partial \lambda_i} \tag{2.3}$$

where the elements of $\mathbf{J}$, the Jacobian matrix, and the vector $\mathbf{f_i}$ are:

$$J_{mn} = \frac{\partial f_m}{\partial y_n} \qquad \mathbf{f}_i = \frac{\partial \mathbf{f}}{\partial \lambda_i} \tag{2.4}$$

The basic idea behind the DDM is that systems (2.1) and (2.3) are decoupled but solved simultaneously, alternating the solution of (2.1) with the solution of (2.3) [Dunker, 1984].

We have calculated the sensitivity coefficients of the mechanism in table 3 with respect to the reaction constants that appear in it. Results will be presented in terms of the dimensionless sensitivity coefficients $\overline{s}_{ij}$ defined as

$$\overline{s}_{ij} = \frac{\lambda_j}{y_i}\frac{\partial y_i}{\partial \lambda_j} = \frac{\partial \ln y_i}{\partial \ln \lambda_j} \tag{2.5}$$

in order to make comparison between them easier [Dougherty and Rabitz, 1980]. The use of dimensional sensitivity coefficients can result in difficulty in assesing the sensitivity to the nonzero initial concentrations [Cho et al., 1986]. However, the dimensionless sensitivity coefficient will always be zero for a zero initial concentration because the nonzero $\partial y_i/\partial \lambda_j$ is multiplied by $\lambda_j = 0$. In this case dimensional sensitivity coefficients should be calculated.

One way of interpreting the dimensionless sensitivity coefficients is the use of a Taylor series expansion of formula (2.5). Then :

$$y_i(t, \lambda_j + \Delta\lambda_j) - y_i(t, \lambda_j) = \overline{s}_{ij} y_i(t, \lambda_j)\frac{\Delta\lambda_j}{\lambda_j} \tag{2.6}$$

Note that the net effect of parameter λ_j on y_i at time t depends not only on $\overline{s}_{ij}(t)$ but on $y_i(t)$ too.

We have calculated the sensitivity of the concentrations of our species to 150 parameters of the mechanism (reaction constants, initial conditions, liquid water content, etc). This required the solution of almost 7500 stiff ODE's and consumed 19 hours of CPU time on a microvax II.

S(IV) to S(VI) Tranformation and Sulfur Chemistry.

The conversion of S(IV) to S(VI) is a dominant chemical process in cloudwater. Absorption of SO_2(g) in cloudwater results in the ionic dissociation of $SO_2 \cdot H_2O$ to HSO_3^- and SO_3^{2-}. Because of this dissociation the solubility of SO_2(g) in water is

enhanced and the total amount of dissolved sulfur always exceeds that predicted by Henry's law for SO_2 alone. The total amount of dissolved S(IV) is therefore quite pH-dependent. The Henry's law coefficient for SO_2 alone, H_{SO_2}, is 1.23 M/atm at 298 K, while for the same temperature the effective Henry's law coefficient for S(IV), $K_{H,S(IV)}$ (equation 1.4), is 1524 M/atm for pH=5, 152 M/atm for pH=4 and 16.4 M/atm for pH=3. Furthermore at the pH range of interest (pH 2-8) virtually all of the S(IV) is in the form of HSO_3^-, whereas at low pH (pH<2) all of the S(IV) occurs as $SO_2 \cdot H_2O$.

The pathways for S(IV) transformation that have been included in the present mechanism involve reactions of S(IV) with O_3, H_2O_2, O_2 (catalysed by Mn^{2+} and Fe^{3+}), OH, SO_5^-, HSO_5^-, SO_4^-, PAN, CH_3OOH, $CH_3C(O)OOH$, HO_2, NO_3, NO_2, N(III), HCHO and Cl_2^-. For the oxidation of S(IV) by OH we have adopted here the mechanism proposed by Jacob [1986]. The products of the above S(IV) reactions include S(VI), SO_4^-, SO_5^-, HSO_5^- and $HOCH_2SO_3^-$. The dimensionless sensitivity coefficients for S(IV) to the various chemical reaction constants appear in table 4.

The dominant reaction throughout the simulation is the oxidation of S(IV) by H_2O_2(aq),

$$S(IV) + H_2O_2 \longrightarrow S(VI) + H_2O \qquad (react.\ 73)$$

Hydrogen peroxide is clearly the most effective oxidant of S(IV) for the pH range of our simulation as for pH>2 the rate of of this reaction is pH independent [Martin and Damschen, 1981; McArdle and Hoffmann, 1983]. Under the conditions of the present simulation the rate of the reaction at t = 30 s was 2.57 ppb SO_2/hr or equivalently 253% SO_2/hr.

The other reactions that influence [S(IV)(aq)] can be divided into two categories:

a) Reactions that influence S(IV) indirectly by producing or consuming H_2O_2 and therefore by changing the rate of reaction 73.

b) Reactions that consume S(IV), influencing S(IV) directly.

TABLE 4. Dimensionless Sensitivity Coefficients for S(IV)(aq)[a]

Time	100 sec		400 sec		800 sec		1800 sec	
	React.	Sens.Coef.	React.	Sens.Coef.	React.	Sens.Coef.	React.	Sens.Coef.
	73	-0.198	73	-0.519	73	-0.662	73	-0.799
	78	-0.323(-2)[b]	7	-0.939(-2)	74	-0.142(-1)	74	-0.262(-1)
	7	-0.298(-2)	78	-0.531(-2)	7	-0.138(-1)	7	-0.216(-1)
	76	-0.263(-2)	74	-0.363(-2)	78	-0.507(-2)	78	-0.628(-2)
	81	-0.228(-2)	76	-0.258(-2)	82	-0.320(-2)	5	0.447(-2)
	72	-0.138(-2)	82	-0.228(-2)	76	-0.280(-2)	82	-0.394(-2)
	74	-0.930(-3)	72	-0.221(-2)	72	-0.249(-2)	76	-0.387(-2)
	82	-0.855(-3)	81	-0.191(-2)	5	0.239(-2)	72	-0.311(-2)
	50	-0.506(-3)	5	0.139(-2)	18	-0.171(-2)	18	-0.281(-2)
	77	-0.372(-3)	18	-0.112(-2)	81	-0.157(-2)	20	0.215(-2)
	87	-0.365(-3)	20	0.804(-3)	20	0.127(-2)	99	-0.186(-2)
	5	0.341(-3)	13	0.701(-3)	13	0.110(-2)	13	0.159(-2)
	18	-0.332(-3)	77	-0.685(-3)	99	-0.103(-2)	81	-0.126(-2)
	96	-0.258(-3)	99	-0.662(-3)	77	-0.736(-3)	77	-0.104(-2)
	99	-0.223(-3)	50	-0.603(-3)	1	0.325(-3)	1	0.998(-3)
	109	-0.223(-3)	87	-0.377(-3)	109	-0.323(-3)	29	0.596(-3)
	20	0.217(-3)	109	-0.280(-3)	87	-0.312(-3)	109	-0.452(-3)
	13	0.184(-3)	96	-0.272(-3)	29	0.287(-3)	6	-0.271(-3)
	101	-0.134(-3)	29	0.136(-3)	96	-0.215(-3)	87	-0.268(-3)
	92	-0.118(-3)	1	0.112(-3)	6	-0.166(-3)	96	-0.149(-3)

[a] Dimensionless sensitivity coefficient for reaction i with reaction constant K_i:

$$\frac{\partial \ln[\mathrm{S(IV)(aq)}]}{\partial \ln K_i}$$

[b] Read -0.323(-2) as -0.323×10^{-2}.

We shall start by examining the indirect influences. The sensitivity coefficients for H_2O_2 are shown in table 5. The main aqueous-phase source of H_2O_2 is:

$$HO_2 + O_2^- \xrightarrow{H_2O} H_2O_2 + O_2 + OH^- \qquad (react.\ 7)$$

and therefore it accelerates the oxidation of S(IV) to S(VI). Reaction 7 is in fact more influential to S(IV) oxidation, in the case considered here, than most of the other direct oxidation reactions for the conversion of S(IV) to S(VI). The rate of this reaction is initially 100% H_2O_2 /hr and, as HO_2 is depleted, it slows down.

The second most important sink of H_2O_2, after the oxidation of S(IV), is its reaction with OH to produce HO_2:

$$OH + H_2O_2 \longrightarrow H_2O + HO_2 \qquad (react.\ 5)$$

This reaction results in a slowing of the conversion of S(IV) by H_2O_2 and after 30 minutes of simulation it is found to be relatively significant for S(IV). The importance of this reaction is less than what its rate suggests because its product, HO_2, leads to H_2O_2 by reaction 7.

Of next importance for the $[H_2O_2(aq)]$ is the reaction of the superoxide ion, O_2^-, with bicarbonate ion to form HO_2^- and carbonate radical ion:

$$HCO_3^- + O_2^- \longrightarrow HO_2^- + CO_3^- \qquad (react.\ 18)$$

Reaction 18 was initially reported by Schmidt [1972] although subsequently Schwartz [1984] concluded that there is insufficient evidence for its occurence in cloudwater. Assuming that the rate constant given in table 3 is correct, the sensitivity analysis shows that this reaction represents a relatively important aqueous-phase source of H_2O_2. Hence some additional studies are necessary to confirm or exclude the occurrence of this reaction.

TABLE 5. Dimensionless Sensitivity Coefficients for $H_2O_2(aq)$[a]

Time	100 sec		400 sec		800 sec		1800 sec	
	React.	Sens.Coef.	React.	Sens.Coef.	React.	Sens.Coef.	React.	Sens.Coef.
	73	-0.606(-1)[b]	73	-0.203	73	-0.336	73	-0.531
	7	0.156(-1)	7	0.175(-1)	7	0.189(-1)	7	0.235(-1)
	5	-0.200(-2)	5	-0.319(-2)	5	-0.406(-2)	5	-0.604(-2)
	18	0.176(-2)	18	0.219(-2)	18	0.249(-2)	74	0.526(-2)
	20	-0.124(-2)	20	-0.165(-2)	20	-0.192(-2)	18	0.327(-2)
	13	-0.117(-2)	13	-0.141(-2)	13	-0.190(-2)	13	-0.324(-2)
	29	-0.246(-3)	76	0.757(-3)	76	0.151(-2)	76	0.324(-2)
	6	0.179(-3)	1	-0.422(-3)	74	0.973(-3)	20	-0.258(-2)
	76	0.172(-3)	29	-0.411(-3)	1	-0.859(-3)	1	-0.204(-2)
	1	-0.105(-3)	6	0.214(-3)	29	-0.538(-3)	78	0.111(-2)
			72	0.125(-3)	78	0.328(-3)	72	0.901(-3)
			74	0.114(-3)	72	0.320(-3)	29	-0.824(-3)
					82	0.241(-3)	82	0.660(-3)

[a] Dimensionless sensitivity coefficient for reaction i with reaction constant K_i:

$$\frac{\partial \ln[H_2O_2(aq)]}{\partial \ln K_i}$$

[b] Read -0.606(-1) as -0.606×10^{-1}.

Another significant sink of H_2O_2 is found to be its reaction with the carbonate radical ion:

$$CO_3^- + H_2O_2 \longrightarrow HO_2 + HCO_3^- \qquad (react.\ 20)$$

This reaction is the inverse of reaction 18.

Finally other sinks or sources of H_2O_2 are reactions 1, 29 and 6. The influence of these reactions on H_2O_2, explains their appearance among the sensitive reactions for S(IV) and S(VI).

For the first five minutes of simulation the second most important direct pathway for S(IV) conversion is its oxidation by OH to produce SO_5^-:

$$HSO_3^- + OH \xrightarrow{O_2} SO_5^- + H_2O \qquad (react.\ 76)$$

After this initial time period the rate of reaction 76 decreases because of the pH decrease and the depletion of OH. We should note that the various gas-phase sources and sinks of OH, which have not been included here, would have as a net result a slower OH depletion. Hence as OH(g) concentration can be higher than the value calculated by our model, the above reaction can be even more influential than shown here. Reaction 76 takes place in two steps; first oxidation of HSO_3^- and SO_3^{2-} by OH(aq) produces the SO_3^- radical and then $SO_3{}^-$ reacts very rapidly with O_2 to produce SO_5^- [Huie and Neta, 1984]. The fate of SO_5^- is reaction via various pathways to produce HSO_5^-, SO_4^- and S(VI) creating a relatively complicated reaction system that we shall examine later.

After the first 10 minutes (Table 4) of the simulation, the second most important pathway for conversion of S(IV) to S(VI) is oxidation by O_2 catalysed by Fe^{3+} and Mn^{2+}:

$$S(IV) + \frac{1}{2}O_2 \xrightarrow{Mn^{2+},Fe^{3+}} S(VI) \qquad (react.\ 74)$$

This reaction has been the subject of considerable interest [Hoffmann and Boyce, 1983; Martin, 1984; Hoffmann and Jacob, 1984; Hoffmann and Calvert, 1985; Clarke and Radojevic, 1986] and important differences in the measured reaction rates, rate laws and pH dependencies have been found [Hoffmann and Jacob, 1984]. Recently Martin [1987] has proposed that the reaction is inhibited by ionic strength, sulfate ion and is self-inhibited, and furthermore, that most of the literature discrepancies may be explained by differences in the above factors. Our sensitivity study in which the previous expressions proposed by Martin [1984] have been used shows that the metal (Fe^{3+} and Mn^{2+}) catalysed oxidation of S(IV) is of major importance for the aqueous-phase sulfate production. Due to the uncertainties existing in the transition metal chemistry and the wide variations of the concentrations of dissolved transition metal ions [Graedel et al., 1986] our analysis of the role of the transition metals will is limited only to reaction 74.

The oxidation of S(IV) by O_3:

$$S(IV) + O_3 \longrightarrow S(VI) + O_2 \qquad (react.\ 72)$$

decreases rapidly as the pH decreases [Hoffmann et al., 1985], and so for the pH range of our simulation, its final contribution to the S(IV) oxidation is far less significant than oxidation of S(IV) by H_2O_2, OH and O_2 (Table 4).

A pathway that becomes progressively important is the oxidation of S(IV) by HSO_5^- to produce sulfate :

$$HSO_5^- + HSO_3^- \xrightarrow{H^+} 2SO_4^{2-} + 3H^+ \qquad (react.\ 82)$$

For the first 15 minutes of simulation the HSO_5^- concentration and the contribution of this pathway to the S(IV) oxidation increase. Later as the pH continues to decrease, HSO_5^- is converted to sulfate and therefore reaction 82 starts slowing down.

There are some reactions that under the conditions used in this study are found moderately significant. They include the oxidation of S(IV) by SO_5^- (reaction 77), oxidation by $CH_3OOH(aq)$ (reaction 99), oxidation by SO_4^- (reaction 87) and oxidation by HO_2 (reaction 101).

The remainder of the reaction pathways for S(IV) included in the present mechanism are found to be insignificant. The oxidation by PAN is very slow for pH less than 5.5. The oxidation of S(IV) by formaldehyde is found to be unimportant, as the corresponding reaction rate decreases dramatically with decreasing pH and will be quite small unless the pH exceeds 5.5. Finally oxidation by nitrogen compounds, NO_3, NO_2 and N(III), is found to be a negligible sink of S(IV) and is not expected to play a role under ordinary conditions.

SO_5^-, SO_4^- and HSO_5^- chemistry

Among the reactions that play an important role in the oxidation of S(IV) (Table 4) appears a group, such as reactions 78 and 81, that do not involve S(IV) directly. These reactions represent intermediate steps in the conversion of S(IV) to S(VI) and involve species like SO_5^-, SO_4^- and HSO_5^-.

The SO_5^-, SO_4^-, HSO_5^- reaction subsystem appears to be rather complicated, therefore we shall try first to identify the important sinks and sources for each of the above species and then we shall examine the influences exerted by these reactions on S(IV) and S(VI). We attempt to gain some insight by looking at the corresponding sensitivity coefficients from three different points of view:

(1) the sensitivity coefficients for S(IV) (Table 4)

(2) the sensitivity coefficients for S(VI) (Table 6) and

(3) the sensitivity coefficients for HSO_5^- (Table 7).

Using the above information we arrive at the following conclusions.

TABLE 6. Dimensionless Sensitivity Coefficients for S(VI)(aq)[a]

Time	100 sec		400 sec		800 sec		1800 sec	
	React.	Sens.Coef.	React.	Sens.Coef.	React.	Sens.Coef.	React.	Sens.Coef.
	73	0.361	73	0.558	73	0.508	73	0.377
	7	0.524(-2)[b]	7	0.101(-1)	74	0.108(-1)	74	0.123(-1)
	72	0.257(-2)	78	0.516(-2)	7	0.106(-1)	7	0.108(-1)
	81	0.241(-2)	82	0.386(-2)	78	0.511(-2)	78	0.474(-2)
	82	0.229(-2)	74	0.363(-2)	82	0.358(-2)	82	0.248(-2)
	78	0.218(-2)	72	0.238(-2)	76	0.241(-2)	76	0.247(-2)
	74	0.171(-2)	76	0.218(-2)	72	0.192(-2)	5	-0.210(-2)
	76	0.112(-2)	81	0.171(-2)	5	-0.182(-2)	72	0.147(-2)
	96	0.918(-3)	5	-0.148(-2)	18	0.131(-2)	18	0.132(-2)
	87	0.891(-3)	18	0.120(-2)	81	0.130(-2)	20	-0.101(-2)
	5	-0.603(-3)	20	-0.861(-3)	20	-0.968(-3)	99	0.871(-3)
	18	0.537(-3)	99	0.710(-3)	99	0.784(-3)	13	-0.813(-3)
	99	0.407(-3)	13	-0.521(-3)	13	-0.705(-3)	1	-0.466(-3)
	20	-0.392(-3)	96	0.497(-3)	77	0.359(-3)	77	0.370(-3)
	13	-0.364(-3)	87	0.414(-3)	96	0.351(-3)	81	0.328(-3)
	92	0.325(-3)	77	0.336(-3)	1	-0.247(-3)	96	0.246(-3)
	101	0.225(-3)	92	0.199(-3)	87	0.243(-3)	29	-0.186(-3)
	90	0.165(-3)	29	-0.134(-3)	29	-0.158(-3)	87	0.137(-3)
	89	0.123(-3)	1	-0.129(-3)	92	0.128(-3)	6	0.127(-3)
			101	0.125(-3)	6	0.127(-3)	109	-0.101(-3)

[a] Dimensionless sensitivity coefficient for reaction i with reaction constant K_i:

$$\frac{\partial \ln[\mathrm{S(VI)(aq)}]}{\partial \ln K_i}$$

[b] Read 0.542(-2) as 0.542×10^{-2}.

TABLE 7. Dimensionless Sensitivity Coefficients for $HSO_5^-(aq)$[a]

Time	100 sec		400 sec		800 sec		1800 sec	
	React.	Sens.Coef.	React.	Sens.Coef.	React.	Sens.Coef.	React.	Sens.Coef.
	78	0.924	78	0.896	78	0.879	82	-1.122
	81	-0.141	82	-0.335	82	-0.618	78	0.859
	82	-0.823(-1)[b]	81	-0.158	81	-0.167	73	0.252
	77	0.687(-1)	77	0.966(-1)	77	0.113	81	-0.183
	73	-0.188(-1)	73	-0.120(-1)	73	0.484(-1)	77	0.133
	83	-0.226(-2)	83	-0.356(-2)	83	-0.436(-2)	74	0.669(-2)
	80	0.112(-2)	80	0.215(-2)	80	0.305(-2)	7	-0.600(-2)
	72	-0.359(-3)	76	0.991(-3)	76	0.215(-2)	83	-0.576(-2)
	87	-0.264(-3)	50	0.544(-3)	50	0.110(-2)	80	0.481(-2)
	7	-0.243(-3)	72	-0.297(-3)	7	0.106(-2)	76	0.475(-2)
	74	-0.163(-3)	87	-0.225(-3)	74	0.908(-3)	5	-0.115(-2)
	76	0.113(-3)	74	-0.124(-3)	5	-0.193(-3)	18	0.759(-3)
			7	-0.119(-3)	87	-0.178(-3)	72	0.744(-3)

[a] Dimensionless sensitivity coefficient for reaction i with reaction constant K_i:

$$\frac{\partial \ln[HSO_5^-(aq)]}{\partial \ln K_i}$$

[b] Read -0.823(-1) as -0.823×10^{-1}.

The main source of SO_5^- is under the present conditions the oxidation of HSO_3^- by OH (reaction 76). A additional source is the oxidation of S(IV) by SO_4^-:

$$SO_4^- + HSO_3^- \xrightarrow{O_2} SO_4^{2-} + H^+ + SO_5^- \qquad (react.\ 87)$$

There are two competing reactions consuming SO_5^-. The first one is its reaction with O_2^- to produce SO_5^- :

$$SO_5^- + O_2^- \xrightarrow{H_2O} HSO_5^- + OH^- + O_2 \qquad (react.\ 78)$$

and the second is its autoconversion to SO_4^- :

$$SO_5^- + SO_5^- \longrightarrow 2SO_4^- + O_2 \qquad (react.\ 81)$$

There is only one significant source of SO_4^-, the autoconversion of SO_5^- by reaction 81. The fate of SO_4^- is mainly conversion to S(VI). There are two main pathways for this conversion, its reaction with Cl^-:

$$SO_4^- + Cl^- \longrightarrow SO_4^{2-} + Cl \qquad (react.\ 96)$$

and its reaction with HSO_3^- (reaction 87). Additional pathways for the above conversion, like the reaction of SO_4^- with H_2O_2 (reaction 92), its reaction with HO_2 and O_2^- (reactions 89 and 90) and finally its reaction with $HCOO^-$ (reaction 95), are of minor importance.

The main sources of HSO_5^- (Table 7) appear to be the fast reaction of SO_5^- with O_2^- (reaction 78) and the oxidation of HSO_3^- by SO_5^- (reaction 77). There is one more minor source, the reaction of SO_5^- with $HCOO^-$:

$$SO_5^- + HCOO^- \xrightarrow{O_2} HSO_5^- + CO_2 + O_2^- \qquad (react.\ 80)$$

The main sink is by far its reaction with HSO_3^- to produce sulfate (reaction 82). A secondary sink is its reaction with OH (reaction 83).

The main reactions that produce and consume SO_4^-, HSO_5^- and SO_5^- are found to be influential on both the S(IV) and S(VI) concentrations. Under the conditions used in this study there are two main pathways involving the above species and resulting in the conversion of S(IV) to S(VI). The first is:

$$S(IV)(+OH) \longrightarrow SO_5^-(+O_2^-) \longrightarrow HSO_5^-(+HSO_3^-) \longrightarrow S(VI)$$

and the second :

$$S(IV)(+OH) \longrightarrow SO_5^- \longrightarrow SO_4^-(+Cl^-, HSO_3^-) \longrightarrow S(VI)$$

The first of these two pathways appears to be faster than the second under the present conditions (Tables 4, 6 and 7) after at least the first few minutes.

An interesting feature of the reaction system is the production and consumption of HSO_5^-. For the first five minutes of our simulation the concentration of HSO_5^- keeps increasing; it then reaches a maximum value and starts decreasing (figure 2). Reaction 78, which is mainly responsible for HSO_5^- production, slows down at this time and reaction 82 becomes dominant (Table 7). Notable is the influence of reaction 73 on the HSO_5^- concentration. Initially one finds that this reaction indirectly negatively influences the HSO_5^- concentration because it consumes S(IV) and therefore inhibits the HSO_5^- production which is at this time the dominant process for HSO_5^-. Subsequently as the consumption of HSO_5^- by HSO_3^- becomes the dominant process, reaction 73 starts enhancing the HSO_5^- concentration as it consumes HSO_3^-. The same change of sign at 300 s is noted for the sensitivity coefficients for reactions 72, 7 and 74 for exactly the same reasons.

$HOCH_2SO_3^-$ *chemistry*

Under the pH conditions studied here hydroxymethanesulfonate ion (HMSA) is produced by the reaction of SO_3^{2-} with formaldehyde:

$$HCHO + SO_3^{2-} \xrightarrow{H_2O} HOCH_2SO_3^- + OH^- \qquad (react.\ 106)$$

HMSA concentration attains a maximum value and then is converted to SO_5^- because of the OH(aq) attack:

$$HOCH_2SO_3^- + OH \xrightarrow{O_2} SO_5^- + HCHO + H_2O \qquad (react.\ 108)$$

The dissociation of $HOCH_2SO_3^-$ by nucleophilic displacement of HSO_3^- by OH^- [Munger et al., 1986] :

$$HOCH_2SO_3^- + OH^- \xrightarrow{O_2} SO_3^{2-} + HCHO + H_2O \qquad (react.\ 107)$$

is slow under the current conditions and is not expected to be influential under ordinary cloud conditions (non-alkaline conditions).

The main features of the sulfur chemistry are summarized in figure 3.

Nitrite and Nitrate Chemistry

From table 8 we note there is no significant reaction producing HNO_3 in the aqueous phase. The main reaction concerning N(V) is, under the present conditions, the photolysis of NO_3^-:

$$NO_3^- \xrightarrow{h\nu, H_2O} NO_2 + OH + OH^- \qquad (react.\ 44)$$

which consumes nitric acid at the negligible rate of 0.03%/hr. Hence the rates of all the nitric acid aqueous-phase reactions are too small to influence the HNO_3(aq)

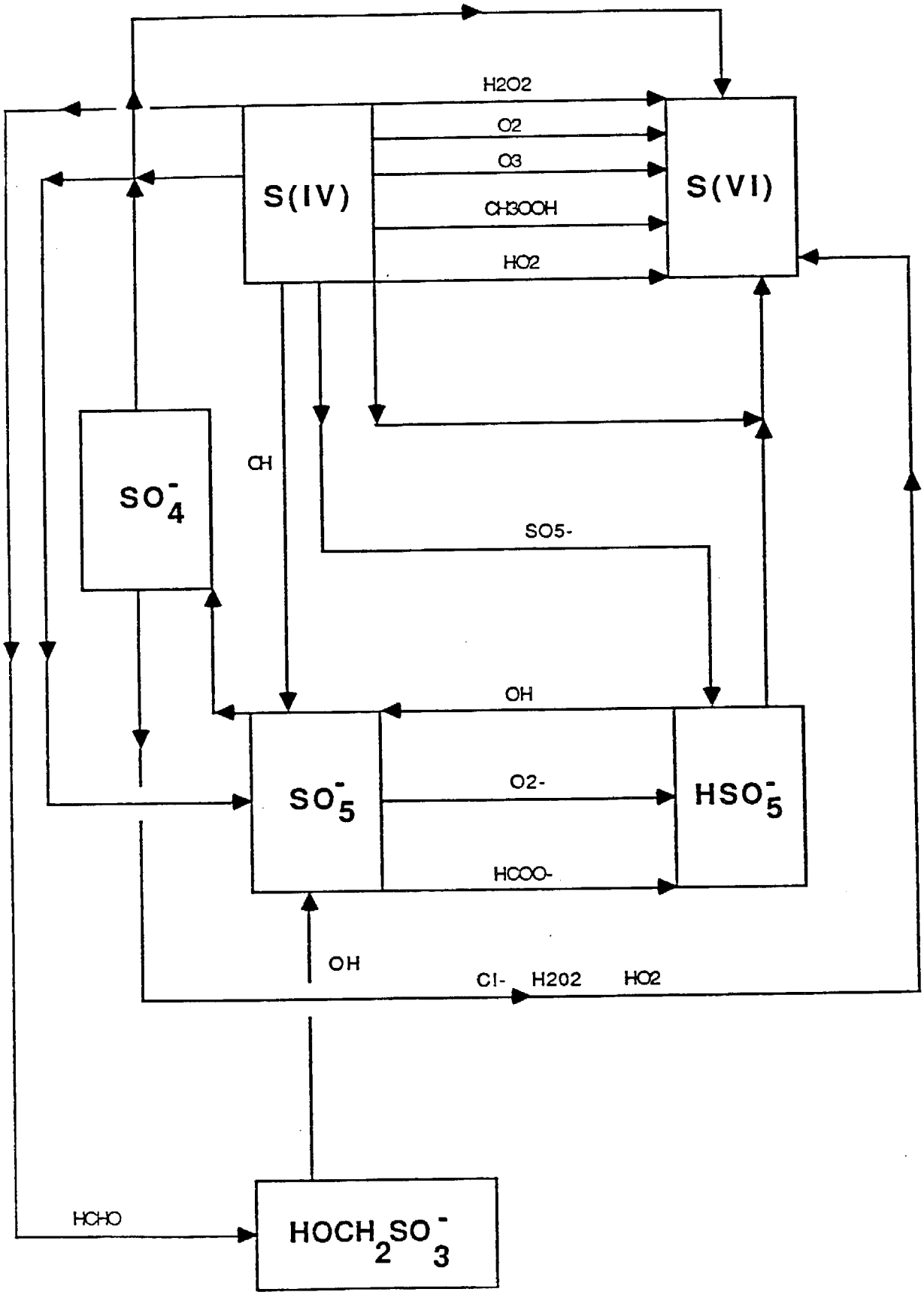

Figure 3. Main pathways for the sulfur reaction system.

TABLE 8. Dimensionless Sensitivity Coefficients for Nitrogen compounds at t=1800 s

Species	$HNO_3(aq)^a$		$PAN(aq)^b$		$NO(aq)^c$		$NO_2(aq)^d$	
	React.	Sens.Coef.	React.	Sens.Coef.	React.	Sens.Coef.	React.	Sens.Coef.
	44	-0.178(-3)[e]	62	-0.204(-4)	35	0.785(-6)	44	0.260(-2)
	62	0.215(-4)	98	-0.324(-6)	36	0.576(-6)	38	0.178(-3)
	73	-0.168(-5)	73	0.191(-6)	33	-0.183(-6)	104	-0.618(-4)
	40	0.772(-6)			73	-0.152(-6)	73	-0.517(-4)
	46	0.218(-6)			38	-0.209(-7)	42	0.482(-5)
	103	0.128(-6)					37	0.234(-5)

[a] Dimensionless sensitivity coefficient for reaction i with reaction constant K_i:

$$\frac{\partial \ln[HNO_3(aq)]}{\partial \ln K_i}$$

[b] Dimensionless sensitivity coefficient for reaction i with reaction constant K_i:

$$\frac{\partial \ln[PAN(aq)]}{\partial \ln K_i}$$

[c] Dimensionless sensitivity coefficient for reaction i with reaction constant K_i:

$$\frac{\partial \ln[NO(aq)]}{\partial \ln K_i}$$

[e] Dimensionless sensitivity coefficient for reaction i with reaction constant K_i:

$$\frac{\partial \ln[NO_2(aq)]}{\partial \ln K_i}$$

[e] Read -0.178(-3) as -0.178×10^{-3}.

concentration under any circumstances. The dominant pathway for determining the aqueous-phase HNO_3 concentration is scavenging of nitric acid from the gas phase.

In the present mechanism (Table 3) there are two aqueous-phase reactions of PAN, its decomposition to NO_3^- (reaction 62) and the oxidation of S(IV) by PAN (reaction 98). Both reactions are found to be very slow and therefore do not influence the PAN(aq) concentration (Table 8). The rate of consumption of PAN by these reactions is about 0.004%/hr.

The results in table 8 show that there is no reaction influencing NO(aq), which is just in Henry's law equilibrium with NO(g).

NO_2 also does not play an important role in the aqueous-phase chemistry (Table 8). The production of NO_2 by NO_3^- photolysis (reaction 44) occurs at about 0.5% NO_2/hr. Reactions that consume NO_2 are also slow because of the low NO_2 solubility in the aqueous phase. The main one is the reaction with S(IV):

$$2NO_2 + HSO_3^- \xrightarrow{H_2O} 3H^+ + 2NO_2^- + SO_4^{2-} \qquad (react.\ 104)$$

which consumes NO_2 at an average rate of 0.02%/hr.

NO_3 is the only highly reactive nitrogen containing species in the aqueous phase. It is consumed rapidly by its reaction with Cl^-:

$$NO_3 + Cl^- \longrightarrow NO_3^- + Cl \qquad (react.\ 49)$$

Additional reactions that consume NO_3 are those with HO_2 (reactions 46 and 47), with H_2O_2 (reaction 48) and with HSO_3^- (reaction 103). The lifetime (time for 99.9 % depletion) of NO_3 in our simulation was in the order of a few minutes.

NO_3 aqueous-phase chemistry may become much more important during the night and under the appropriate conditionsNO_3 can constitute a relatively significant aqueous-phase source of NO_3^- [Chameides, 1986].

An important feature of HNO_2 is that as the cloudwater pH decreases, its solubility also decreases and it is transferred from the aqueous to the gas phase. Thus the reactions that influence the HNO_2(aq) concentration are both those that involve HNO_2 and those that influence the cloudwater pH, such as reactions 73, 78 and 7. The main reaction involving HNO_2 is under the present conditions its attack by OH:

$$NO_2^- + OH \longrightarrow NO_2 + OH^- \qquad (react.\ 38)$$

which consumes HNO_2 at an average rate of 0.9%/hr. Hence the resulting change of [HNO_2(aq)] is small (the corresponding sensitivity coefficient is -0.02). Other slightly important reactions for HNO_2 include reaction 104, which is the main aqueous-phase source of HNO_2, and reaction 40.

Formaldehyde and Formic Acid Chemistry

The main aqueous-phase reaction involving organic species is the attack of OH on the diole:

$$H_2C(OH)_2 + OH \xrightarrow{O_2} HCOOH + HO_2 + H_2O \qquad (react.\ 50)$$

This reaction consumes 12% HCHO /hr and therefore we expect a small decrease in the concentration of HCHO(g) because of the presence of the cloud. The main aqueous-phase source of formaldehyde is the attack of OH on CH_3OH:

$$CH_3OH + OH \longrightarrow HCHO + HO_2 + H_2O \qquad (react.\ 67)$$

but this source is more than an order of magnitude less important for HCHO than reaction 50 (Table 9). An additional small sink for HCHO is reaction 106, while some sources of HCHO that under different conditions may play a small role are the reaction of CH_3OOH with OH (reaction 70), the photolysis of CH_3OOH (reaction 65), and the reaction of CH_3OH with SO_4^- (reaction 102).

TABLE 9. Dimensionless Sensitivity Coefficients for HCHO(aq)[a]

Time	100 sec		400 sec		800 sec		1800 sec	
	React.	Sens.Coef.	React.	Sens.Coef.	React.	Sens.Coef.	React.	Sens.Coef.
	50	-0.243(-1)[b]	50	-0.357(-1)	50	-0.429(-1)	50	-0.559(-1)
	13	-0.417(-2)	13	-0.531(-2)	13	-0.628(-2)	13	-0.684(-2)
	67	0.558(-3)	67	0.857(-3)	67	0.103(-2)	67	0.134(-2)
	106	-0.381(-4)	106	-0.541(-4)	106	-0.627(-4)	106	-0.761(-4)
	70	0.321(-4)	70	0.467(-4)	70	0.561(-4)	70	0.732(-4)
	102	0.297(-5)	102	0.351(-5)	102	0.375(-5)	65	0.779(-5)

[a] Dimensionless sensitivity coefficient for reaction i with reaction constant K_i:

$$\frac{\partial \ln[\mathrm{HCHO(aq)}]}{\partial \ln K_i}$$

[b] Read -0.243(-1) as -0.243×10^{-1}.

Reaction 50 is primarily responsible for the production of formic acid in the aqueous-phase. The average rate of this reaction for the present pH range is 250% HCOOH/hr and therefore the presence of the cloud enhances the HCOOH(g) concentration. Reaction 73 causes a decrease of the pH and therefore results in a decrease of [HCOOH(aq)] (Table 10). In our case the effects of reaction 50 are stronger but the sensitivity coefficient of reaction 73 is of the same order of magnitude as that of reaction 50. Hence in other cases (high SO_2(g) concentration) the effects of reaction 73 may dominate. As in the previous cases the [HCOOH(aq)] is influenced by the pH determining reactions such as 74, 7, 78, 72 etc.

The main aqueous-phase sink of HCOOH is its reaction with OH(aq):

$$HCOO^- + OH \xrightarrow{O_2} CO_2 + HO_2 + OH^- \qquad (react.\ 57)$$

and

$$HCOOH + OH \xrightarrow{O_2} CO_2 + HO_2 + H_2O \qquad (react.\ 52)$$

Under the conditions considered here these reactions are two orders of magnitude less significant than reaction 50. The above two reactions can be considered as competitive with reaction 50 as they both consume OH. The ratio of the rate of reaction 50 (R50) over the sum of the rates of reactions 52 and 57 (R52+R57) can be expressed as a function of the pH and the ratio of the gas-phase pressures (p_{HCHO}/p_{HCOOH}) for a constant temperature. The ratio of the gas-phase pressures is under ordinary conditions (before cloud formation) higher than 10 and for all the pH of interest we expect a net production of formic acid.

Some additional sinks of formic acid include its reactions with SO_5^- (reaction 80) and SO_4^- (reaction 95). The remainder of the aqueous-phase sinks of HCOOH appear to be negligible.

Table 10. Dimensionless Sensitivity Coefficients for HCOOH(aq)[a]

Time	100 sec		400 sec		800 sec		1800 sec	
	React.	Sens.Coef.	React.	Sens.Coef.	React.	Sens.Coef.	React.	Sens.Coef.
	50	0.495	50	0.589	50	0.629	50	0.682
	73	-0.829(-1)[b]	73	-0.174	73	-0.170	73	-0.123
	57	-0.425(-1)	57	-0.484(-1)	13	0.637(-1)	13	0.914(-1)
	13	0.361(-1)	13	0.425(-1)	57	-0.502(-1)	57	-0.515(-1)
	78	-0.194(-2)	7	-0.316(-2)	74	-0.367(-2)	74	-0.417(-2)
	7	-0.120(-2)	78	-0.245(-2)	7	-0.355(-2)	7	-0.339(-2)
	52	-0.795(-3)	74	-0.119(-2)	78	-0.210(-2)	78	-0.167(-2)
	72	-0.572(-3)	52	-0.109(-2)	52	-0.126(-2)	52	-0.158(-2)
	81	-0.411(-3)	82	-0.873(-3)	82	-0.872(-3)	76	-0.827(-3)
	82	-0.393(-3)	72	-0.723(-3)	76	-0.811(-3)	5	0.707(-3)
	74	-0.391(-3)	76	-0.683(-3)	5	0.616(-3)	82	-0.596(-3)
	76	-0.260(-3)	5	0.467(-3)	72	-0.613(-3)	67	0.519(-3)
	95	-0.221(-3)	18	-0.376(-3)	18	-0.439(-3)	72	-0.466(-3)
	67	0.212(-3)	67	0.315(-3)	67	0.385(-3)	18	-0.442(-3)
	87	-0.196(-3)	80	-0.298(-3)	80	-0.354(-3)	80	-0.404(-3)
	80	-0.185(-3)	81	-0.284(-3)	20	0.326(-3)	20	0.338(-3)
	96	-0.148(-3)	20	0.270(-3)	99	-0.263(-3)	99	-0.291(-3)
	18	-0.138(-3)	95	-0.214(-3)	95	-0.202(-3)	95	-0.178(-3)

[a] Dimensionless sensitivity coefficient for reaction i with reaction constant K_i:

$$\frac{\partial \ln[\mathrm{HCOOH(aq)}]}{\partial \ln K_i}$$

[b] Read -0.829(-1) as -0.829×10^{-1}.

Other Organic Species

The main sink for methanol, CH_3OH, is its transformation to formaldehyde by OH (reaction 67), which occurs at a rate of 0.09% CH_3OH/hr. Since methanol is not produced in the aqueous-phase, one expects a very small decrease in the $CH_3OH(g)$ because of the cloud's presence.

A moderate sink for CH_3OOH is the oxidation of S(IV) via reaction 99. The average rate of this reaction is 0.2% CH_3OOH/hr, a rate that is not particularly important for CH_3OOH under the present circumstances but may be influential in case of larger S(IV) concentrations. The main source for CH_3OOH is the reaction of CH_3O_2 with O_2^-:

$$CH_3O_2 + O_2^- \xrightarrow{H_2O} CH_3OOH + O_2 + OH^- \qquad (react.\ 64)$$

The main sink of CH_3O_2 is reaction 64, with an average rate of 0.5% CH_3O_2/hr. Its main aqueous phase source is its production by the attack of OH on CH_3OOH:

$$CH_3OOH + OH \longrightarrow CH_3O_2 + H_2O \qquad (react.66)$$

As both these reactions are of minor importance (sensitivity coefficients less than 0.006) we do not expect a substantial change in $CH_3O_2(g)$ concentration because of the aqueous-phase CH_3O_2 sinks.

The only reaction of $CH_3C(O)OOH$ included in the mechanism is the oxidation of HSO_3^-:

$$HSO_3^- + CH_3C(O)OOH \longrightarrow SO_4^{2-} + H^+ + \text{prd.} \qquad (react.\ 100)$$

This reaction occurs with a rate of 0.7% $CH_3C(O)OOH$/hr and does not play a major role in the reaction system.

The carbonate radical ion is a highly reactive species. It is produced by the rapid reaction of HCO_3^- with O_2^- (reaction 18) the occurence of which, as we noted, is still

a subject of discussion. The main sinks are first the reaction of CO_3^- with hydrogen peroxide (reaction 20) and second its reaction with O_2^- (reaction 19).

Oxygen and Hydrogen Chemistry

Ozone is not produced at all in the aqueous-phase but is consumed via 12 different reactions. Because of the small solubility of ozone most of these reactions are too slow to influence $[O_3(aq)]$ (Table 11). Its main aqueous-phase sink is its reaction with O_2^-:

$$O_3 + O_2^- \xrightarrow{H_2O} OH + 2O_2 + OH^- \qquad (react.\ 13)$$

Although the rate of this reaction is just 0.03 % O_3/hr, because of the small ozone solubility this rate results in a lifetime of $O_3(aq)$ of the order of 1 s. The oxidation of S(IV) via reaction 72 decreases as pH decreases and therefore is an order of magnitude less important for ozone than reaction 13.

There are 16 reactions producing the hydroxyl radical, OH, and 19 consuming it. Its main sink is the reaction with the diole $H_2C(OH)_2$ (reaction 50). Other sinks are the reactions with hydrogen peroxide (reaction 5), with $HCOO^-$ (reaction 57) and with HSO_3^- (reaction 76). Moderate sinks are the reactions of OH with methanol (reaction 67) and HO_2 (reactions 3 and 4). The main aqueous-phase sources of OH are the reaction of O_2^- with ozone (reaction 13) and the photolysis of hydrogen peroxide (reaction 1). Secondary sources are the photolysis of NO_3^- (reaction 44) and the oxidation of S(IV) by HO_2 (reaction 101).

HO_2 is another highly reactive radical produced by 29 reactions and consumed by 22 reactions. The main aqueous-phase sources of HO_2 include reactions 50, 5, 20, 57, 67 and 29. Main sinks are reactions 13, 7, 18 and 78. Secondary sinks are reactions 3, 4 and 6.

Chlorine Chemistry

TABLE 11. Dimensionless Sensitivity Coefficients for $O_3(aq)$[a]

Time	100 sec		400 sec		800 sec		1800 sec	
	React.	Sens.Coef.	React.	Sens.Coef.	React.	Sens.Coef.	React.	Sens.Coef.
	13	-0.153(-3)[b]	13	-0.218(-3)	13	-0.251(-3)	13	-0.307(-3)
	72	-0.697(-5)	72	-0.140(-4)	72	-0.189(-4)	72	-0.245(-4)
	73	0.525(-6)	73	0.192(-5)	73	0.316(-5)	7	-0.216(-4)
	16	-0.130(-6)	16	-0.507(-6)	16	-0.930(-6)	16	-0.173(-5)
							11	-0.109(-6)

[a] Dimensionless sensitivity coefficient for reaction i with reaction constant K_i:

$$\frac{\partial \ln[O_3(aq)]}{\partial \ln K_i}$$

[b] Read -0.153(-3) as -0.153×10^{-3}.

Chlorine chemistry is characterised by various equilibria. First an equilibrium exists between two forms of radical chlorine [Jayson et al., 1973]:

$$Cl_2^- \rightleftharpoons Cl + Cl^-$$

Reactions 21 and 22 result in an equilibrium between Cl^- and $ClOH^-$:

$$Cl^- + OH \rightleftharpoons ClOH^-$$

Because both reactions are quite fast the equilibrium is established in our simulation in about 1s. Reactions 23 and 24 are relatively fast also and reach equilibrium after the first two minutes of simulation.

Using the above aqueous-phase equilibria the reactions between Cl_2^- and HO_2 and O_2^- :

$$HO_2 + Cl_2^- \longrightarrow 2Cl^- + O_2 + H^+ \qquad (react.\ 25)$$

$$O_2^- + Cl_2^- \longrightarrow 2Cl^- + O_2 \qquad (react.\ 26)$$

can be combined, the intermediate chlorine compounds can be eliminated and the net result is that reactions 25 and 26 constitute an alternate pathway for the reactions of HO_2 and O_2^- with OH:

$$HO_2 + OH \longrightarrow H_2O + O_2 \qquad (react.\ 3)$$

$$O_2^- + OH \longrightarrow OH^- + O_2 \qquad (react.\ 4)$$

Comparison of the rates of the above reactions at 298 K results in the following:

$$r_{25} = 5.3\ 10^{13}[Cl^-]^2[H^+]r_3 \qquad M/s$$

and

$$r_{26} = 8.3\ 10^{12}[Cl^-]^2[H^+]r_4 \qquad M/s$$

Thus the relative importance of these pairs of pathways depends on the pH and the concentration of Cl^-. For our simulation the maximum value of $[H^+]$ is 200 μM and that of $[Cl^-]$ 60 μM. For these values the pathway starting with reaction 25 can be one order of magnitude faster than reaction 3, and the pathway starting with reaction 26 one-half an order of magnitude faster than reaction 4. Reactions 3 and 4 are moderate sinks of HO_2 and so reactions 25 and 26, even if sometimes faster, are still of minor importance. The sensitivity coefficient of H_2O_2 to the reaction 25 after 1800 s is just -0.3×10^{-3}.

Using the same procedure as above the reaction of Cl with HO_2:

$$HO_2 + Cl \longrightarrow Cl^- + O_2 + H^+ \qquad (react.\ 27)$$

can be viewed as one more alternate pathway for reaction 3. The rate of reaction 27 in our case can be the most comparable to reaction 3 and therefore it is unimportant for HO_2.

The reaction between H_2O_2 and Cl_2^- :

$$H_2O_2 + Cl_2^- \longrightarrow 2Cl^- + HO_2 + H^+ \qquad (react.\ 28)$$

is an alternate pathway for the reaction of H_2O_2 and OH (reaction 5). The maximum rate of this pathway in our case is one order of magnitude less than the rate of the direct reaction 5 and therefore it is of minor importance for H_2O_2. The sensitivity coefficient of H_2O_2 to this reaction after 1800 s is -0.4×10^{-3}.

Another alternate pathway for reaction 5 is the reaction of H_2O_2 with Cl:

$$H_2O_2 + Cl \longrightarrow Cl^- + HO_2 + H^+ \qquad (react.\ 29)$$

Kinetic calculations show that the rate of this pathway can be at most 8 times faster than the direct pathway 5 and therefore reaction 29 is a relatively important sink of hydrogen peroxide even if it is less influential than reaction 5 (Table 5).

The oxidation reaction of S(IV) by Cl_2^-:

$$HSO_3^- + Cl_2^- \xrightarrow{O_2} SO_5^- + 2Cl^- + H^+ \qquad (react.\ 109)$$

constitutes an additional pathway for the oxidation of S(IV) by OH (reactions 75 and 76). The kinetic calculations show that the rate of this reaction can be at most comparable to the rate of reaction 76 and therefore reaction 109 is only slightly important for S(IV).

The reactions of Cl^- with NO_3 (reaction 49) and SO_4^- (reaction 96) have been already been discussed. Other reactions of chlorine species like reactions 30, 42 and 61 are quite slow.

Importance of Initial Gas and Aqueous-Phase Concentrations

The sensitivity coefficients for all the species with respect to all the initial gas phase concentrations as well as the initial aqueous-phase concentrations of S(VI), N(V), HCl and NH_3 have been calculated. This calculation serves a dual purpose. First it demonstrates quantitatively the dependence of the whole reaction process on the initial conditions used in this study and it provides further insight to the interaction between the two phases.

Effects on the S(IV) to S(VI) conversion

The major variables among the initial conditions influencing the sulfate concentration are the gas-phase concentrations of $SO_2(g)$ and $H_2O_2(g)$ (Table 12). The calculated dimensionless sensitivity coefficients are about 0.6. This result has an important consequence on the control of cloud acidity. Based on the calculated sensitivity coefficient if ambient levels of $SO_2(g)$ are decreased by 10%, the sulfate concentration in cloudwater will approximately decrease by 6%. This important feature of the reaction system can

TABLE 12

Dimensionless Sensitivity Coefficients for S(VI)(aq), N(V)(aq) and HSO_5^- to initial conditions

Time	100 sec		400 sec		800 sec		1200 sec	
	Species	Sens.Coef.	Species	Sens.Coef.	Species	Sens.Coef.	Species	Sens.Coef.
S(VI)(aq) [a]								
	$[S(VI)]_o$ [b]	0.579	$(SO_2)_o$ [c]	0.664	$(SO_2)_o$	0.681	$(SO_2)_o$	0.672
	$(SO_2)_o$	0.405	$(H_2O_2)_o$	0.632	$(H_2O_2)_o$	0.638	$(H_2O_2)_o$	0.626
	$(H_2O_2)_o$	0.381	$[S(VI)]_o$	0.287	$[S(VI)]_o$	0.189	$[S(VI)]_o$	0.159
	$(HO_2)_o$	0.027	$(NH_3)_o$	0.029	$(HO_2)_o$	0.014	$(HO_2)_o$	0.013
	$(O_3)_o$	0.010	$(HNO_3)_o$	-0.020	$(OH)_o$	0.010	$(OH)_o$	0.009
	$(NH_3)_o$	0.007	$(HCl)_o$	-0.019	$(NH_3)_o$	0.006	$(O_3)_o$	0.002
	$(HNO_3)_o$	-0.007	$(HO_2)_o$	0.018	$(HNO_3)_o$	-0.003	$(NH_3)_o$	0.002
	$(HCl)_o$	-0.006	$(OH)_o$	0.010	$(O_3)_o$	0.003	$(HNO_3)_o$	-0.001
	$(OH)_o$	0.005	$(O_3)_o$	0.006	$(HCl)_o$	-0.002	$(HCl)_o$	-0.001
	$(HCHO)_o$	-0.004	$(HCHO)_o$	-0.002	$(HCHO)_o$	-0.001		
	$[HCl]_o$	-0.002	$[HCl]_o$	-0.001				
N(V)(aq) [a]								
	$(HNO_3)_o$	0.966	$(HNO_3)_o$	0.965	$(HNO_3)_o$	0.965	$(HNO_3)_o$	0.965
	$[N(V)_o$	0.034	$[N(V)_o$	0.034	$[N(V)_o$	0.034	$[N(V)_o$	0.034
							$(PAN)_o$	0.131(-4)
$HSO_5^-(aq)$ [a]								
	$(NH_3)_o$	1.050	$(HO_2)_o$	1.490	$(HO_2)_o$	1.378	$(HO_2)_o$	1.322
	$(HNO_3)_o$	-0.970	$(NH_3)_o$	1.066	$(NH_3)_o$	1.067	$(NH_3)_o$	1.061
	$(HCl)_o$	-0.898	$(HNO_3)_o$	-0.984	$(HNO_3)_o$	-0.986	$(HNO_3)_o$	-0.980
	$[S(VI)]_o$	-0.652	$(HCl)_o$	-0.920	$(HCl)_o$	-0.922	$(HCl)_o$	-0.916
	$(SO_2)_o$	0.464	$[S(VI)]_o$	-0.588	$(OH)_o$	0.674	$(OH)_o$	0.697
	$[HCl]_o$	-0.341	$(HCHO)_o$	-0.323	$[S(VI)]_o$	-0.565	$[S(VI)]_o$	-0.552
	$(HCHO)_o$	-0.331	$[HCl]_o$	-0.308	$(HCHO)_o$	-0.327	$(SO_2)_o$	-0.356
	$(HO_2)_o$	0.182	$(OH)_o$	0.301	$[HCl]_o$	-0.296	$(HCHO)_o$	-0.330
	$(O_3)_o$	0.153	$(O_3)_o$	0.186	$(O_3)_o$	0.200	$[HCl]_o$	-0.289
	$(H_2O_2)_o$	-0.129	$(SO_2)_o$	0.177	$(SO_2)_o$	-0.146	$(O_3)_o$	0.207
	$[N(V)_o$	-0.082	$(H_2O_2)_o$	-0.149	$(H_2O_2)_o$	-0.131	$(H_2O_2)_o$	-0.090
	$[NH_3]_o$	0.082	$[N(V)_o$	-0.074	$[N(V)_o$	-0.071	$[N(V)_o$	-0.069
	$(OH)_o$	0.041	$[NH_3]_o$	0.074	$[NH_3]_o$	0.071	$[NH_3]_o$	0.069

[a] Dimensionless sensitivity coefficient of species I (concentration c_i) to the initial concentration of species J, c_{jo}:

$$\frac{\partial \ln c_i}{\partial \ln c_{jo}}$$

[b] $[I]_o$ is the initial aqueous-phase concentration of species I.

[c] $(I)_o$ is the initial gas-phase concentration of species I.

be explained considering the complicated interaction among the S(IV), S(VI) concentrations and the cloudwater pH [Chameides, 1982].

Species that directly affect the cloudwater pH determine to a large extent the [S(IV)(aq)] and therefore influence the sulfate formation. They include gases like $NH_3(g)$, HNO_3, HCl, and species that initially exist in cloudwater like SO_4^{2-}, Cl^-, NO_3^- and NH_4^+ (Table 14).

Additional species whose initial concentrations influence the sulfate formation include those that oxidize S(IV), like OH and O_3, and species that produce $H_2O_2(aq)$, like HO_2. Formaldehyde is of some influence also as its reaction in the aqueous-phase with OH constitutes a major sink of OH(aq) and at the same time a major source of $HO_2(aq)$.

Nitrogen Chemistry

The negligibly small sensitivity coefficients for all other species for nitrate (Table 12) show that the only pathway for nitric acid cloud acidity is the scavenging of the gaseous and aerosol phase nitric acid.

Formic acid and Formaldehyde chemistry

The conversion of formaldehyde to formic acid is relatively sensitive to the OH(g) concentration, to species that affect the OH(aq) concentration like ozone (because of reaction 13), and finally to species that influence the cloudwater pH (Table 13).

The concentration of formic acid in the aqueous-phase is much more sensitive to the various gas-phase concentrations than [HCHO(aq)] is. The hydroxyl radical concentration is once more of primary importance here with a sensitivity coefficient of about 0.6. As the aqueous-phase solubility of HCOOH is a strong function of pH, the influence of species like ammonia and nitric acid is important to [HCOOH(aq)]. The sensitivity of the HCOOH(aq) concentration to the HCOOH(g) concentration decreases

TABLE 13
Sensitivity Coefficients for HCHO(aq) and HCOOH(aq) to initial conditions

Time	100 sec		400 sec		800 sec		1200 sec	
	Species	Sens.Coef.	Species	Sens.Coef.	Species	Sens.Coef.	Species	Sens.Coef.
HCHO(aq) [a]								
	$(HCHO)_o$ [b]	0.998	$(HCHO)_o$	0.996	$(HCHO)_o$	0.993	$(HCHO)_o$	0.990
	$(O_3)_o$	-0.016	$(OH)_o$	-0.022	$(OH)_o$	-0.040	$(OH)_o$	-0.045
	$(OH)_o$	-0.011	$(O_3)_o$	-0.016	$(O_3)_o$	-0.022	$(O_3)_o$	-0.024
	$(HNO_3)_o$	0.005	$(NH_3)_o$	-0.009	$(NH_3)_o$	-0.011	$(NH_3)_o$	-0.012
	$(HCl)_o$	0.005	$(HNO_3)_o$	0.008	$(HNO_3)_o$	0.010	$(HNO_3)_o$	0.011
	$(NH_3)_o$	-0.005	$(HCl)_o$	0.008	$(HCl)_o$	0.010	$(HCl)_o$	0.011
	$(SO_2)_o$	0.004	$(SO_2)_o$	0.006	$(SO_2)_o$	0.008	$(SO_2)_o$	0.009
	$(H_2O_2)_o$	0.002	$(H_2O_2)_o$	0.004	$(H_2O_2)_o$	0.005	$(H_2O_2)_o$	0.005
	$[S(VI)]_o$ [c]	0.002	$[S(VI)]_o$	0.003	$[S(VI)]_o$	0.003	$[S(VI)]_o$	0.003
					$(CH_3OH)_o$	0.001	$(CH_3OH)_o$	0.001
HCOOH(aq) [a]								
	$(NH_3)_o$	0.623	$(NH_3)_o$	0.501	$(OH)_o$	0.601	$(OH)_o$	0.627
	$(HNO_3)_o$	-0.578	$(HCOOH)_o$	0.466	$(HCOOH)_o$	0.414	$(HCOOH)_o$	0.388
	$(HCOOH)_o$	0.569	$(HNO_3)_o$	-0.461	$(NH_3)_o$	0.412	$(O_3)_o$	0.385
	$(HCl)_o$	-0.530	$(HCl)_o$	-0.427	$(HNO_3)_o$	-0.377	$(NH_3)_o$	0.379
	$(O_3)_o$	0.248	$(OH)_o$	0.376	$(O_3)_o$	0.369	$(SO_2)_o$	-0.377
	$(HCHO)_o$	0.211	$(O_3)_o$	0.335	$(SO_2)_o$	-0.364	$(HNO_3)_o$	-0.346
	$(SO_2)_o$	-0.180	$(SO_2)_o$	-0.322	$(HCl)_o$	-0.353	$(HCl)_o$	-0.326
	$[S(VI)]_o$	-0.168	$(H_2O_2)_o$	-0.274	$(H_2O_2)_o$	-0.295	$(H_2O_2)_o$	-0.293
	$(H_2O_2)_o$	-0.143	$(HCHO)_o$	0.247	$(HCHO)_o$	0.259	$(HCHO)_o$	0.263
	$(OH)_o$	-0.095	$[S(VI)]_o$	-0.134	$[S(VI)]_o$	-0.110	$[S(VI)]_o$	-0.101
	$[HCl]_o$	-0.085	$[HCl]_o$	-0.068	$[HCl]_o$	-0.057	$[HCl]_o$	-0.052
	$[NH_3]_o$	0.021	$[NH_3]_o$	0.017	$[NH_3]_o$	0.014	$[NH_3]_o$	0.014
	$[N(V)_o$	-0.021	$[N(V)_o$	-0.017	$[N(V)_o$	-0.014	$[N(V)_o$	-0.014
	$(CH_3OH)_o$	-0.005	$(CH_3OH)_o$	-0.006	$(CH_3OH)_o$	-0.007	$(CH_3OH)_o$	-0.008
	$(HO_2)_o$	-0.003	$(HO_2)_o$	-0.004	$(HO_2)_o$	-0.004	$(HO_2)_o$	-0.004

[a] Dimensionless sensitivity coefficient of species I (concentration c_i) to the initial concentration of species J, c_{jo}:

$$\frac{\partial \ln c_i}{\partial \ln c_{jo}}$$

[b] $(I)_o$ is the initial gas-phase concentration of species I.

[c] $[I]_o$ is the initial aqueous-phase concentration of species I.

rapidly so that one expects that after sufficient time the aqueous-phase concentration will be almost independent of the initial gas-phase concentration of HCOOH (Table 13).

HSO_5^-

Since the fate of HSO_5^- is a strong function of pH, the HSO_5^-(aq) concentration is found to depend on the concentrations of ammonia, nitric acid, etc. Decrease of the pH, or increase of HNO_3(g) and HCl(g) results in a dramatic drop of the HSO_5^- aqueous-phase concentration (Table 12).

Liquid Water Content w_L

The liquid water content is one of the important input parameters of a cloud-chemistry model [Chameides, 1982]. Typical values of w_L are $10^{-7} - 10^{-6}$ (l water/ l air) for clouds and $5 \times 10^{-8} - 5 \times 10^{-7}$ (l water/ l air) for fogs [Pruppacher, 1980]. In our simulation a value of 4×10^{-7} (l water/ l air) has been used.

In order to investigate the importance of w_L on the whole system we have calculated the sensitivity coefficients of all species in both phases with respect to w_L. We shall restrict ourselves here to the importance of w_L on the sulfate and formic acid formation.

Since a change of w_L represents a change of the amount of the aqueous-phase, it is crucial to calculate not only the sensitivity of the S(IV)(aq) and S(VI)(aq) concentrations to w_L but also to examine how the total sulfate, $S(VI)_{tot}$ and the total $S(IV)_{tot}$ in the system vary with w_L (Table 14).

Increase of the cloud liquid water content has as its main effect the dissolution of larger quantities of SO_2(g) in the aqueous-phase and therefore increase of the S(IV) amount available to be oxidized. Thus the total sulfate increases with increasing w_L and the total S(IV) actually decreases. But as increased w_L results in higher dilution,

TABLE 14. Dimensionless Sensitivity Coefficients to the Water Liquid Content w_L [a]

Species	400 sec	800 sec	1200 sec	3600 sec
S(IV)(aq)	0.707	0.607	0.544	0.435
S(VI)(aq)	-0.698	-0.748	-0.764	-0.874
$S(IV)_{tot}$	-0.126	-0.187	-0.232	-0.361
$S(VI)_{tot}$	0.302	0.252	0.236	0.126
HCOOH(g)	0.052	0.101	0.127	0.231
HSO_5^-(aq)	0.994	0.896	0.861	0.841

[a] Dimensionless sensitivity coefficient for species I with concentration c_i:

$$\frac{\partial \ln c_i}{\partial \ln w_l}$$

the concentration of S(VI) is found to decrease, even if the global amount of sulfate increases. This higher dilution results in a pH increase and increase of the S(IV)(aq) concentration. Summarizing, an increase of w_L results in an increase of the S(IV)(aq) concentration but decrease of the total amount of S(IV), decrease of the sulfate concentration but increase of the total sulfate amount and finally to a pH increase (sensitivity coefficient for the H^+ concentration is -0.7).

The above results demonstrate the importance of the liquid water content. Using the above sensitivity coefficients as an approximation we can extrapolate and predict that for an increase of w_L from 4×10^{-7} to 1.3×10^{-6} (l water/ l air), a change that is possible inside the same cloud [Pruppacher, 1980], the sulfate produced after one hour will increase by 30%.

Since the increase of the liquid water content results in an important pH increase, it influences all the pH-sensitive species. For example, $[HSO_5^-]$ will increase rapidly (Table 14) with increasing w_L.

The production of formic acid is enhanced by the increase of the liquid water content (Table 14) as the sensitivity coefficient of HCOOH(g) to w_L is 0.23 after the first hour. This increase can be explained by the pH increase and the subsequent increase of the aqueous-phase OH production rate.

Accomodation Coefficient and Droplet Radius

The sensitivity coefficients of some key species with respect to the accomodation coefficient a_w and the droplet radius α are shown in table 15. The same accomodation coefficient for all the species has been used in the above calculation.

Our results are consistent with the predictions of Jacob [1986], Schwartz [1984] and Chameides [1984]. When a_w is in the order of 0.01, as in our case, the interfacial mass transport does not substantially influence the concentrations of most species in

TABLE 15. Dimensionless Sensitivity Coefficients to a_w and the Radius α

Species	100 sec	400 sec	1200 sec	3600 sec
Accomodation coefficient a_w [a]				
S(VI)(aq)	0.007	0.005	0.003	0.002
H_2O_2(aq)	0.003	0.004	0.006	0.008
OH(aq)	0.063	0.081	0.101	0.187
HO_2(aq)	0.022	0.014	0.010	0.014
HCOOH(g)	0.005	0.013	0.014	0.018
Droplet radius α [b]				
S(VI)(aq)	-0.010	-0.008	-0.005	-0.003
H_2O_2(aq)	-0.004	-0.006	-0.010	-0.012
OH(aq)	-0.095	-0.122	-0.154	-0.281
HO_2(aq)	-0.033	-0.021	-0.015	-0.020
HCOOH(g)	-0.008	-0.021	-0.022	-0.028

[a] Dimensionless sensitivity coefficient of species I with concentration c_i:

$$\frac{\partial \ln c_i}{\partial \ln a_w}$$

[b] Dimensionless sensitivity coefficient of species I with concentration c_i:

$$\frac{\partial \ln c_i}{\partial \ln \alpha}$$

our reaction system. The increase of a_w has as its main effect the acceleration of the transfer of the OH and HO_2 radicals from the gas to the aqueous-phase. Therefore the production of HCOOH and H_2O_2 increases in the aqueous phase. The positive contribution of this increase to the conversion of S(IV) to S(VI) appears to be very small for this range of a_w. Species like HCHO(aq), HNO_3(aq), NH_3(aq) that for the present a_w reach Henry's law equilibria in a few minutes [Jacob, 1985], are not influenced at all by a_w, at least after this equilibration period.

Increase of cloud droplet radius has exactly the same effects as decrease of the accomodation coefficient, that is decrease of the mass-transfer rate between the gas and the aqueous-phase. The corresponding sensitivity coefficients, calculated for the present case, are larger than the coefficients for a_w and exactly the opposite phenomena are observed.

Temperature Effects

The temperature influences the reaction system in various ways. A change of temperature results in changes in the cloud water liquid content w_L, in the rate of the gas-phase reactions, in the rate of mass transport between the two phases, in the solubilities of the species in the aqueous-phase, in the rate of the reactions in the aqueous-phase etc. Our study of the temperature effects will be necessarily preliminary not only because of the restrictions of our model (w_L independent of temperature, no gas-phase reactions), but additionally because of the uncertainities on the temperature dependence of the various reaction, Henry's law, equilibria etc. constants.

We have studied four cases for different temperatures and the results after one hour of simulation are presented in table 16. A temperature decrease mainly results in the increase of the solubility of the gas-phase species in the aqueous-phase and at the same time in the decrease of the rates of the aqueous-phase reactions. As it can be

TABLE 16. Concentrations of Various Species After 1 hr for Different Temperatures

Species	298°K	283°K	273°K	263°K
pH	3.71	3.69	3.69	3.69
S(IV)(aq) (μM)	0.025	0.050	0.090	0.191
S(VI)(aq) (μM)	75.1	75.7	80.2	80.3
H_2O_2(aq) (μM)	13.5	15.6	25.1	30.7
HCOOH(aq) (μM)	0.161	0.423	0.708	1.71
SO_2(g) (mol/l)	1.31(-10)[a]	1.29(-10)	1.10(-10)	1.10(-10)
H_2O_2(g) (mol/l)	7.51(-12)	2.72(-12)	1.96(-12)	1.00(-12)
HCOOH(g) (mol/l)	1.00(-13)	1.01(-13)	1.03(-13)	1.05(-13)
$(HCOOH)_{tot}$ (mol/l)	1.64(-13)	2.70(-13)	3.86(-13)	7.89(-13)

[a] Read 1.31(-10) as 1.31×10^{-10}.

seen in table 16 these effects almost cancel each other resulting in the same pH, sulfate concentration and HCOOH(g) concentrations. Additionally the S(IV)(aq), H_2O_2(aq), HCOOH(aq) concentrations increase substantially if temperature decreases.

Condensed Mechanism

The sensitivity analysis has shown that 48 reactions in the mechanism are completely unimportant under the initial conditions studied. The corresponding dimensionless sensitivity coefficients are less than 10^{-5}. Therefore it is possible to propose a condensed mechanism consisting of the following reactions:

Oxygen-Hydrogen Chemistry: 1, 3, 4, 5, 6, 7, 13, 16.

Carbonate Chemistry: 17, 18 (if the reaction rate in table 3 is correct), 19, 20.

Chlorine Chemistry: 21, 22, 23, 24, 25, 26, 28, 29.

Nitrogen Chemistry: 38, 40, 44, 47, 49.

CH_4 Oxidation Chemistry: 50, 52, 57, 60, 61, 62, 63, 64, 66, 67, 70.

Sulfur Chemistry: 72, 73, 74, 75, 76, 77, 78, 80, 81, 82, 83, 87, 89, 90, 92, 93, 95, 96, 99, 100, 101, 104, 106, 108, 109.

The results of a simulation, for the initial conditions of table 1, using the above simplified reaction mechanism differ by only the numerical error from the results of the full mechanism of table 3. Because the above mechanism has been derived by local sensitivity analysis its validity cannot be guaranteed very far from the conditions used in this study. Even if the condensed mechanism has been tested for several additional sets of conditions (with pH$<$ 6) and the results were again within numerical error from the results of the full mechanism caution should be employed before its use for conditions very different than ours.

Comparison of the DDM with the Indirect Method

In order to check the accuracy of the results obtained using the Direct Decoupled

Method we have calculated several sensitivity coefficients using the Indirect Method. For the latter we have employed the simple one sided difference formula:

$$s_{ij} = \frac{\partial y_i}{\partial \lambda_j} \mid_{\lambda_k} \approx \frac{y_i(\lambda_j + \Delta\lambda_j;\ \lambda_k\ j \neq k) - y_i(\lambda_j;\ \lambda_k\ j \neq k)}{\Delta\lambda_j} \tag{5.1}$$

and in nondimensionalized form:

$$\bar{s}_{ij} = \frac{\lambda_j}{y_i}\frac{\partial y_i}{\partial \lambda_j} \mid_{\lambda_k} \approx \frac{1}{\delta}\ \frac{y_i(\lambda_j + \Delta\lambda_j;\ \lambda_k\ j \neq k) - y_i(\lambda_j;\ \lambda_k\ j \neq k)}{y_i(\lambda_j;\ \lambda_k\ j \neq k)} \tag{5.2}$$

where $\delta = \Delta\lambda_j/\lambda_j$.

Another alternative is the use of a centered difference formula instead of formula (5.2).

$$\bar{s}_{ij} = \frac{\lambda_j}{y_i}\frac{\partial y_i}{\partial \lambda_j} \mid_{\lambda_k} \approx \frac{1}{2\delta}\ \frac{y_i(\lambda_j + \Delta\lambda_j;\ \lambda_k\ j \neq k) - y_i(\lambda_j - \Delta\lambda_j;\ \lambda_k\ j \neq k)}{y_i(\lambda_j;\ \lambda_k\ j \neq k)} \tag{5.3}$$

One of the main disantvantages of the indirect method is that cancellation can occur in the numerator of formula (5.2). In our calculation only the first three or four digits appear free of round-off error. Hence for small δ's some of the sensitivity coefficients calculated with the indirect method are inaccurate because of the round-off error in the y_i's. If we attempt to use a larger δ the finite difference approximation becomes progressively inaccurate. We have found that in this case the indirect method gives usually unreliable results if $\bar{s}_{ij} \leq 0.001$. As some of the sensitivity coefficients are large and some small, it is impossible to compute all of them accurately with one choice of δ [Dunker, 1980]. In our calculations we have used $\delta = 0.05$ and for some small sensitivity coefficients (≤ 0.005) $\delta = 0.5$.

Results obtained by both methods are shown in table 17. The results appear to be in very good agreement. One main advantage of the DDM is that the sensitivity coefficients are calculated exactly. If T is the time required for the execution of one simulation the calculation of our 150 sensitivity coefficients costs 151 T using the Indirect Method with one sided differences and 300 T using the numerically better centered

TABLE 17. Comparison of Sensitivity Analysis Methods

Time	100 sec		400 sec		1100 sec	
	DDM	Indirect	DDM	Indirect	DDM	Indirect
Reaction 73 [a]						
S(IV) (aq)	-0.211	-0.210	-0.518	-0.517	-0.723	-0.693
S(VI) (aq)	0.361	0.353	0.522	0.543	0.463	0.446
N(III) (aq)	-0.125	-0.127	-0.258	-0.245	-0.247	-0.238
H_2O_2 (aq)	-0.060	-0.058	-0.203	-0.201	0.410	-0.405
HCOOH (aq)	-0.088	-0.102	-0.174	-0.116	-0.155	-0.175
NH_3 (aq)	0.001	0.001	0.002	0.003	0.002	0.003
HSO_5^- (aq)	-0.020	-0.078	-0.012	-0.069	0.107	0.043
$HOCH_2SO_3^-$ (aq)	-0.095	-0.087	-0.291	-0.340	-0.456	-0.440
SO_2 (g)	-0.053	-0.051	-0.203	-0.204	-0.406	-0.393
HNO_3 (g)	$\leq$ 0.001		0.304	0.306	0.318	0.319
H_2O_2 (g)	-0.051	-0.049	-0.197	-0.198	-0.406	-0.389
NH_3 (g)	-0.104	-0.130	-0.302	-0.302	-0.316	-0.310
Reaction 50 [b]						
HCHO (aq)	-0.024	-0.025	-0.036	-0.041	-0.047	-0.057
HCOOH (aq)	0.495	0.512	0.588	0.612	0.649	0.697
HCHO (g)	-0.023	-0.023	-0.035	-0.040	-0.047	-0.057
HCOOH (g)	0.480	0.498	0.586	0.629	0.648	0.698
Reaction 74 [c]						
S(IV) (aq)	-.0009	-.0008	-.0036	-.0034	-0.018	-0.019
S(VI) (aq)	.0017	.0016	.0036	.0032	0.012	0.012
N(III) (aq)	-.0005	-.0005	-.0017	-.0015	-.0063	-.0061
SO_2 (g)	-.0023	-.0021	-.0017	-.0012	-.0101	-.0106
HNO_3 (g)	$\leq$ 0.0001		.0017	.0016	0.0081	.0077

[a] Dimensionless sensitivity coefficient of species i with concentration c_i to reaction 73:

$$\frac{\partial \ln c_i}{\partial \ln K_{73}}$$

[b] Dimensionless sensitivity coefficient of species i with concentration c_i to reaction 50:

$$\frac{\partial \ln c_i}{\partial \ln K_{50}}$$

[c] Dimensionless sensitivity coefficient of species i with concentration c_i to reaction 74:

$$\frac{\partial \ln c_i}{\partial \ln K_{74}}$$

differences. Use of the DDM requires 11 T for four sensitivity coefficients and 39 T for the calculation of the whole set of 150. The DDM is expected to perform even better for smaller Jacobians [Dunker, 1980].

Conclusions

A sensitivity analysis of a comprehensive chemical mechanism for aqueous-phase atmospheric chemistry has been perfomed, using the Direct Decoupled Method (DDM). The dominant reaction throught the simulation is the oxidation of S(IV) by H_2O_2. Other important oxidation pathways for S(IV) include reactions with O_2 (catalysed by Fe^{3+} and Mn^{2+}), with OH to produce SO_5^-, with ozone, and with HSO_5^-. Reactions that produce or consume H_2O_2 influence the conversion of S(IV) to S(VI) directly and to a large extent. Such reactions are the production of H_2O_2 in the aqueous-phase by HO_2, the reaction of H_2O_2 with OH, and the reaction of the superoxide ion with bicarbonate ion. The concentration of peroxymonosulfate is found to be a strong function of pH.

The rate of all the aqueous-phase reactions for nitric acid, NO and NO_2 are too small to influence their aqueous-phase concentrations. Therefore the dominant pathway for the HNO_3 acidity is scavenging of nitric acid from the gas phase.

The presence of a cloud enhances the production of formic acid. Formaldehyde reacts with OH to produce HCOOH which (at least for pH less than 5) is transfered to the gas-phase. This reaction is more important for HCOOH(g) than for HCHO(g). The main aqueous-phase sink for HCOOH is its reaction with OH.

The initial gas-phase concentrations of SO_2, H_2O_2, HO_2, OH, O_3, HCHO, NH_3, HNO_3, HCl and the initial aqueous-phase concentrations of S(VI), N(V), NH_3 and HCl are the initial conditions of primary importance for the reaction system.

The liquid water content is one of the most important parameters of the mecha-

nism. Increase of w_L results in an increase of the S(IV)(aq) concentration but decrease of the total amount of S(IV), decrease of the sulfate concentration but increase of the total sulfate amount.

For the value of the accomodation coefficient used in this study (a_w=0.01), the rates of the aqueous-phase reactions are not substantially limited by interfacial or gas-phase mass-transport. Therefore the importance of the accomodation coefficient and the average droplet radius is small. The temperature has opposite effects on the solubility of the various species and on the reaction constants. The net result is a small temperature influence.

Acknowledgement

This work was supported by State of California Air Resources Board Agreement A732-043.

References

Anbar, M., and P. Neta, A compilation of specific bimolecular rate constants for the reactions of hydrated electrons, hydrogen atoms and hydroxyl radicals with inorganic and organic compounds in aqueous solution, *Int. J. Appl. Radiat. Isot.*, 18, 493-523, 1967.

Behar, D., G. Czapski, and I. Duchovny, Carbonate radical in flash photolysis and pulse radiolysis of aqueous carbonate solutions, *J. Phys. Chem.*, 74, 2206-2210, 1970.

Bielski, B. H. J., Reevaluation of the spectral and kinetic properties of HO_2 and O_2^- free radicals, *Photochem. Photobiol.*, 28, 645-649, 1978.

Bothe, E., and D. Schulte-Frohlinde, Reaction of dihydroxymethyl radical with molecular oxygen in aqueous solution, *Z. Naturforsch. B, Anorg. Chem. Org. Chem.*, 35, 1035-1039, 1980.

Boyce, S. D., and M. R. Hoffmann, Kinetics and mechanism of the formation of hydroxymethanesulfonic acid at low pH, *J. Phys. Chem.*, 88, 4740-4746, 1984.

Chameides, W. L., and D. D. Davis, The free-radical chemistry of cloud droplets and its impact upon the composition of rain, *J. Geophys. Res.*,87:4863-4877, 1982.

Chameides, W. L., The photochemistry of a marine stratiform cloud, *J. Geophys. Res.*,89:4739-4755, 1984.

Chameides, W. L., Possible role of NO_3 in the nighttime chemistry of a cloud, *J. Geophys. Res.*, 91:5331-5337, 1986.

Chen, S., V. W. Cope, and M. Z. Hoffman, Behavior of CO_3^- radicals generated in the flash photolysis of carbonatoamines complexes of cobalt(III) in aqueous solution, *J. Phys. Chem.*, 77, 1111-1116, 1973.

Christensen, H., K. Sehested, and H. Corfitzen, Reactions of hydroxyl radicals with hydrogen peroxide at ambient and elevated temperatures, *J. Phys. Chem.*, 86, 1588-1590, 1982.

Cho, S, and G. R. Carmichael, Sensitivity analysis of the role of free radical, organic and transition metal reactions in sulfate production in clouds, *Atmos. Environ.*, 20, 10, 1959-1968, 1986.

Clarke, A. G., and M. Radojevic, Oxidation of SO_2 in rainwater and its role in acid rain chemistry, *Atmos. Environ.*, 21, 1115-1123, 1987.

Cukier R. I., H. B. Levine and K. E. Shuler, Nonlinear Sensitivity analysis of Multi-Parameter Model Systems, *J. Comp. Phys.*, 26, 1-42, 1978.

Damschen, D. E., and L. R. Martin, Aqueous aerosol oxidation of nitrous acid by O_2, O_3, and H_2O_2, *Atmos. Environ.*, 17, 2005-2011, 1983.

Dickinson, R. P., and Gelinas R. J., Sensitivity analysis of ordinary differential

equation systems-a direct method *J. Comp. Phys.*, 21,123-143, 1976.

Dogliotti, L., and E. Hayon, Flash photolysis of persulfate ions in aqueous solutions. Study of the sulfate and ozonide radical ions, *J. Phys. Chem.*, 71, 2511-2516, 1967.

Dougherty, E. P., Hwang J. T., and Rabitz H., Further developments and applications of the Green's function method of sensitivity analysis in chemical kinetics, *J. Chem. Phys.*, 71, 1794-1808, 1979.

Dougherty, E. P., and Rabitz H., Computational kinetics and sensitivity analysis of hydrogen-oxygen combustion, *J. Chem. Phys.*, 72, 6571-6586, 1980.

Dunker, A. M., The response of an atmospheric reaction-transport model to changes in input functions, *Atmos. Environ.*, 14, 671-678, 1980.

Dunker, A. M., The decoupled direct method for calculating sensitivity coefficients in chemical kinetics. *J. Chem. Phys.*, 81, 2385-2393, 1984.

Falls, A. H., G. J. McRae , and J. H. Seinfeld, Sensitivity and uncertainty of reaction mechanisms for photochemical air pollution, *Int. J. Chem. Kinet.*, 11, 1137-1162, 1979.

Frank, P. M., Introduction to system Sensitivity Theory, Academic, New York, 1978.

Fuchs, N. A., and A. G. Sutugin, High-dispersed aerosols, in International Reviews of aerosol Physics and Chemistry, vol. 2, edited by G. M. Hidy and J. R. Brock, pp. 1-60, Pergamon, New York, 1971.

Gardner J. A., Watson L. R., Adewuyi Y. G., Davidovits P., Zahniser M. S., Worsnop D. R., and C. E. Kolb, Measurement of the mass accomodation coefficient of SO_2(g) on water droplets. *J. Geophys. Res.*, 92, 10887-10895, 1987.

Graedel, T. E., and C. J. Weschler, Chemistry within aqueous atmospheric aerosols

and raindrops. *Rev. Geophys. Space Phys.*, 19:505-539, 1981.

Graedel, T. E., and K. I. Goldberg, Kinetic studies of raindrop chemistry, 1. Inorganic and organic processes. *J. Geophys Res.*,88C:10, 865-10, 882, 1983.

Graedel, T. E., M. L. Mandich and C. J. Weschler, Kinetic model studies of atmospheric droplet chemistry 2. Homogeneous transition metal chemistry in raindrops, *J. Geophys Res.*, 91: 5205-5221, 1986.

Gratzel, M., A. Henglein, and S. Taniguchi, Pulsradiolytische Beobachtungen uber die reduktion des NO_3^--Ions unt uber Bildungund Zerfall des persalpetrigen Saure in wassriger Losung, *Ber. Bundsenges. Phys. Chem.*, 74, 292-298, 1970.

Hagesawa, K., and P. Neta, Rate constants and mechanisms of reaction for Cl_2^- radicals, *J. Phys. Chem.*, 82, 854-857, 1978.

Hales, J. M., and D. R. Drewes, Solubility of ammonia in water at low concentrations, *Atmos. Environ.*, 13, 1133-1147, 1979.

Havas, M., Hutchinson, T.C., and Likens, G.E., Red herrings in acid rain research, *Environ. Sci. Technol.*, 18, 176A-186A, 1984.

Hoffmann, M. R., and S.D. Boyce, Catalytic Autoxidation of Aqueous Sulfur Dioxidein Relationship to Atmospheric Systems, *Adv. Environ. Sci. Tech.*, 12, 148-189, Wiley-Interscience, New York, 1983.

Hoffmann, M. R., and J. G. Calvert, Chemical Transformation Modules for Eulerian Acid Deposition Models. Vol. 2 - The Aqueous-phase chemistry, U.S Environmental Protection Agency, Research Triangle Park, North Carolina (EPA/600/3-85/017), 1985.

Hoffmann, M. R., and D. J. Jacob, Kinetics and Mechanisms of the catalytic oxidation of dissolved sulfur dioxide in aqueous solution: an application to night-time fog water chemistry, SO_2, NO and NO_2 Oxidation Mechanisms,

edited by Calvert J. G., pp. 101-172, Butterworth, Boston, Mass., 1984.

Hoigne, J., and H. Bader, Rate constants of reactions of ozone with organic and inorganic compounds in water, 1, Non-dissociating organic compounds, *Water Res.*, 17, 173-183, 1983a.

Hoigne, J., and H. Bader, Rate constants of reactions of ozone with organic and inorganic compounds in water, 2, Dissociating organic compounds, *Water Res.*, 17, 185-194, 1983b.

Huie, R. E., and P. Neta, Chemical behavior of SO_3^- and SO_5^- radicals in aqueous solutions, *J. Phys. Chem.*, 88, 5665-5669, 1984.

Huie, R. E., and P. Neta, Rate constants for some oxidations of S(IV) by radicals in aqueous solutions, *Atmos. Environ.*, 21, 8, 1743-1747, 1987.

Jacob, D. J., and M. R. Hoffmann, A dynamic model for the production of H^+, NO_3^-, and SO_4^{2-}, in urban fog, *J. Geophys. Res.*, 88, 6611-6621, 1983.

Jacob, D. J., Comment on "The photochemistry of a remote marine stratiform cloud" by William L. Chameides, *J. Geophys. Res.*, 90, 5864, 1985.

Jacob, D. J., Chemistry of OH in remote clouds and its role in the production of formic acid and peroxymonosulfate, *J. Geophys. Res.*, 91 (D9), 9807-9826, 1986.

Jayson, G. G., B. J. Parsons, and A. J. Swallow, Some simple, highly reactive, inorganic chlorine derivatives in aqueous-solution, *Trans. Farad. Soc.*, 69, 1597-1607, 1973.

Koda M., Dogru A. H., and J. H. Seinfeld, Sensitivity analysis of partial differential equations with application to reaction and diffusion processes, *J. Comp. Phys.*, 30, 259-282, 1979.

Kozac-Channing, L. F., and G. R. Heltz, Solubility of ozone in aqueous solutions of 0-0.6 M ionic strength at 5-30°C, *Environ. Sci. Technol.*, 17(3), 145-149,

1983.

Latimer, W. M., The Oxidation States of the Elements and Their Potentials in Aqueous Solutions, Prentice-Hall, New York, pp. 70-89, 1952.

Le Henaf, P., Methodes d'etude et proprietes des hydrates, hemiacetals et hemiacetals derives des aldehydes et des cetones, *Bull. Soc. Chim. France*, 4687-4700, 1968.

Ledbury, W., and E. W. Blair, The partial formaldehyde vapour pressure of aqueous solutions of formaldehyde, Part II, *J. Chem. Soc.*, 127, 2832-2839, 1925.

Lee, Y-N, Kinetics of oxidation of aqueous sulfur(IV) by nitrogen dioxide, in Precipitation Scavenging, Dry Deposition, and Resuspension, Volume I, H. R. Pruppacher, R. G. Semonin, and W. G. N. Slinn, eds., Elsevier, New York, 1983.

Lee, Y-N, Kinetics of some aqueous-phase reactions of peroxyacetyl Nitrate, in Gas-Liquid Chemistry of Natural Waters, Vol. 1, 21/1-21/7, Brookhaven National Laboratory (BNL 51757), 1984a.

Lee, Y-N, Atmospheric aqueous-phase reactions of nitrogen species, in Gas-Liquid Chemistry of Natural Waters, Brookhaven National Laboratory, 1984b.

Lee, Y-N, and J. A. Lind, Kinetics of aqueous-phase oxidation of nitrogen(III) by hydrogen peroxide, *J. Geophys. Res.*, 91(D2), 2793-2800, 1986.

Lilie, J., A. Henglein, and R. J. Hanrahan, Reactions of the carbonate radical anion with organic and inorganic solutes in aqueous solution, presented at the 176th meeting of the American Chemical Society, Miami Beach, Florida, 1978.

Lind, J. A., and G. L. Kok, Henry's law determinations for aqueous solutions of hydrogen peroxide, methylhydroperoxide, and peroxyacetic acid, *J. Geophys. Res.*, 91(D7), 7889-7895, 1986.

Marsh A. R. W., and W. J. McElroy, The dissociation constant and Henry's law constant of HCl in aqueous solution, *Atmos. Environ.*, 19, 1075-1080, 1985.

Martin, L. R., and Damschen, D. E., Aqueous Oxidation of Sulfur Dioxide by Hydrogen Peroxide at low pH, *Atmos. Environ.*, 15, 1615-1622, 1981.

Martin, L. R., Kinetic Studies of Sulfite Oxidation in Aqueous Solution, in SO_2, NO, and NO_2 Oxidation Mechanisms: Atmospheric Considerations, edited by Calvert J. G., pp. 63-100, Butterworth, Boston, Mass., 1984.

Martin, L. R., and M. W. Hill, The iron catalysed oxidation of sulfur: recociliation of the literature rates, (preliminary communication), *Atmos. Environ.*, 6, 1487-1490, 1987.

McArdle, J. V., and Hoffmann, M. R., Kinetics and Mechanism of the Oxidation of Aquated Sulfur Dioxide by Hydrogen Peroxide at Low pH, *J. Phys. Chem.*, 87, 5425-5429, 1983.

Mozurkewich, M., P. H. McMurry , A. Gupta, and J. G. Calvert, Mass accomodation coefficient for HO_2 radicals on aqueous particles, *J. Geophys. Res.*, 92, 4163-4170, 1987.

Munger, J. W., C. Tiller, and M. R. Hoffmann, Identification of hydroxymethanesulfonate in fog water, *Science*, 231, 247-249, 1986.

Oblath, S. B., S. S. Markowitz, T. Novakov, and S. G. Chang, Kinetics of the formation of hydroxylamine disulfonate by reaction of nitrite with sulfites, *J. Phys. Chem.*, 85, 1017-1021, 1981.

Oran, E. S., and J.P. Boris, Numerical Simulation of reactive flow, Elsevier Science Publishing Co., Inc., New York, 1987.

Perrin, D. D., Ionization Constants of Inorganic Acids and Bases in Aqueous Solution, 2nd edition, Pergamon Press, New York, 1982.

Pruppacher, H. R., and J. D. Klett, Microphysics of Cloud and Precipitation, D.

Reidel, Dordrecht, The Netherlands, 1980.

Rettich, T. R., Some photochemical reactions of aqueous nitric acid, *Diss. Abstr. Int. B.*, 38, 5968, 1978.

Ross, A. B., and P. Neta, Rate constants for reactions of inorganic radicals in aqueous solution, U.S. Department of Commerce, Washington, D. C., (NSRDS-NBS 65), 1979.

Schmidt, K. H., Electrical conductivity techniques for studying the kinetics of radiation-induced chemical reactions in aqueous solutions, *Int. J. Radiat. Phys. Chem.*, 4, 439-468, 1972.

Schofield, C.L., Acid rain/fisheries, Proceedings International Symposium on Acidic Precipitation and Fishery impacts in Northeast North America, R.E. Johnson (Ed.), Ithaca, NY, 57-67, 1982.

Scholes, G., and R. L. Willson, γ-radiolysis of aqueous thymine solutions. Determination of relative reaction rates of OH radicals, *Trans. Faraday Soc.*, 63, 2982-2993, 1967.

Schwartz, S. E., Mass-transport considerations pertinent to aqueous-phase reactions of gases in liquid-water clouds, in Chemistry of Multiphase Atmospheric Systems (W. Jaeschke, ed.), Heidelberg: Springer, 415-471, 1986.

Schwartz, S. E., Gas- and aqueous-phase chemistry of HO_2 in liquid water clouds. *J. Geophys. Res.*, 89, 11,589-11,598, 1984.

Schwartz, S. E., and W. H. White, Solubility equilibrium of the nitrogen oxides and oxyacids in dilute aqueous solution, *Adv. Environ. Sci. Eng.*, 4, 1-45, 1981.

Sehested, K., O. L. Rasmussen, and H. Fricke, Rate constants of OH with HO_2, O_2^-, and $H_2O_2^+$ from hydrogen peroxide formation in pulse-irradiated oxygenated water, *J. Phys. Chem.*, 72, 626-631, 1968.

Sehestad, K., J. Holcman, and E. J. Hart, Rate constants and products of the reactions of e^-_{aq}, O_2^-, and H with ozone in aqueous solutions, *J. Phys. Chem.*, 87, 1951-1954, 1983.

Sehested, K., J. Holcman, E. Bjergbakke, and E. J. Hart, A pulse radiolytic study of the reaction OH + O_3 in aqueous medium, *J. Phys. Chem.*, 88, 4144-4147, 1984.

Seigneur, C., and P. Saxena, A study of atmospheric acid formation in different environments, *Atmos. Environ.*, 18:2109-2124, 1984.

Seinfeld, J. H., Atmospheric Chemistry and Physics of Air Pollution, John Wiley, New York, 1986.

Shapilov, O. D., and Y. L. Kostyukovskii, Reaction kinetics of hydrogen peroxide with formic acid in aqueous solutions, *Kinet. Katal.*, 15, 1065-1067, 1974.

Smith, R. M., and A. E. Martell, Critical Stability Constants, Vol. 4: Inorganic Complexes, Plenum Press, New York, 1976.

Snider, J. R., and G. A. Dawson, Tropospheric light alcohols, carbonyls, and acetonitrile: Concentrations in the southwestern United States and Henry's law data, *J. Geophys. Res.*, 90, 3797-3805, 1985.

Sorensen, P. E., and V. S. Andersen, The formaldehyde-hydrogen sulphite system in alkaline aqueous solution: kinetics, mechanism, and equilibria, *Acta Chem. Scand.*, 24, 1301-1306, 1970.

Staehelin, J., R. E. Buhler, and J. Hoigne, Ozone decomposition in water studied by pulse radiolysis, 2, OH, and HO_4 as chain intermediates, *J. Phys. Chem.*, 88, 5999-6004, 1984.

Staehelin, J., and J. Hoigne, Decomposition of ozone in water: rate of initiation by hydroxide ions and hydrogen peroxide, *Environ. Sci. Technol.*, 16, 676-681, 1982.

Stolarski, R. S., Butler D. M., and R. D. Rundel, Uncertainty propagation in a stratospheric model, II. Monte Carlo analysis of Imprecision due to reaction rates, *J. Geophys. Res.*, 83(C6), 3074-3078, 1978.

Strehlow, H., and I. Wagner, Flash photolysis in aqueous nitrite solutions, *Z. Phys. Chem. Wiesbaden*, 132, 151-160, 1982.

Systems Applications, Inc., Development of a Comprehensive Chemistry Acid Deposition Model (CCADM) Volume I: Technical Document, SYSAPP-87/002, 1987.

Treinin, A., and E. Hayon, Absorption spectra and reaction kinetics of NO_2, N_2O_3, and N_2O_4 in aqueous solutions, *J. Am. Chem. Soc.*, 92, 5821-5828, 1970.

Weeks, J. L., and J. Rabani, The pulse radiolysis of deaerated aqueous carbonate solutions, I, Transient optical spectrum and mechanism; II, pK for OH radicals, *J. Phys. Chem.*, 70, 2100-2106, 1966.

Weinstein, J., and B. H. J. Bielski, Kinetics of the interaction of HO_2 and O_2^- radicals with hydrogen peroxide; the Haber-Weiss reaction, *J. Am. Chem. Soc.*, 101, 58-62, 1979.

Young, J.R., and F.W. Lurmann, ADOM/TADAP Model Development Program: Volume 7 - Aqueous Phase Chemistry. ERT Doc. No. P-B980-535, Environmental Research and Technology, Inc., Newburry Park, CA, 1984.

CHAPTER 3

MATHEMATICAL MODELLING OF ACID DEPOSITION DUE TO RADIATION FOG

(Submitted for publication in *Journal of Geophysical Research*, January 1989)

Mathematical Modeling of Acid Deposition Due to Radiation Fog

Spyros N. Pandis and John H. Seinfeld

Department of Chemical Engineering and Environmental Quality Laboratory,

California Institute of Technology, Pasadena, CA 91125, USA

Abstract

A Lagrangian model has been developed to study acidic deposition due to radiation fog. The model couples submodels describing the development and dissipation of radiation fog, the gas-phase chemistry and transfer and the aqueous-phase chemistry. The model is applied to a radiation fog episode in Bakersfield in the San Joaquin Valley of California over the period January 4-5, 1985. Model predictions for temperature profile, fog development, liquid water content, gas-phase concentrations of SO_2, HNO_3 and NH_3, pH, aqueous-phase concentrations of SO_4^{2-}, NH_4^+ and NO_3^-, and finally deposition rates of the above ions are compared with the observed values. The deposition rates of the major ions are predicted to increase significantly during the fog episode with the most notable being the increase of sulfate deposition. Pathways for sulfate production that are of secondary importance in a cloud environment may become significant in a fog. Expressing the mean droplet settling velocity as a function of the liquid water content is found to be quite influential in the model's predictions.

Introduction

The importance of acid fog as a component of the general acidic deposition phenomenon has recently been recognized. For example, Hoffmann and co-workers [Waldman et al.,1982; Munger et al., 1983; Jacob et al., 1985] have reported pH values of fogs in Southern California as low as 1.69. These fogs were much more acidic, and concentrations of anions and cations such as SO_4^{2-}, NO_3^- and NH_4^+ were higher by one to two orders of magnitude than in precipitation in the same areas. Field measurements have provided valuable information concerning the chemical composition of acid fog, but the physicochemical processes leading to this composition have yet to be elucidated.

Mathematical models describing atmospheric processes are a major tool in our effort first to understand and then to control acidic deposition. The first step in acidic deposition processes is the emission to the atmosphere of SO_2 and NO_x. SO_2 and NO_x can be oxidized in the atmosphere, yielding sulfuric and nitric acid vapors. Due to its very low vapor pressure, sulfuric acid is rapidly incorporated into aerosol particles, while nitric acid may be scavenged by particles or droplets or remain in the gas-phase. Inside a cloud or a fog, gas-phase species like SO_2, HNO_3, NH_3, H_2O_2, and aerosol particles are scavenged by water droplets resulting in a solution that can be significantly acidic. It was initially believed that the scavenging of these acids by cloud, fog and rain droplets was the major source of sulfuric and nitric acid observed in precipitation. It is now recognized that cloudwater and fogwater acidity may result not only from incorporation of strong acids present in clear air but also from aqueous-phase oxidation reactions, most notably oxidation of S(IV) to S(VI). Several analyses of aqueous-phase atmospheric chemistry have been performed using mechanisms of varying complexity [Graedel and Goldberg, 1983; Jacob and Hoffmann, 1983; Chameides, 1984; Seigneur and Saxena, 1984; Schwartz, 1984; Jacob, 1986; Pandis and Seinfeld, 1989]. These studies are based on reaction mechanisms of the aqueous-phase chemistry in clouds

or fog with or without gas-phase reactions, but with no treatment of cloud or fog dynamics. The importance of parameters such as amount of liquid water, the droplet lifetime, and the amount of polluted air mixed in the cloud system to the chemical composition of the aqueous-phase has been stressed in these studies.

Tremblay and Leighton [1984, 1986] developed a model of cloud dynamics with a simple treatment of cloud chemistry. Their initial one-dimensional model [1984] was later extended to a three-dimensional model [1986]. Walcek and Taylor [1986] used a one dimensional steady-state cumulus cloud model with detailed aqueous but no gas-phase chemistry to study vertical distribution of acidity and sulfate production. Seigneur and Saxena [1988] presented a model with a simple treatment of cloud physics (updraft and precipitation) and detailed cloud chemistry and investigated sulfate formation in stratus and cumulus clouds. Several attempts have been made to model the life-cycle of radiation fog with no treatment of atmospheric chemistry [Fisher and Caplan, 1963; Zdunkowski and Nielsen, 1969; Lala et al., 1975; Brown and Roach, 1976; Brown, 1980; Forkel et al., 1983; Turton and Brown, 1987; Forkel et al., 1987].

Each of all the above studies has focused either on the chemical processes associated with the gas and aqueous-phase or the physics of clouds and fog. This study combines for the first time a detailed description of gas and aqueous-phase atmospheric chemistry with a basic treatment of radiation fog dynamics. The inclusion of the fog dynamics enables us to study the wet deposition of pollutants during fog episodes, the vertical variability of acidity and pollutant concentrations in a fog, and the changes of concentration of aqueous and gaseous species during the various stages of fog development.

A Lagrangian trajectory model has been used in this study for the description of the radiation fog development and gas and aqueous-phase chemistry. A trajectory model that follows a parcel of air as it traverses the airshed has been found to be

a valuable tool for the simulation of the chemical and physical processes occuring in a particular location. Even if such a model is not ideally suited for the prediction of concentration changes over extended spatial and temporal scales where an Eulerian description is preferable, the small computing cost of a trajectory model compared to an Eulerian grid model makes it ideal for the testing of chemical reaction mechanisms and model assumptions and for studing the sensitivity of the model to various inputs and parameters. Furthermore, the relatively low computing cost allows the use of higher vertical resolution than in a three-dimensional model and thus affords the opportunity to explore phenomena sensitive to height above the ground.

In this paper, we begin with a physical description of the system of interest, with emphasis on the physics of radiation fog. Next we present separately the gas-phase chemistry, aqueous-phase chemistry and radiation fog dynamics submodels and then describe the complete model. The full model is then evaluated against data obtained during a well-documented radiation fog episode in the San Joaquin Valley of California [Waldman, 1986; Jacob et al., 1987]. Sensitivity studies address the effects of fog formation on the deposition rates and on the aerosol mass and the chemical pathways that contribute to sulfate formation.

Radiation fog and acid deposition

By definition, a fog is a cloud of liquid water droplets near the earth's surface that reduces visibility to less than 1 km [Eagleman, 1985]. If humid air near the ground is cooled sufficiently it becomes saturated and a fog develops. Typical fogs are classified according to the process that causes the cooling of the air. The types identified are upslope, advection, frontal and radiation fogs [Eagleman, 1985]. Upslope fog is generated by the cooling of the air as it is forced to rise over hills and mountains. Advection fog is created through contact cooling of warm air with a cold surface or

through advection of cold air over warm water. Frontal fog can be created as weather, especially warm fronts, passes through an area. Finally, radiation fog (or ground fog) is generated as the earth's surface cools by loss of radiation to space at night.

This study focuses on the development of radiation fog because it is one of the most frequently encountered fog forms in heavily polluted areas [Munger et al., 1989]. It is important to note, however, that the main ideas concerning the modelling of radiation fog can be extended and applied to other fog categories and especially to advection and upslope fog.

The various stages in the development of a typical radiation fog can be visualized by following the movement of an air parcel during a 24 hour period. During the daytime the air parcel collects water vapor and aerosol particles (sea salt, dust, primary and secondary particles of anthropogenic origin). The air temperature is high and the relative humidity is low. In the late afternoon the heat loss of the ground due to radiation to space exceeds the heating rate due to solar radiation and the ground's temperature starts decreasing. After sunset, as the cooling of the ground continues, the air within the lowest few meters also cools, due to heat transfer to the cooler ground. The radiational heat loss of the surface is partially balanced by heat conducted upwards to the ground surface because of the temperature gradient created in the first few centimeters in the soil. At a specific relative humidity, which for most soluble components in the atmosphere is well below 100%, aerosol particles that are not already liquid deliquesce into aqueous solution drops. As the ambient relative humidity keeps increasing, the droplets undergo a slow equilibrium growth by water vapor diffusion [Pruppacher and Klett, 1980]. The air near the ground approaches saturation. At this stage dew deposition occurs.

Whether fog forms at this point depends on several factors such as cloud cover (clouds reduce radiative cooling), wind speed (turbulent diffusion tends to dry and

may warm the air), and water vapor concentration. If there are no clouds and the wind speed is very low and the water vapor concentration is high enough, then fog starts forming in the lowest few meters. When the relative humidity reaches a critical supersaturation, depending on the size and chemical composition of the aerosol present, the droplets become activated and grow freely by water vapor diffusion.

The air near the top of the fog is cooling rapidly due to radiation of the fog droplets to space and consequently the fog propagates upward. At the same time as the fog's thickness increases, the radiative losses of the ground decrease due to the liquid water shield over it, and the ground temperature starts increasing from heat conduction upward through the soil. The air near the ground thus warms and the fog near the ground thins out.

When the sun comes out, fog dissipation is accelerated and liquid water evaporates rapidly at both the top and bottom of the fog. As the relative humidity decreases, the water evaporates from the fog droplets leaving aerosol particles. The fog life-cycle affects the aerosol concentration and composition in various ways. The aerosol particles grow because of water vapor diffusion and their gravitational settling and subsequent deposition are accelerated. At the same time, fog droplets scavenge soluble gases like nitric acid and ammonia and act as the medium for various aqueous-phase reactions, including the oxidation of absorbed SO_2 to sulfate.

Model Description

A complete model for acidic deposition due to fog should include descriptions of several physicochemical processes for all three phases existing in the atmosphere, namely the gaseous, the aqueous and the aerosol phase (Figure 1). Important processes that should be modelled are the emission of gas-phase species (SO_2, NH_3, NO_x, hydrocarbons) and particles, the reactions of species in the gas-phase, the nucleation

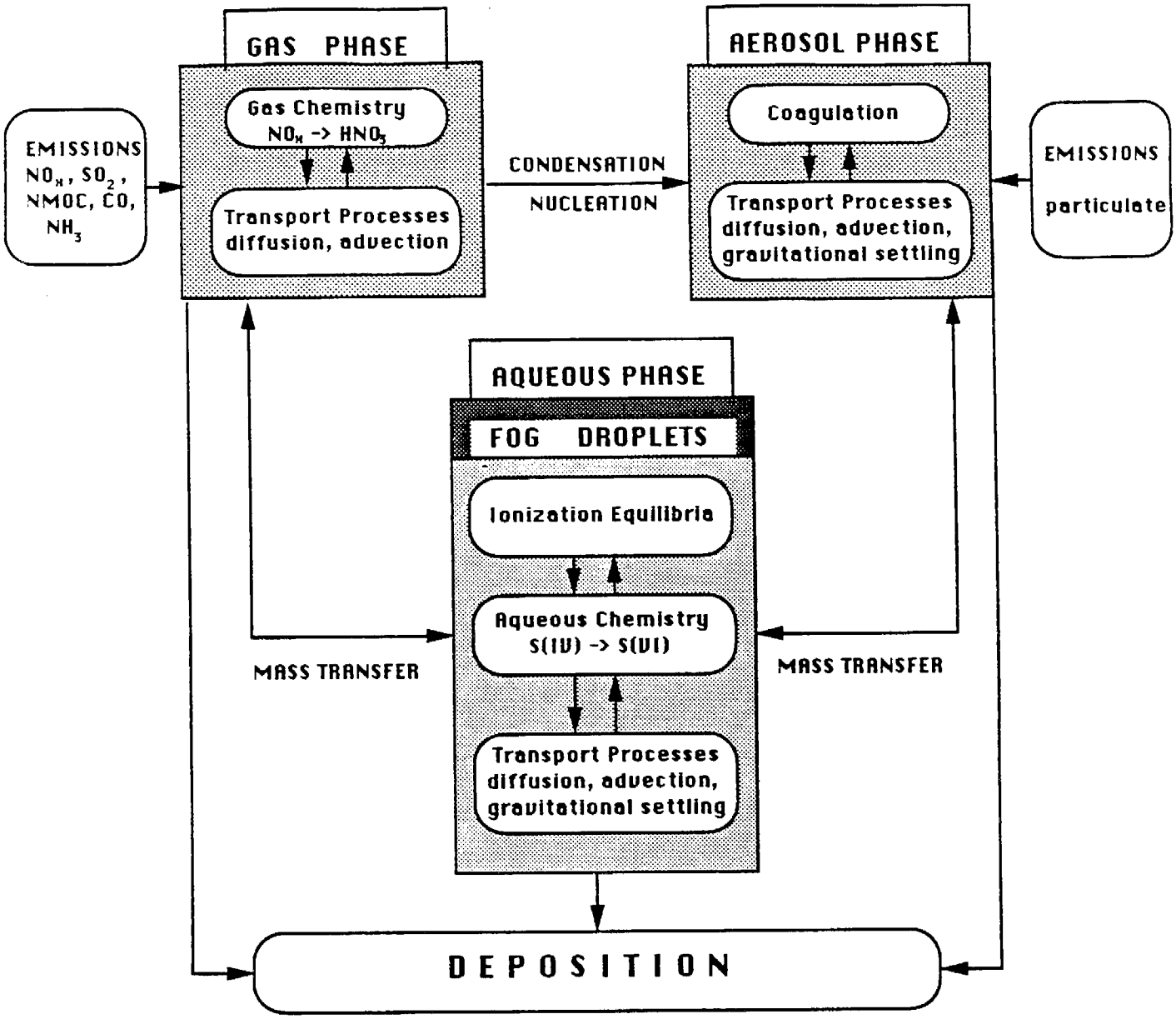

Figure 1 Atmospheric processes leading to acid deposition.

and condensation of gaseous species to aerosol particles, and the mass transfer (diffusion and advection) and dry deposition of gases and aerosol. Additionally, a description of the physical process that causes the cooling of the moist air (radiative cooling for radiation fog) is necessary. The condensation of water vapor on the aerosol particles that serve as condensation nuclei and the subsequent growth of the water droplets is the next step. After the appearance of the aqueous-phase one should account for the scavenging of gaseous species by the water droplets, their ionization and aqueous-phase reactions. The gravitational settling of droplets and their deposition on the ground must also be described. The last step of the phenomenon is the evaporation of the aqueous-phase leaving an aerosol residue.

A full description of all the above processes requires a model capable of predicting the changes of the aerosol and water droplet size-chemical composition spectrum. The present study focuses on the chemical changes in both the gas and aqueous-phases and an explicit treatment of the aerosol microphysics has not been included. Size-dependent processes of interest such as the aerosol particle scavenging by fogwater, gravitational settling, and radiative cooling of fog droplets have been parametrized. The model is capable of predicting the liquid water profile, and the gas and aqueous-phase concentration profiles for all species but does not account for the size or composition spectrum of aerosol particles or fog droplets.

The mathematical model employed in this study consists of three interacting submodels simulating gas-phase chemistry, fog development and aqueous-phase chemistry. These three models will initially be described independently.

1. Gas-phase model

The gas-phase model describes atmospheric chemical reactions, turbulent vertical diffusion, horizontal advective transport, and ground level pollutant deposition. It is

based on the numerical solution of the Lagrangian trajectory form of the atmospheric diffusion equation presented in McRae et al. [1982]. Except for the changes mentioned below the methods employed here are as described by McRae et al. [1982].

The detailed SAPRC/ERT gas-phase chemical reaction mechanism (Carter et al., 1986) with the modifications and extensions of Carter and Atkinson [1988] has replaced the previously used mechanism. It contains 154 reactions and 62 species (39 active, 7 accumulating and 16 steady state species). The photochemical mechanism preparation and emissions processing software of Carter and Atkinson [1988] has been used to prepare the gas-phase mechanism dependent part of the code.

2. Radiation fog model

The governing equations of the radiation model are the one-dimensional continuity equations for heat (for air and soil), water vapor and liquid water:

$$\frac{\partial T}{\partial t} = -\frac{1}{\rho c_p}\frac{\partial F_N}{\partial z} + \frac{\partial}{\partial z}\left[K_h\left(\frac{\partial T}{\partial z} + \Gamma\right)\right] + \frac{L}{\rho c_p}C \tag{1}$$

$$\frac{\partial T_s}{\partial t} = K_s\frac{\partial^2 T_s}{\partial z^2} \tag{2}$$

$$\frac{\partial q}{\partial t} = \frac{\partial}{\partial z}\left(K_q\frac{\partial q}{\partial z}\right) - C \tag{3}$$

$$\frac{\partial w}{\partial t} = \frac{\partial}{\partial z}\left(K_w\frac{\partial w}{\partial z}\right) + \frac{\partial G}{\partial z} + C \tag{4}$$

where T is the air temperature (in K), ρ the air density (in g m^{-3}), c_p the specific heat of air (in J K^{-1} g^{-1}), F_N the net radiative flux (in W m^{-2}), K_h, K_q, K_w the exchange coefficients for heat, water vapor and liquid water respectively (in m^2 s^{-1}), Γ is the

adiabatic lapse rate ($\Gamma = 0.0098$ K m^{-1}), L the latent heat of vaporization (in J / g water), C the condensation rate (in g water m^{-3} s^{-1}), T_s the temperature in the soil (in K), K_s the soil thermal conductivity (in m^2 s^{-1}), q is the water vapor concentration (in g water m^{-3}), w is the liquid water concentration (in g water m^{-3}) and G is the gravitational flux of liquid water (in g water m^{-2} s^{-1}).

The radiation flux F_N is calculated using the radiation scheme of Zdunkowski et al. [1982] for the solar and infrared emission spectrum. This scheme incorporates the effects of atmospheric water vapor, carbon dioxide, ozone, nitrogen dioxide, aerosol particles and multiple layers of clouds or fog. A total of 74 grid points extending from the ground surface to a height of 50 km have been found to provide sufficient accuracy for the solution of the equations for the radiative fluxes in this study.

The exchange coefficients for heat, water vapor and liquid water are assumed equal in this model [Brown and Roach, 1975]. They are given by the [Shir, 1973] :

$$K_{h,q,w} = \frac{K^n}{\phi_{h,q,w}(z/L)} \tag{5}$$

where K^n refers to neutral conditions and is given by :

$$K^n = \frac{1}{2} k u_* z \left[\exp\left(\frac{-4z}{H}\right) + \frac{1}{1 + 16(z/H)^{1.6}} \right] \tag{6}$$

In the above formulas $H = 0.455 u_*/f$ scales the boundary layer height [Shir, 1973], u_* is the friction velocity, f the Coriolis parameter, L is the Monin-Obukhov length, and $\phi_{h,q,w}$ is the appropriate Monin-Obukhov profile function. The simplifying assumption is made that $\phi_h = \phi_q = \phi_w$. The Monin-Obukhov profile functions used in this study are [Zdunkowski et al., 1976] :

1) Unstable Regime

$$\phi_h\left(\frac{z}{L}\right) = 0.76\left(1 - 16\frac{z}{L}\right)^{-\frac{1}{2}} \qquad \text{for } \frac{z}{L} > -10. \tag{7}$$

The functions are evaluated at $z/L = -10$ if $z/L < -10$.

2.) Stable Regime

$$\phi_h\left(\frac{z}{L}\right) = 0.74 + 9.62\frac{z}{L} + 29.6\left(\frac{z}{L}\right)^2, \quad \frac{z}{L} < 0.08 \tag{8a}$$

$$\phi_h\left(\frac{z}{L}\right) = 1.2 + 6.1\frac{z}{L}, \quad \frac{z}{L} > 0.08 \tag{8b}$$

The thermal conductivity of the soil, K_s, is assumed to remain constant for all depths during the simulation.

The gravitational flux of liquid water G is defined in terms of a mean settling velocity $u_{\mathbf{av}}$ by

$$G = w\, u_{\mathbf{av}} \tag{9}$$

If the droplet size distribution, $n(r, z)$, and the settling velocity of droplets as a function of size, $u(r)$, are known, the mean settling velocity, $u_{\mathbf{av}}$, can be obtained from

$$u_{\mathbf{av}} = \frac{\int_0^\infty n(r,z)u(r)r^3 dr}{\int_0^\infty n(r,z)r^3 dr} \tag{10}$$

Because the fog droplet distribution at height z is not calculated by this model we have parametrized the mean settling velocity $u_{\mathbf{av}}$ following Brown and Roach [1976] and Forkel et al. [1983, 1987] as :

$$u_{\mathbf{av}} = a_g w \tag{11}$$

Various measured fog droplet spectra [Waldman, 1986] have been used to calculate an average a_g value of 0.120 $\mathrm{m}^4\ \mathrm{g}^{-1}\mathrm{s}^{-1}$. The terminal velocity of droplets in Equation (10) has been calculated using Stokes law.

To avoid an explicit treatment of the fog microphysics we assume that inside the fog the water vapor pressure always attains its saturation value [Brown and Roach, 1976]. Various field measurements suggest that fogs generally have low supersaturations, with largest values during the initial stage of fog development. Therefore our assumption leads to a small loss of accuracy in the calculated liquid water values but at the same time reduces drastically the computing time requirements as we do not have to solve the droplet growth equation [Brown, 1980]. The integration of Equations (1), (3) and (4) is performed in two steps. In the first, the equations are integrated for one timestep neglecting the condensation/evaporation term ($C = 0$). This integration results in values of the air temperature, water vapor and liquid water concentrations, T_o, q_o, w_o, respectively. In general, the water vapor concentration will be different from the saturation concentration, q_{so}, at temperature T_o. If the air is supersaturated, some water vapor has to be condensed. If it is subsaturated, some of the existing liquid water is evaporated. Therefore, the three variables are adjusted to T', q', w', where q' is the saturation concentration corresponding to T'. The new values are calculated by solving the water mass balance, the energy balance and the Clausius-Clapeyron equations simultaneously [McDonald, 1963].

Boundary conditions

Equations (1), (3) and (4) are solved in the region extending from the ground surface to a height of 300 m. This region has been chosen large enough to include the fog top in most radiation fog episodes. Equation (2) is solved from a depth of 1 m below the surface to the ground surface. The grid used is unequally spaced with 52 points above ground level for the solution of Equations (1), (3), and (4), and 13 points inside the soil for the solution of Equation (2). The grid is much denser near the ground surface. This grid selection was proven to provide both accuracy and speed

for subsequent calculations.

The boundary conditions applied to the top ($z = 300$ m) of the model region are:

$$T = \text{constant} = T_{\text{top}}$$

$$q = \text{constant} = q_{\text{top}}$$

$$w = 0$$

for the bottom level:

$$T_s = \text{constant} = T_{\text{bot}} \text{ at } z = -1 \text{ m}$$

Finally for the ground surface the liquid water concentration is assumed to be zero, $w = 0$, and the air and soil temperature are considered to be the same, $T = T_s$. From the continuity of heat fluxes at the air-soil interface [Turton and Brown, 1987],

$$-F_N + F_H + F_L - F_S = 0 \text{ at } z = 0$$

where F_N is the net radiative flux (long-wave and short-wave) incident at the surface, F_H and F_S are the sensible heat fluxes reaching the interface through the air and the soil and F_L is the latent heat flux. The surface water vapor concentration q_1 is calculated by [Turton and Brown, 1987] :

$$q_1 = f_p q_{\text{sat}}(T_1) + (1 - f_p) q_2 \tag{12}$$

where $q_{\text{sat}}(T_1)$ is the saturation water vapor concentration of the ground surface which has temperature T_1, q_2 is the water vapor concentration for the first grid point above ground level and f_p is given by [Turton and Brown, 1987] :

$$f_p = (z_2/K_{h1})/(z_2/K_{h1} + r_s) \tag{13}$$

where r_s is the surface resistance. A value of 60 s m^{-1} is used in this study following Turton et al. [1987]. For dew deposition that is $q_{sat}(T_1) < q_2$, f_p is set equal to unity.

The system of the four partial differential equations is solved using the Crank-Nicolson method with a timestep of 1 s. No stability difficulties were encountered for this timestep.

3) Aqueous-phase model

The aqueous-phase chemical reaction mechanism used in this study is described Pandis and Seinfeld [1989]. The mechanism includes the dynamic exchange of species between the gaseous and aqueous phases in a homogeneous parcel of air containing liquid water droplets. The chemical mechanism includes 49 individual aqueous-phase species, 17 aqueous-phase ionic equilibria, 20 gas-phase aqueous-phase reversible reactions and 109 aqueous-phase reactions.

Full Model Description

The full Lagrangian model describes the physicochemical processes occurring in a vertical column containing a prescribed number of computational grid cells (12, in the present computation). The region where the fog is expected to grow (the first 300 meters above the ground) is divided into 9 cells, while the remaining three cells cover the height from 300 to 1000 m. The size of each vertical cell remains constant during the simulation (Figure 2).

Each simulation is divided in three stages. In the first, the stage before fog development, the model operates like an ordinary air quality trajectory model with only the gas-phase submodel active [McRae, 1982]. The variables calculated by the model in this stage are the gas-phase concentrations c_{gi}. Their change is calculated by

$$c_g^{(t+\Delta t)} = A_{gas}(\Delta t) c_g^{(t)} \tag{14}$$

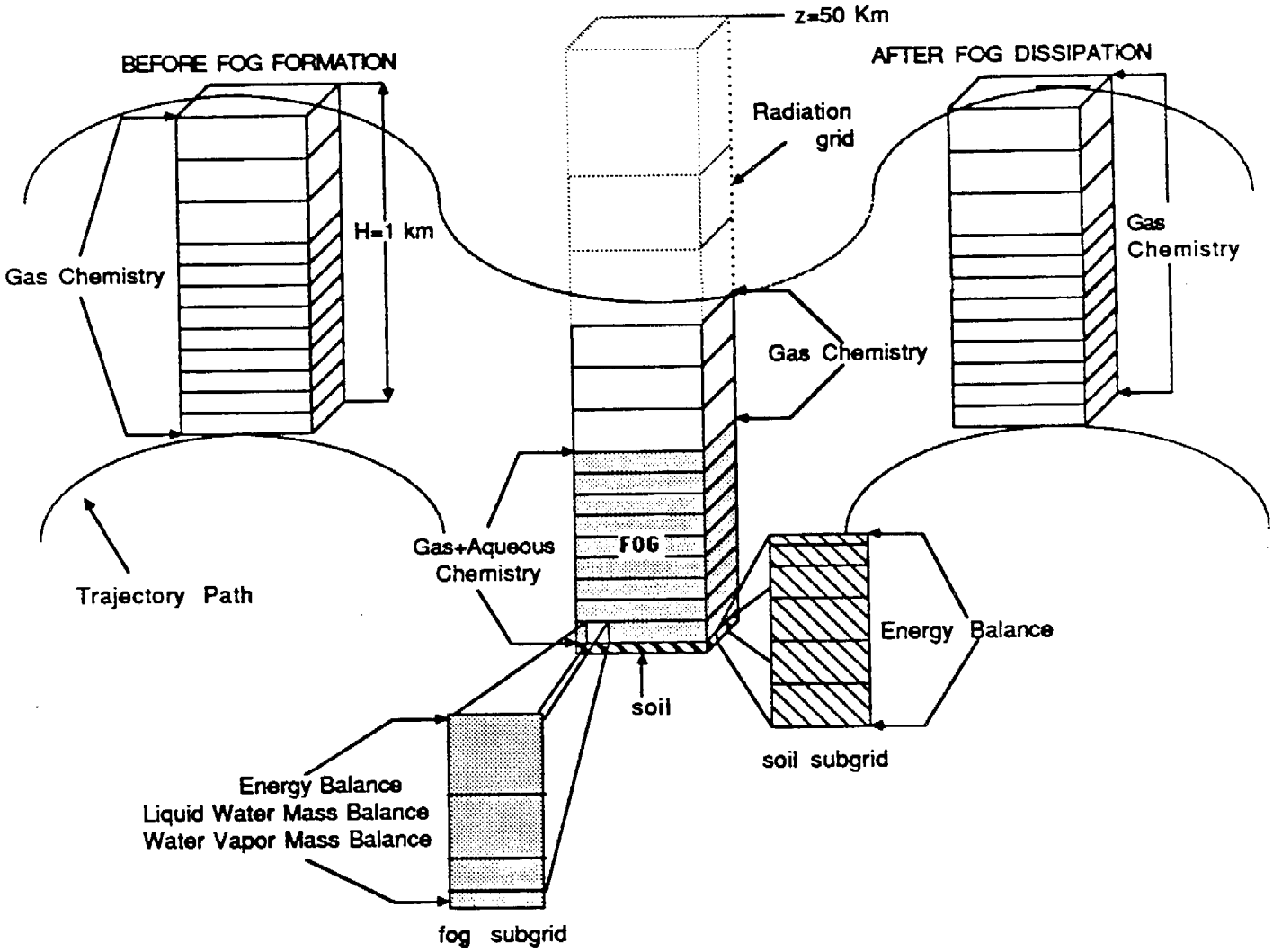

Figure 2 Schematic representation of the vertically resolved Lagrangian trajectory model for radiation fog.

where A_{gas} is the gas-phase operator described for the gas phase submodel.

At this stage the temperature and relative humidity constitute an input to the model. When the relative humidity exceeds 90%, the first stage is considered over, and we enter the fog development stage. Initial temperature and relative humidity profiles are provided as an input and the fog submodel becomes active. The first 9 of the 12 major cell of the gas submodel are divided into smaller cells for the solution of the fog model equations (1), (3) and (4). When liquid water is created in a cell, the aqueous-phase chemistry submodel is also used. The existing aerosol particles are assumed to be completely scavenged by fog droplets upon the formation of a liquid water phase [Ten Brink et al., 1987]. In this way the aerosol mass provides the initial concentrations of sulfate, nitrate and ammonia in fogwater.

The aqueous-phase chemistry calculation is performed within the fog region of the main grid. The liquid water content for each of these cells is an average over the liquid water profile provided by the fog submodel.

During radiation fog, wind speeds remain generally under 2 m s^{-1} [Forkel et al., 1987; Waldman, 1986], therefore during the life cycle of the radiation fog one can assume that the Lagrangian cell is stationary. Under this assumption, the energy balance is valid because the cell remains more or less over the same piece of land throughout the simulation.

The full set of partial differential equations for the fog, gaseous and aqueous phases is solved using an operator splitting technique, in order to decouple the fog growth, the gas-phase chemistry and vertical transport, and the aqueous-phase chemistry. If F_i is the variable vector containing the gas and aqueous phase concentrations and fog variables, its value at time $t + \Delta t$ is obtained from that at time t by:

$$F_i^{(t+\Delta t)} = A_{gas}(\Delta t)A_{fog}(\Delta t)A_{aq}(2\Delta t)A_{fog}(\Delta t)A_{gas}(\Delta t)F_i^{(t)} \qquad (15)$$

where A_{gas}, A_{aq} and A_{fog} are the gaseous-chemistry, aqueous-chemistry and fog operators described above.

The second stage of simulation ends when the fog dissipates. At this point, when all the liquid water has been evaporated the fog and aqueous chemistry operators become inactive, and the model becomes once more an ordinary gas-phase only model.

Application of the Model to the San Joaquin Valley of California on 4-5 January 1985

The Lagrangian radiation fog model has been applied to simulate atmospheric conditions in the San Joaquin Valley of California (Bakersfield's Meadows Field Airport) from 1700 PST on 4 January to 1000 PST on 5 January 1985. The main goals of this simulation are to evaluate the model's performance against a well documented episode and to improve our understanding of the interaction of the various physical and chemical processes taking place during a radiation fog. About 10 CPU hours on a micro-Vax III were required for the simulation.

During the 4th and 5th of January 1985 an extensive sampling network was operated in the San Joaquin Valley of California as a part of a two month study [Waldman, 1986; Jacob et al., 1987]. The gas-phase concentrations of SO_2 , HNO_3, and NH_3 were monitored. Aerosol samples were collected on open-faced Teflon filters, and fogwater samples were collected with a rotating arm collector. The fog liquid water content was determined from the collection rate of the rotating arm collector assuming a collection efficiency of 60%. The fogwater pH and the aqueous-phase concentrations of S(IV), HCHO, NH_4^+, SO_4^{2-}, NO_3^-, Cl^- and trace metals (Fe, Mn, Na, K, Ca, Mg, Pb, and Cu) were measured. The aerosol concentrations of NH_4^+, NO_3^-, SO_4^{2-}, Cl^- and several trace metals were determined. Additionally, the fog deposition rates for the major ions were monitored using polystyrene petri dishes and polyethylene buckets. Surface

winds in the valley were determined at several sites and vertical profiles of temperature, relative humidity, wind speed and wind direction were recorded every 4-8 using a tethersonde. An inert tracer was continously released for 23 hours between 1800 PST on 4 January and 1700 PST on 5 January 1985 to monitor the fate of sulfur dioxide in the valley. The complete data sets have been reported by Waldman [1986] along with detailed descriptions of the sampling techniques used.

Input Data for the model

All the field data used are from the work of Waldman [1986] and Jacob et al. [1987] for the Bakersfield site unless another source is mentioned. Measured vertical profiles for temperature are presented in Figure 4. The profiles for 1700 PST have been used as initial conditions for the fog model. The profiles predicted by the fog model are also presented in the same figure. Due to lack of any other information the initial soil temperature has been chosen to vary according to $T_s = 278.25 - 12.25z$ for $-0.4\text{m} < z \leq 0$ and ($T_s = 283.15$ K) for -1 m $< z \leq -0.4$ m in agreement with Forkel et al. [1984]. Representative soil properties assumed here are, $K_s = 3.210^{-7}$ m^2s^{-1}, $c_s = 1255$ J kg K^{-1} and $\rho_s = 1600$ kg m^{-3} [Zdunkowski and Nielsen, 1969]. The wind speeds at the 2.85 m level during this night were lower than 2 m s^{-1}. A constant value of 1.5 m s^{-1} has been assumed for the simulation.

The emissions are taken from the NAPAP 5.2 1980 emissions inventory [U.S. Environmental Protection Agency, 1986] for a winter weekday, with the exception of SO_2 and NH_3 emissions. The SO_2 emission rate is assumed constant at 7.1×10^{-10} kg m^{-2} s^{-1}, obtained from a 1984 SO_2 inventory for the San Joaquin Valley [Aerovironment, Inc., 1984]. An NH_3 emission rate of 3.4×10^{-11} kg m^{-2} s^{-1} has been used for the San Joaquin Valley based on the estimation of Jacob [1985].

Initial gas-phase concentrations for SO_2, NH_3, HNO_3, and aerosol particle mass

concentrations for SO_4^{2-}, NO_3^-, and NH_4^+ are based on the corresponding ground-level measurements. The remainder of the gas-phase concentrations are computed by an extra simulation using the gas-phase submodel from 0000 to 1700 PST on January 4. Due to lack of other information, an initial H_2O_2 vapor concentration of 2 ppb has been assumed based on the measurements of Heikes et al. [1987]. The aqueous-phase concentrations of Fe^{3+} and Mn^{2+} are assumed to be 225 and 33 μg / liter water according to the observations of Waldman [1986] for this fog episode.

Fog Development

The radiation model predicts that radiation fog starts developing just after sunset (1700 PST), reaches a maximum height of about 230 m, and dissipates by 1000 PST, the morning of the next day. The predicted fog evolution is shown in Figure 3. The predicted start and end of the radiation fog agrees exactly with the observations of Waldman [1986]. The predicted fog height agrees with the relative humidity profiles measured by tethersonde. These profiles suggest that the first 210 m, 240 m and 270 m of the atmosphere were saturated at 0030, 0530 and 0900 PST, respectively. The predicted and observed temperature profiles (Figure 4) are in close agreement.

The hourly averaged liquid water content predicted at ground level is compared to the measured values in Figure 5. The maximum liquid water attained in the fog is predicted to be 0.28 g m^{-3} matching very closely the 0.29 g m^{-3} reported. The model appears to have a tendency of slightly overpredicting the liquid water content of the fog.

The predicted hourly averaged liquid water deposition rates are presented in Figure 6. A maximum of 24.6 g m^{-2} hr^{-1} is attained around midnight. These liquid water rates are closely consistent with the deposition velocities of 1 to 3 cm s^{-1} reported by Waldman [1986].

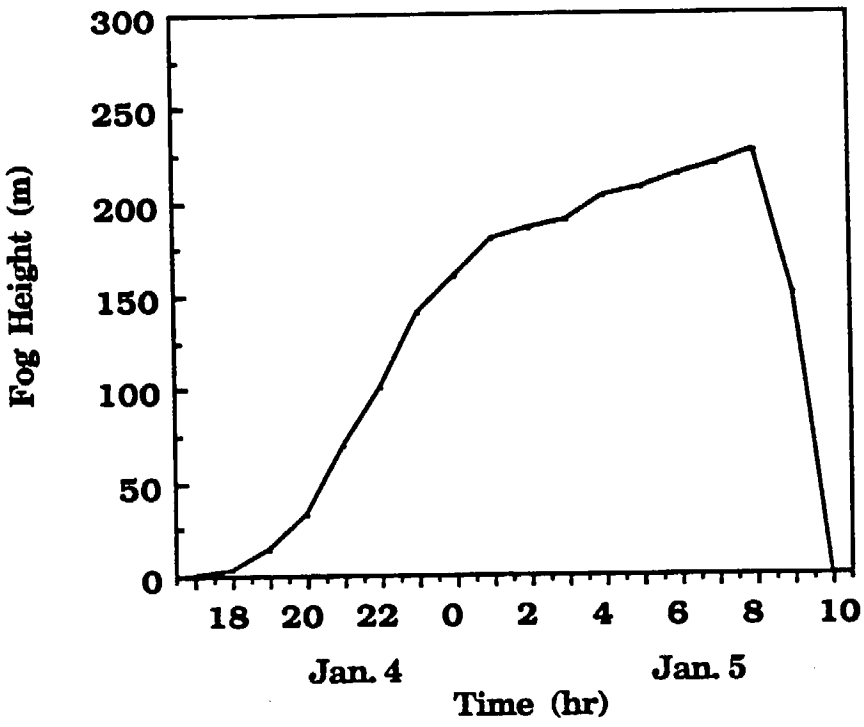

Figure 3 Predicted top of the fog layer.

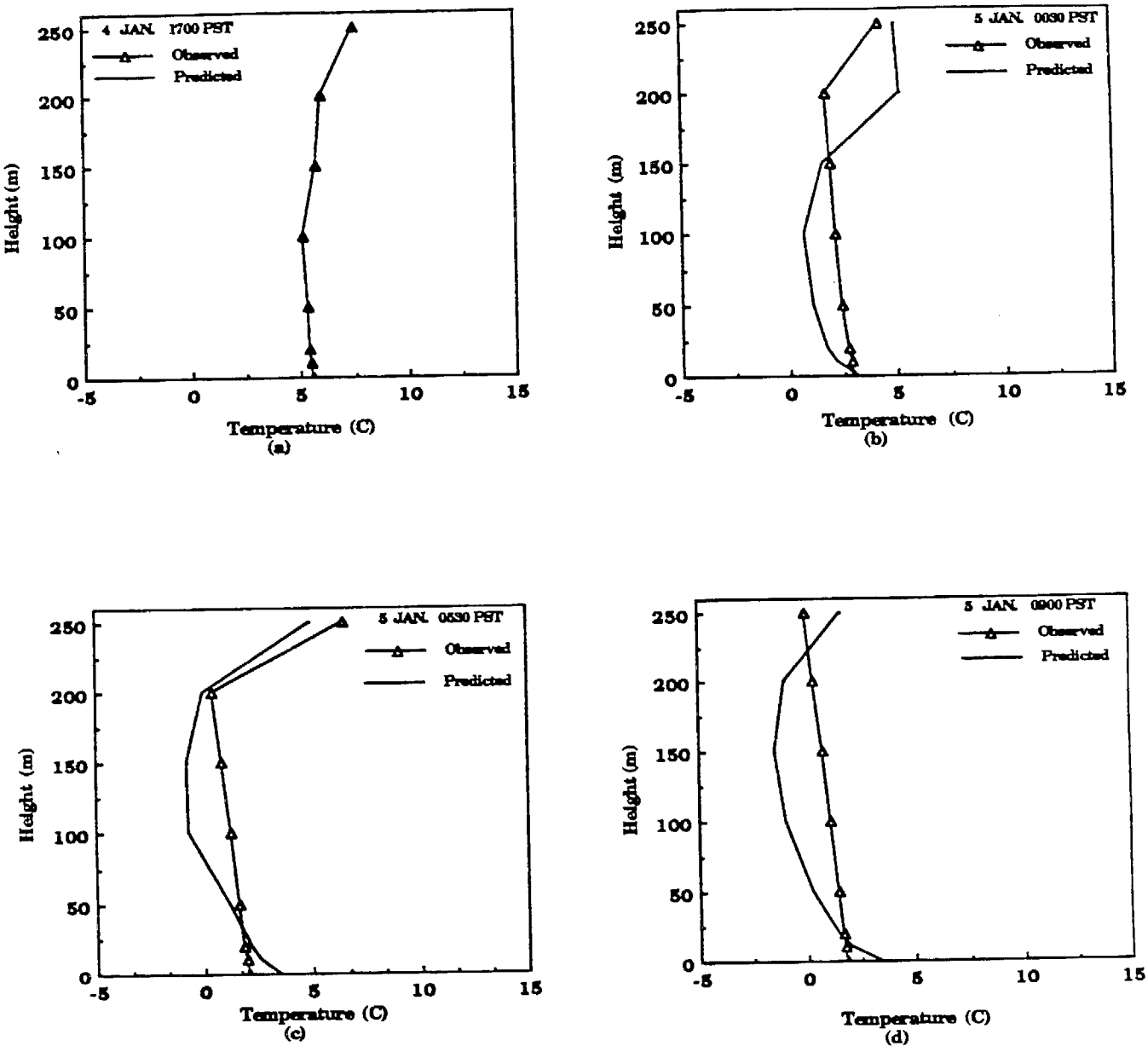

Figure 4 Comparison of the vertical temperature profiles predicted by the model with the observations of Waldman (1986).

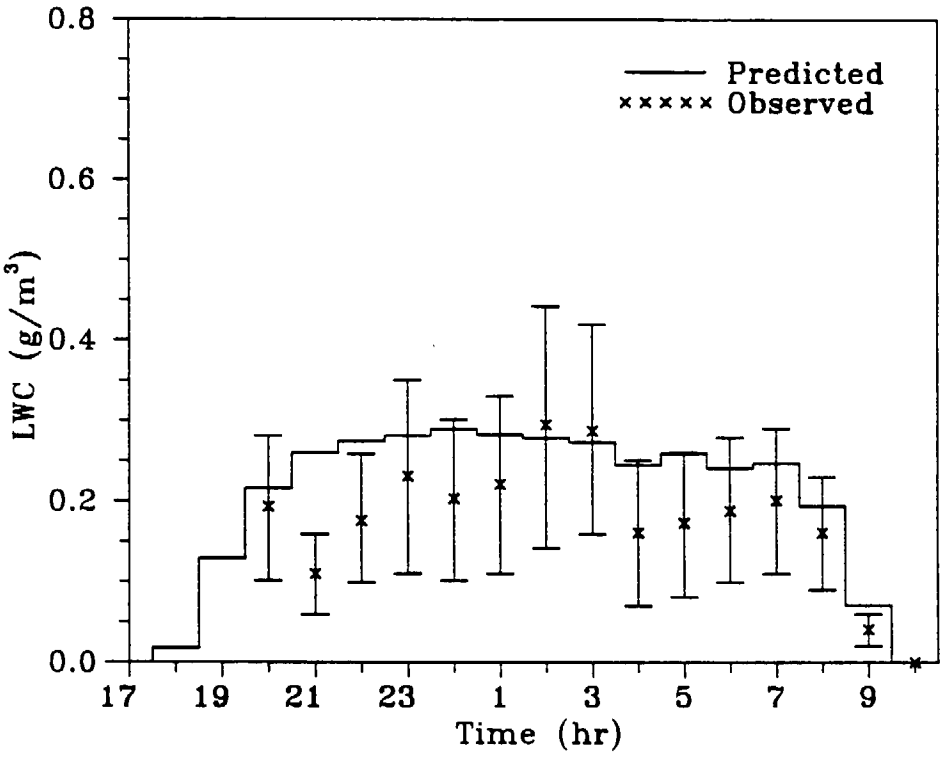

Figure 5 Comparison of the predicted hourly averaged liquid water content for the ground-level grid cell with the observations of Waldman (1986). The uncertainty in the measurements as reported by Waldman (1986) is indicated by the data ranges.

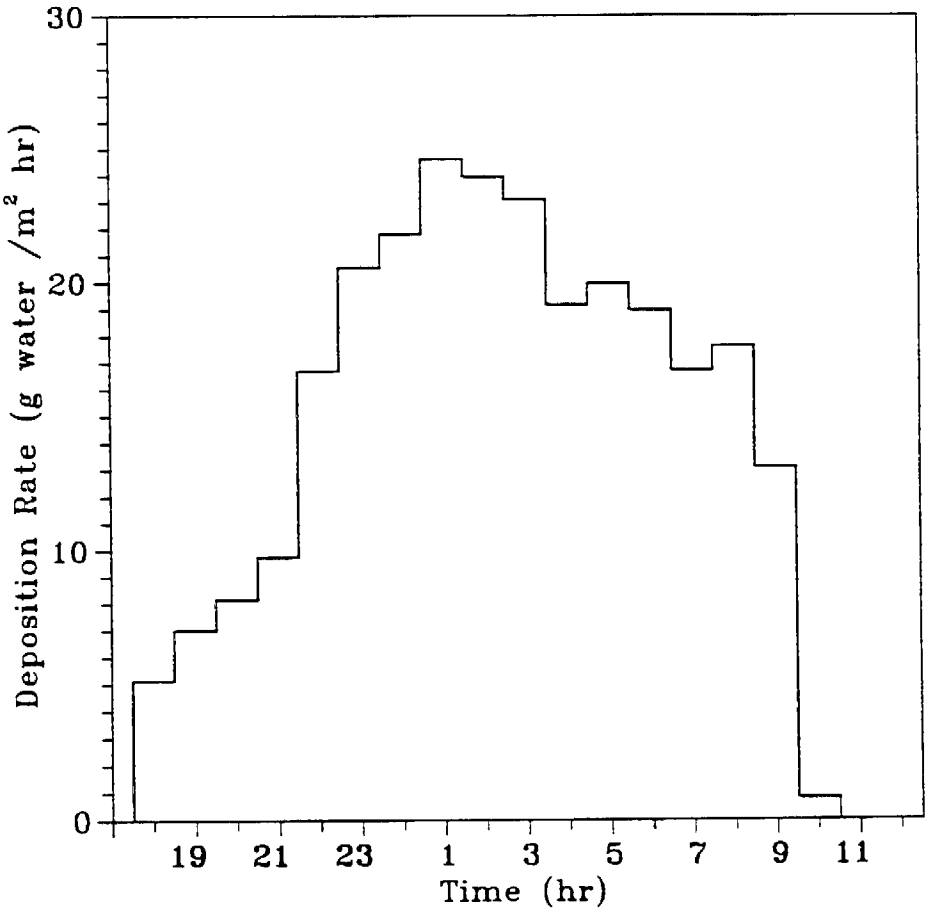

Figure 6 Predicted hourly averaged liquid water deposition rates.

The results indicate that the radiation fog submodel is very succesful in describing the observed fog development and in predicting variables of interest like the liquid water content, the liquid water deposition rates and the fog height.

Three representative calculated liquid water profiles are shown in Figure 7. An interesting feature is that after the initial fog development stage, after midnight in this simulation, the liquid water profile starting at a few meters high and ending near the fog top remains relatively flat.

Species concentrations in the aqueous and gas-phase

Predicted and observed hourly averaged values for the pH and the aqueous-phase concentrations of NH_4^+, SO_4^{2-} and NO_3^- are presented in Figure 8.

The pH of the fog at ground level is initially around 7.0, gradually drops to 4.5 at 0700 PST as the fog is developing and in the dissipation stage of the fog it drops further reaching a value of 3.3 at 0900 PST. The pH prediction of the model is very good with a small tendency to underestimate.

The major ionic species in fogwater are in this case NH_4^+, SO_4^{2-} and NO_3^-. The high pH during most of the fog is a result of the ammonia emissions in the area due to widespread agricultural and livestock activities. The maximum predicted concentration of NH_3, 2000 μeq /liter, as well as the rest of the predicted values, are in close agreement with the reported values.

The SO_4^{2-} is the anion that closely balances NH_4^+. The hourly averaged sulfate concentrations do match closely the observed concentrations with a tendency of the model to overpredict the sulfate concentrations. The reasons for this overprediction will be examined later. A result of this sulfate overprediction is the pH underprediction observed above.

The aqueous-phase concentration of nitric acid remains much smaller than the am-

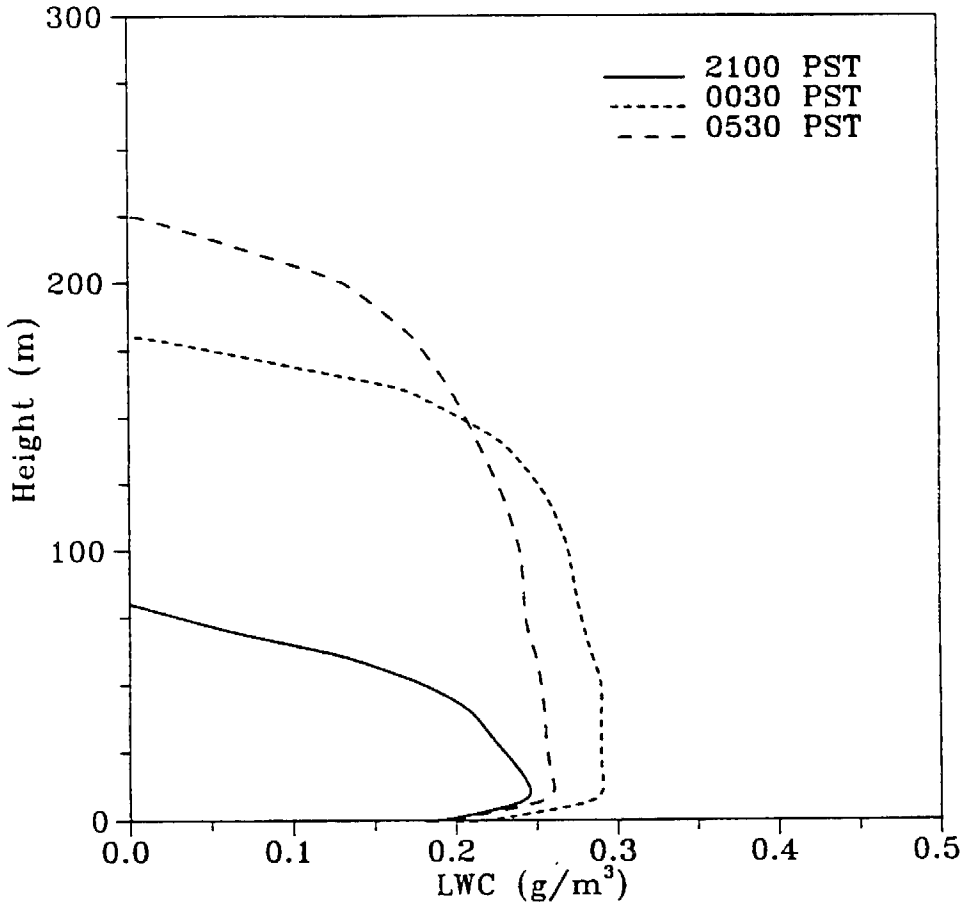

Figure 7 Predicted vertical liquid water concentration profiles for 2100, 0030, and 0530 PST.

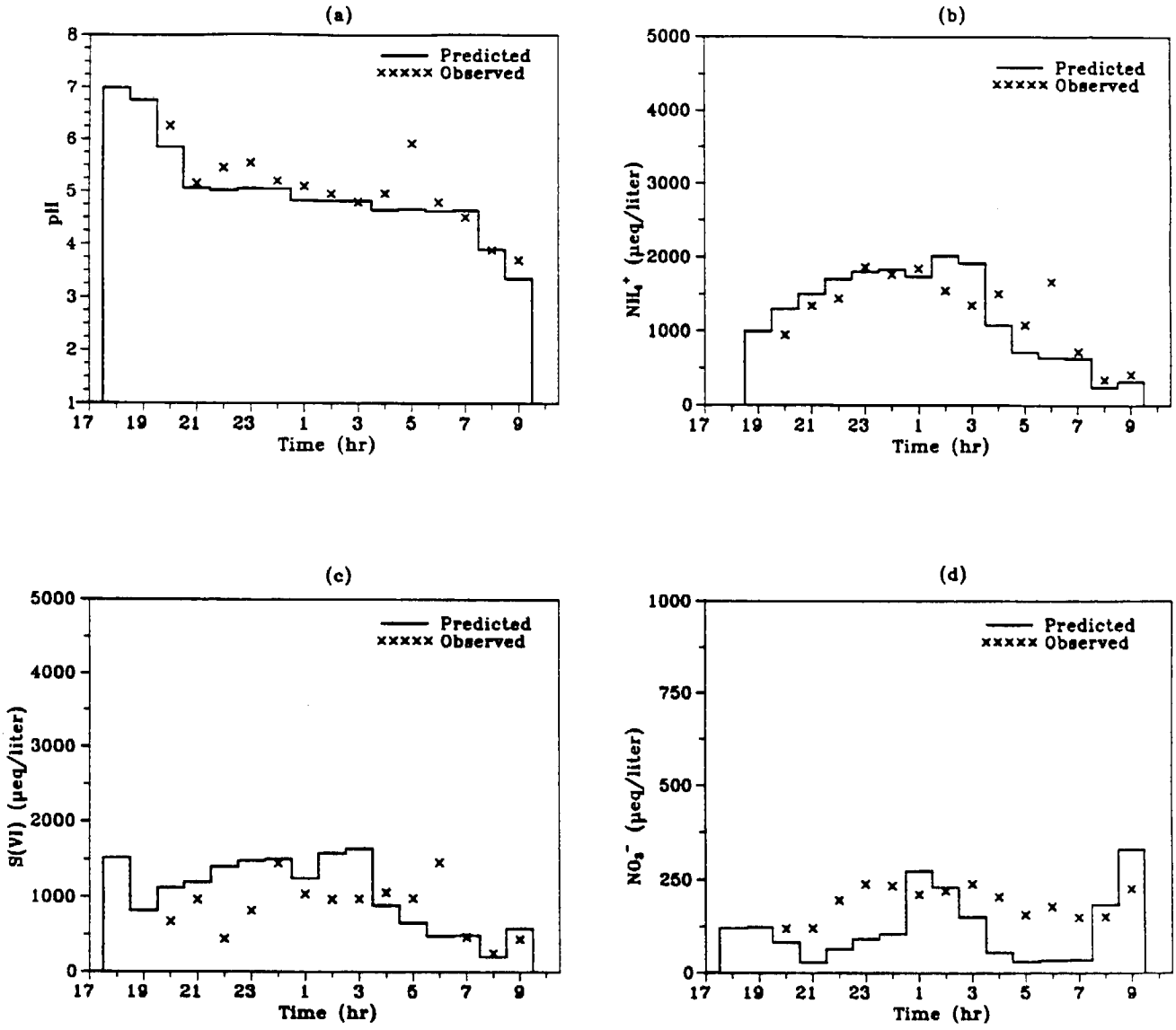

Figure 8 Comparison of the predicted hourly averaged (a) pH values, (b) NH_4^+, (c) S(VI), (d) NO_3^- concentration for the ground-level grid cell with the observations of Waldman (1986).

monia and sulfate concentrations throughout the simulation until the fog dissipation stage. The maximum predicted concentration (excluding the fog dissipation) of nitric acid is 270 μeq / liter versus the maximum observed value 240 μeq / liter. The model results indicate a larger variation in the nitrate concentrations than observed and generally the observed values are somewhat higher than predicted. Possible explanations include the use of an incorrect initial gas and nitrate aerosol concentration profile, or an underprediction of the gas-phase nitric acid production rate.

The predicted and observed gas-phase concentrations of SO_2 at ground level are shown in Figure 9. The model predictions once more match adequately the observed values. An average concentration of 40 ppb is maintained during the night.

The behavior of the gas-phase concentrations of HNO_3, NH_3 and H_2O_2 is quite interesting (Figure 10). At 2300 the fog has reached a height of 140 meters. When the aqueous phase is not present in a cell these three species exist in the gas-phase. When the fog enters a cell these species rapidly disappear either because of their high solubility in the aqueous phase (NH_3 and HNO_3) or because of fast reactions in the aqueous-phase (H_2O_2). In this respect the gravitational settling of the fog results in a 'cleaning' of the lower atmosphere of these three species. The above model predictions agree with the reported gas phase concentrations of HNO_3 and NH_3 [Waldman, 1986] and the mutual exclusivity of SO_2 and H_2O_2 in in clouds reported by Kelly et al. [1985].

Effect of the fog development on the aerosol mass

The influence of the fog development on the dry aerosol mass concentration in the modelling region can be examined (Figure 11). The concentrations of sulfate, nitrate and ammonium before the fog development are the observed values that have already been used as initial conditions. To estimate the corresponding concentrations after the fog dissipation we use the concentrations of these species at 0845. The average

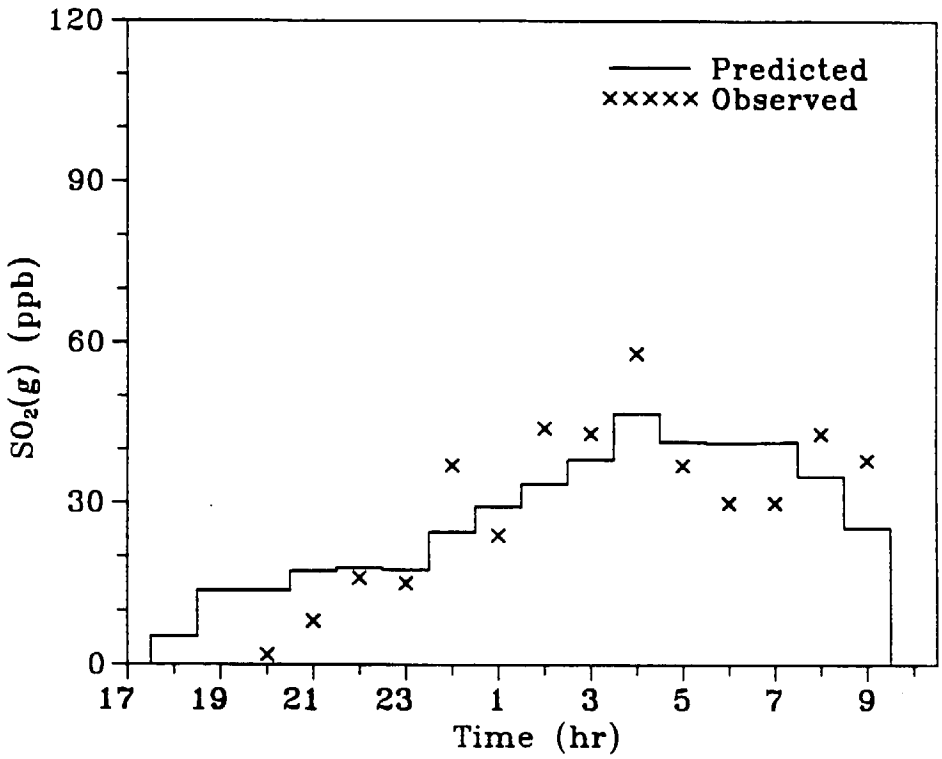

Figure 9 Comparison of the predicted hourly averaged $SO_2(g)$ concentration for the ground-level grid cell with the observations of Waldman (1986).

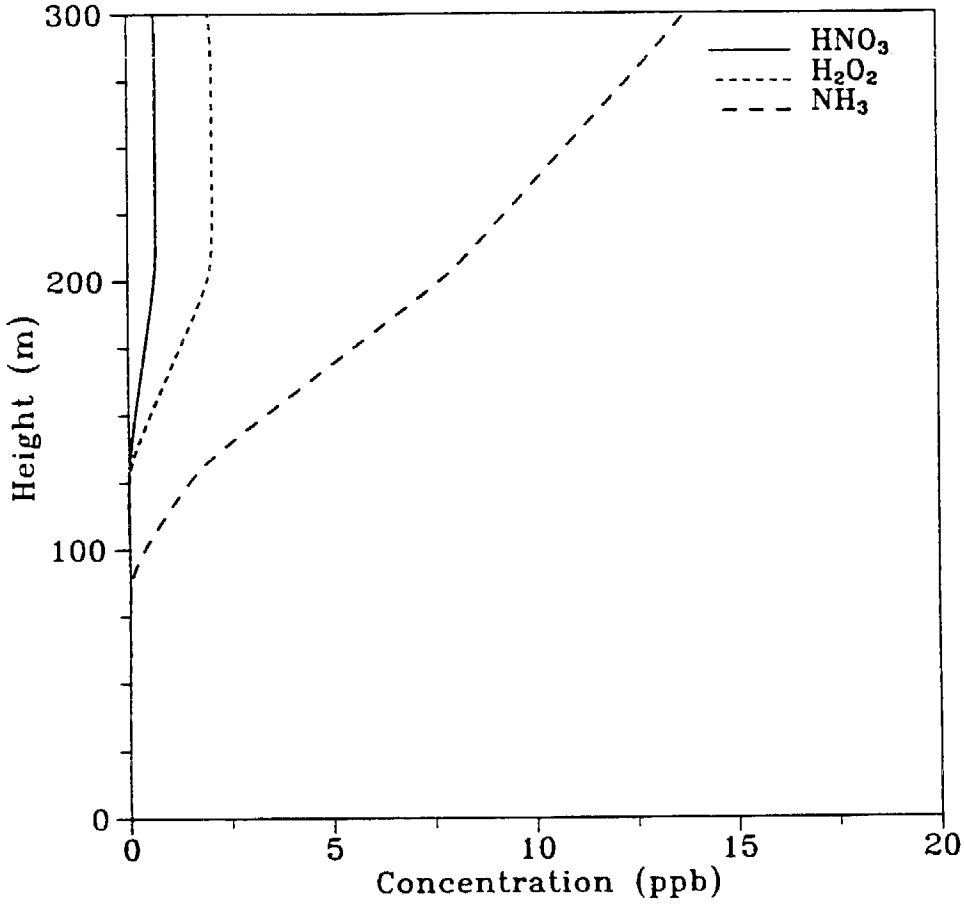

Figure 10 Predicted HNO_3, H_2O_2, and NH_3 vertical gas-phase concentration profiles for 2300 PST.

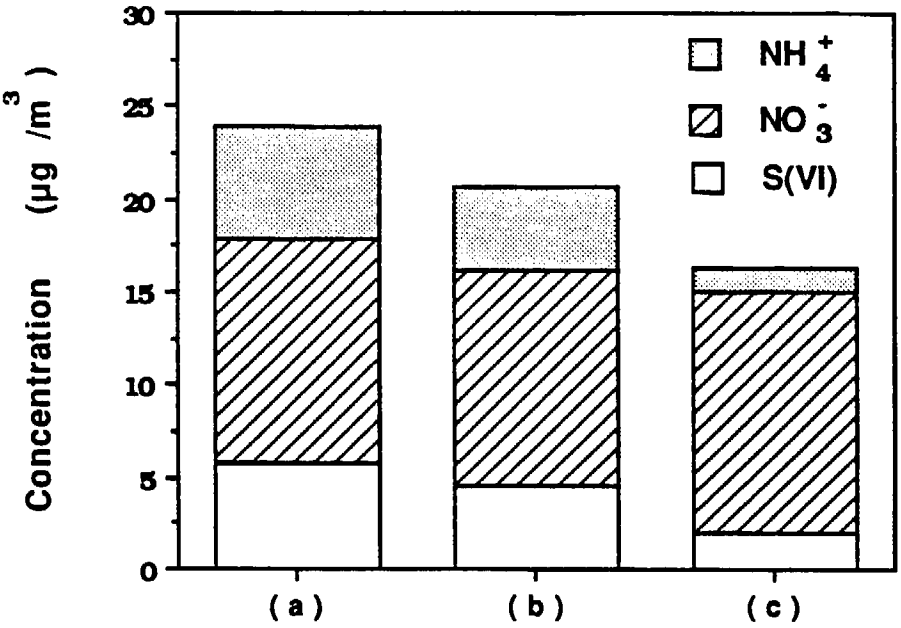

Figure 11 Concentrations of the principal ionic species in the aerosol phase (a) vertically averaged concentration before fog formation (observed values used as initial conditions in the simulation) , (b) predicted vertically averaged concentration after fog dissipation, (c) predicted concentration for the ground-level grid cell after fog dissipation.

concentrations refer to the entire modelling region (1000 m). A large part of this region has not been influenced substantially by the fog that occupied the lower 250 m only.

The predicted aqueous-phase concentrations for sulfate and ammonium suggest that for the case studied here, the corresponding aerosol concentrations will be reduced especially near the ground. The nitrate concentration remains practically unchanged. The reasons for this behavior lie in the sinks and sources of these species under foggy conditions. The only source of ammonia is the ground-level emissions. The fog accelerates significantly the deposition of ammonia resulting in a significant decrease of the ammonium concentration in the aerosol phase. The decrease of the sulfate concentration is found to be less than that of ammonium due to the production of sulfate in the aqueous phase. The relatively small change in the nitrate concentrations is due to the production of nitric acid in the gas phase during the last hour of the fog life. This production is much faster near the ground where the NO_2 concentrations are higher in the early morning. This HNO_3(g) is dissolved rapidly in the still existing aqueous-phase resulting in a higher nitrate concentration.

An additional important question that should be addressed in the future concerns the effects of the fog formation on the number concentration of aerosol particles as well as their size distribution. The present model can only predict aerosol mass and a rigorous discription of the aerosol particle microphysics must be added to address the above question.

Wet deposition rates

The average predicted and observed wet deposition rates for the major ionic species are presented in Figure 12. The observed values are measured at the ground level. The model tends to overpredict the deposition of all three species. The main reason for this

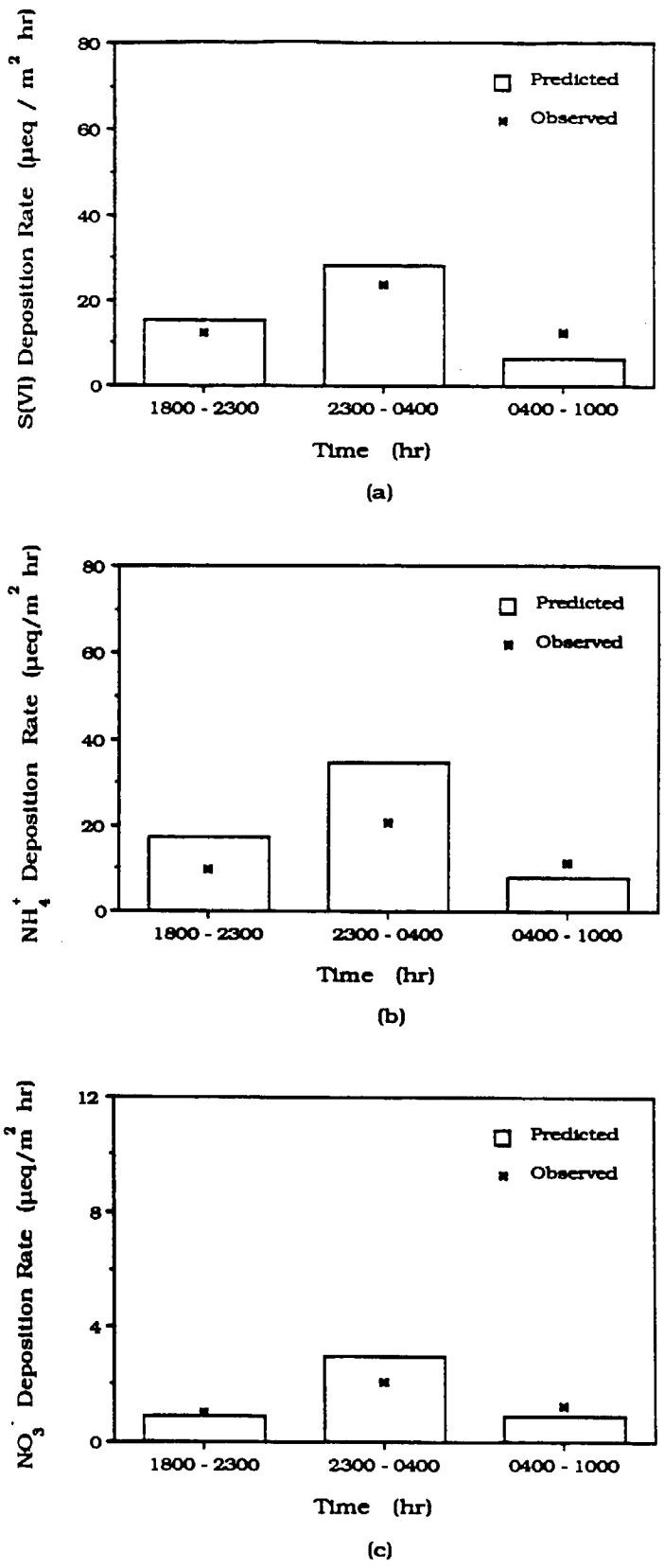

Figure 12 Comparison of the predicted average wet deposition rates over three time periods with the observations of Waldman (1986) for (a) S(VI), (b) NH_4^+, (c) NO_3^-.

is probably our assumption that the fog deposition velocity depends linearly on the liquid water content. Waldman [1986] reports that during this episode the liquid water variations appeared to be principally a function of droplet number concentration and the mass median diameters remained in a relative narrow range. Therefore we have probably overpredicted the fog deposition velocity especially for the high liquid water values.

During the fog dissipation stage (0400 to 1000) the deposition rates are underpredicted because of the underprediction at this time of the corresponding aqueous-phase concentrations (Figures 8b, 8c and 8d). The observed values of ammonia deposition rates are according to Waldman a lower bound due to ammonia losses so disparity between the model and the actual values is less than appears in Figure 12b.

An interesting question that can be addressed is the effect of the fog formation on the total deposition rates. We have performed an additional simulation for the imaginary scenario that no fog was formed during the night of 4 to 5 of January. During this scenario the only mechanism for deposition is the dry deposition of gases and aerosol. The calculation was performed according to the model described by McRae et al. [1982]. Due to the various simplifications used the dry deposition rates are only reasonable estimates.

The results of this simulation are presented as the average deposition rates for the 16 hour period from 1800 January 4 to 1000 January 5 (Figure 13). These calculations suggest that because of the fog formation the total average deposition rate increased almost three times. The deposition of S(IV) is found to increase only 25% because the gas-phase concentration decreases during the fog period. The most interesting change is the deposition of sulfate that increases about 30 times because of the sulfate production in fogwater. Ammonia and nitric acid gas phase concentrations are very low inside the fog so the corresponding dry deposition rates are very small and the net increase is

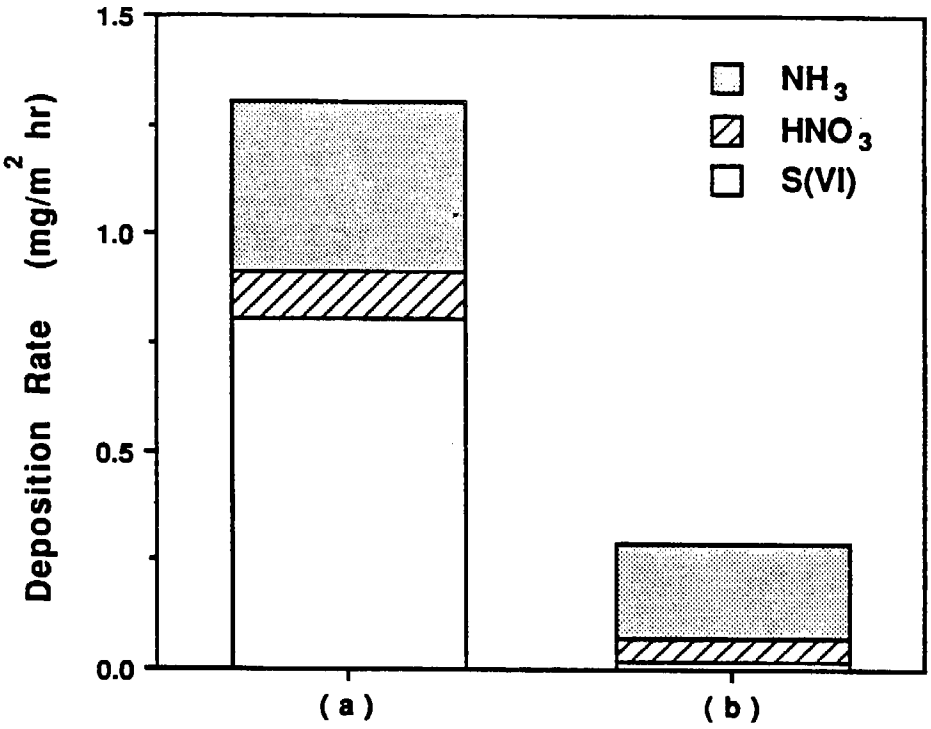

Figure 13 Comparison of the predicted average deposition rates for the same 16 hour period in (a) presence of radiation fog, (b) absence of radiation fog.

only twofold.

Sulfate Production

The main chemical change taking place in fogwater is the oxidation of S(IV) to S(VI) [Pandis and Seinfeld, 1989]. A mass-balance for sulfur is presented in Figure 14 including the deposited masses of S(IV)(aq), SO_2(g) and S(VI). The mass of sulfur existing as S(IV)(aq) has not been included in the figure because it is much smaller than the rest of the entries.

During this fog episode the main pathways for the production of sulfate are the oxidation of S(IV) by H_2O_2, O_2 (catalysed by Fe^{3+} and Mn^{2+}), HSO_5^- and NO_2 (Figure 15). Hydrogen peroxide oxidizes S(IV) rapidly but is also depleted rapidly because of the excess of SO_2(g) in cases like the present one. One would expect that under these conditions the contribution of hydrogen peroxide to the SO_2 oxidation would be negligible shortly after the fog develops. This is, however, not the case. Due to the very stable conditions during the radiation fog life, hydrogen peroxide continues to exist in significant concentrations above the fog (Figure 10). As the fog continues to grow, new hydrogen peroxide is entrained into the fog and is available to oxidize S(IV). This process continues for almost 8 hours after the beginning of fog development, until 0200. After this time the contribution of hydrogen peroxide to S(IV) oxidation is indeed zero.

Due to the ammonia that gets continously dissolved in the aqueous-phase the pH of the fog is always greater than 4 except during the last two hours of fog life. Under these conditions the Fe^{3+} and Mn^{2+}-catalysed oxidation of S(IV) is predicted to be a major contributor to sulfate formation. After hydrogen peroxide is depleted from the fog region, this reaction becomes the major pathway for the S(IV) to S(VI) transformation.

The gas phase concentration of ozone during the night remains close to zero and

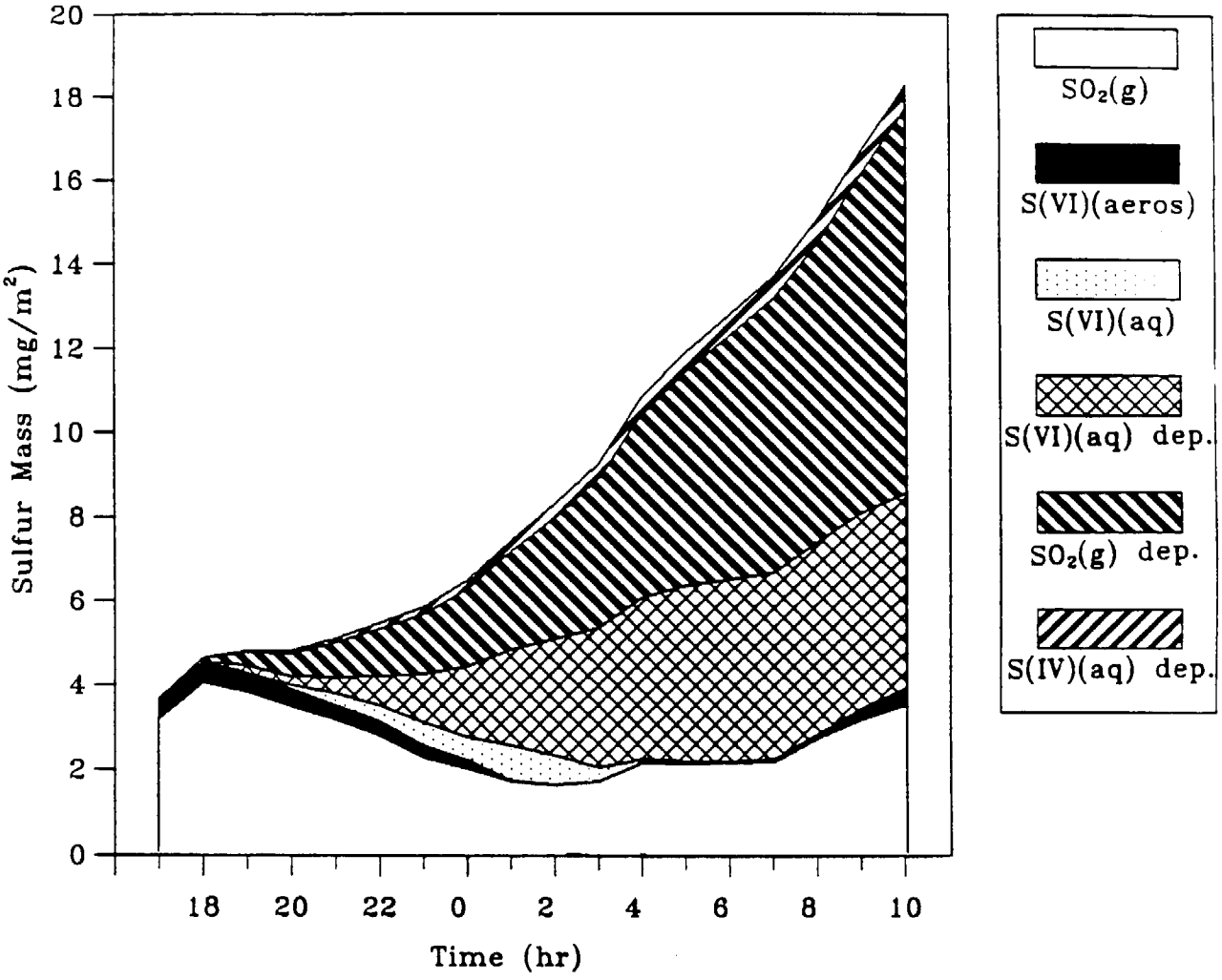

Figure 14 Predicted sulfur mass balance for the lower 250 m of the atmosphere.

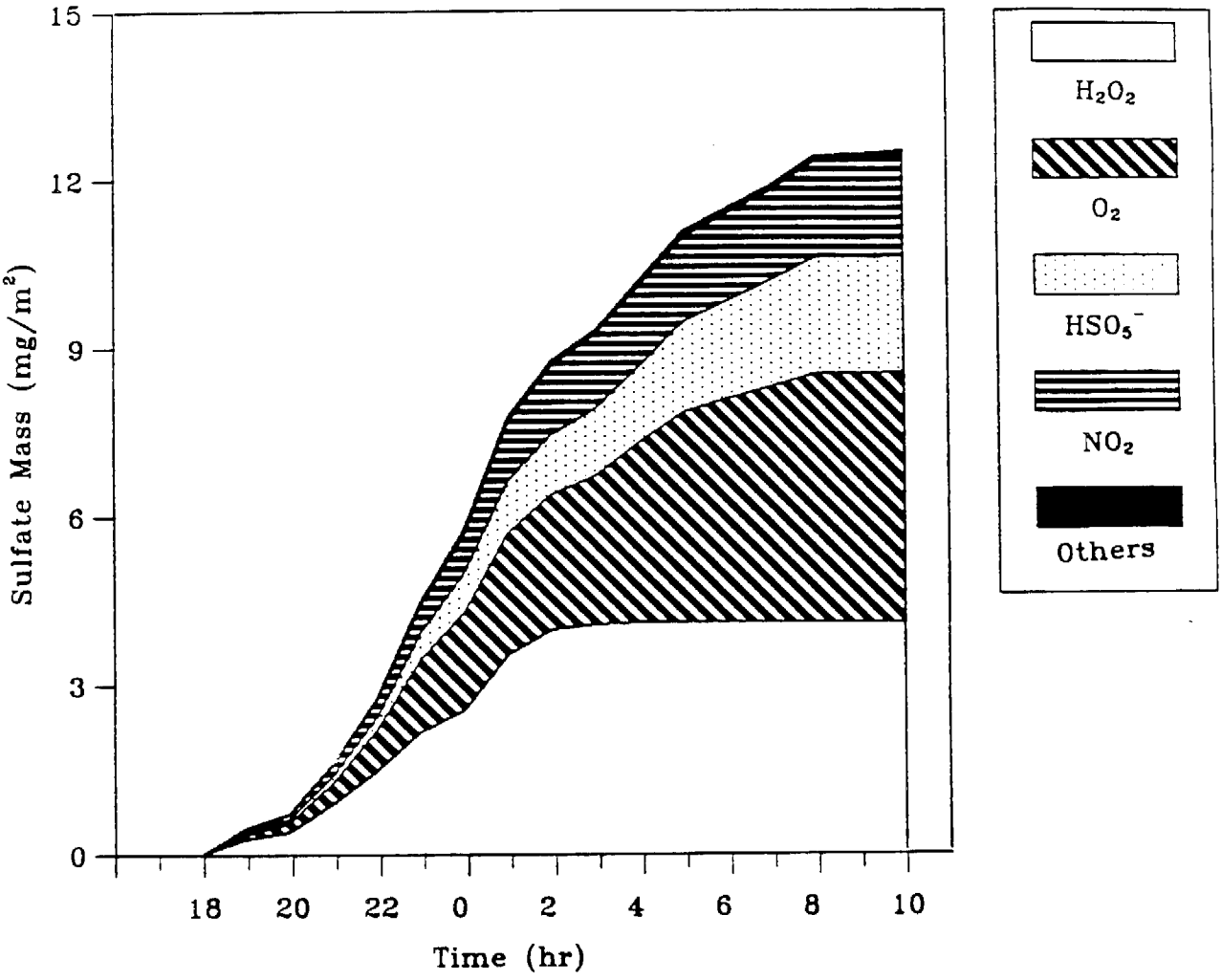

Figure 15 Pathways for the production of sulfate during the radiation fog episode.

therefore the oxidation of S(IV) by ozone in the aqueous-phase is negligible. When ozone concentrations start to increase (around 0800) the fog has already begun to dissipate and the fog pH is lower than 4 resulting again in negligible S(IV) oxidation by ozone.

An important pathway for sulfate production during this fog episode is the oxidation of S(IV) by HSO_5^-:

$$HSO_5^- + HSO_3^- \xrightarrow{H^+} 2HSO_4^- + 3H^+$$

HSO_5^- is one of the products appearing in the oxidation chain initiated by the attack of OH(aq) to S(IV) and propagated by further reactions of the radicals SO_4^-, SO_5^- and HSO_5^- [Jacob, 1986; Pandis and Seinfeld, 1989].

A reaction that under the present conditions is found to contribute considerably to the sulfate production is that of S(IV) with NO_2:

$$2NO_2 + HSO_3^- \xrightarrow{H_2O} SO_4^{2-} + 3H^+ + 2NO_2^-$$

This reaction has been studied by Lee and Schwartz [1983] at pH 6.4, 5.8 and 5.0 and was described as a reaction that is first order in NO_2 and first order in S(IV), with a pH dependent rate constant. The evaluation of this rate expression was considered tentative by Lee and Schwartz in view of evidence for the formation of a long-lived intermediate species. The apparent rate constant was found to increase with increasing pH. This reaction was considered of secondary importance at the concentrations and pH values representative of clouds. Under the conditions of the radiation fog in the San Joaquin Valley the importance of this reaction increases considerably over that in clouds. The major reason is that the emitted NH_3 is scavenged by the fog droplets maintaining a low fogwater acidity. Therefore this reaction is not self limiting in fog to the extent that it is in clouds. Other reasons for the significance of this reaction for

this case are the relatively high gas phase concentrations of SO_2 and NO_2. Radiation fogs develop under stable meteorological conditions, and in polluted environments they occur at the same altitude as the sources of SO_2 and NO_x. Consequently the gas phase concentrations of SO_2 and NO_2 can be much higher in a fog than inside a cloud and the aqueous-phase reaction of S(IV) with NO_2 can be much faster.

Due to the remaining questions concerning the kinetics of this reaction our results should be considered tentative. The fact that the model overpredicts the sulfate concentrations could be the result of a high initial H_2O_2 concentration, an overprediction of the oxidation of S(IV) by NO_2, or an overprediction of the S(IV) oxidation rate by O_2 (catalysed by Fe^{3+} and Mn^{2+}).

Sensitivity to deposition

The sensitivity of the model to the expression of the mean settling velocity, u_{av}, as a function of the liquid water content has been investigated by performing an additional simulation using the value $a_g = 0.06$ (case II) instead of $a_g = 0.12$ used for the base case (case I). Therefore, for the same liquid water content, the settling velocity in case II is half the settling velocity of case I. This reduction in settling velocity accelerates the fog growth by 10-20 m, and increases the liquid water content of the fog by almost 30%. The mature fog in case II has a liquid water content of 0.38 g water m^{-3}. The rate of liquid water mass deposited to the ground in case II is only around 10% less than that in case I. This is due to the fact that the decrease of the water deposition rate because of the smaller value of the parameter a_g is partially balanced by the increase of the liquid water content.

The aqueous-phase concentrations of the main ionic species, S(VI), NH_4^+ and NO_3^- in case II, are initially (at 2000 PST) around 25% lower than the corresponding concentrations in case I because the incease of the liquid water causes a higher dilution.

Therefore case I is characterized initially by higher ionic concentrations and higher water deposition rates than case II, or equivalently by higher initial ionic deposition rates. This difference in the deposition rates of the major ions causes a convergence of the calculated ionic concentrations and after 0400 PST the calculated concentration difference is less than 5%. At the same time the total mass of the ionic species dissolved in the aqueous-phase is for case II as much as 30% larger compared to case I due to the higher liquid water content.

Summarizing, a 50% decrease in the parameter a_g causes an average increase of the fog liquid water content by 30%, an average decrease of the liquid water deposition rate by 10%, an initial decrease of 25% in the aqueous-phase concentrations of the major ions that finally reduces to less than 5% and an increase of the total mass of the major ions in the aqueous-phase by as much as 30%. These results indicate that a good estimate of a_g is required by the model and furthermore that the gravitational settling of fog droplets affects considerably the chemical composition of fogwater.

An additional test has been performed to study the importance of the deposition process in acidic deposition. In an imaginary scenario the water droplet settling has been neglected and the liquid water content has been assigned a constant value of 0.3 g m^{-3}, conditions that can be generally applied to a cloud simulation (case III). Only one computational cell has been used for this simulation and the rest of the conditions (initial gas and aerosol concentrations, emissions etc) are the same as in the base case (case I). The fact that all the liquid water remains in the modelling region results in much higher concentrations of the major ionic species. The average S(VI), NH_4^+, and NO_3^- are 2.5, 3 and 2.7 times larger in case III than in the base case. The pH in case III remains higher than in the base case until the fog dissipation stage when the pH is practically the same for both case. The higher pH in case III can be explained by the fact that the neutralizing agent, ammonia, is not depleted from the system, keeping

the pH at higher values. The gradual increase in the sulfate and nitrate concentrations finally compensates for this higher ammonia concentration and the pH difference for the two cases becomes essentially zero after 0600 PST.

Conclusions

The physical and chemical processes leading to acidic deposition during a radiation fog episode have been studied using a one-dimensional mathematical model. The model used in this study combines a detailed description of gaseous and aqueous-chemistry with a dynamic model describing radiation fog development. Variables predicted by the model include the vertical profiles of temperature, relative humidity and liquid water content, the vertical concentration profiles of species in the gaseous and aqueous-phase and the wet deposition rates for all species.

Application of the model to a radiation fog episode in Bakersfield in the San Joaquin Valley of California over the period January 4-5, 1985 shows that the model predictions for temperature profile, fog development, liquid water content, gas-phase concentrations of SO_2, HNO_3 and NH_3, pH, aqueous-phase concentrations of SO_4^{2-}, NH_4^+ and NO_3^-, and finally deposition rates of the above ions match well the observed values.

The formation of the specific radiation fog causes reduction of the aerosol NH_4^+ and SO_4^{2-} content. The NO_3^- content remains practically the same as that predicted in the absence of a fog due to production of nitric acid in the gas-phase during the last three hours of the fog life and subsequent dissolution of the HNO_3 in the existing aqueous-phase. The deposition rates of the major ions are found to increase drastically during the fog episode with most notable the increase of sulfate deposition.

Several differences exist between a radiation fog and a representative cloud environment. Radiation fog develops typically under stable conditions resulting in weak

mixing and significant gradients in the vertical profiles of species like hydrogen peroxide, ammonia and nitric acid. The deposition process during a dense radiation fog leads to rapid removal from the atmosphere of the major ionic species and tends to keep their corresponding fogwater concentrations to lower values. Because of the proximity of the fog to ground-level sources of pollutants like SO_2 and NO_x, the corresponding gas-phase concentrations can reach much higher levels than in a cloud. In such a case, pathways for the sulfate production that are of secondary importance in a cloud environment may become significant in a fog.

Expressing the mean droplet settling velocity as a function of the liquid water content is found to be very influential in the prediction of the fog liquid water content, the total masses of the major ionic species in the aqueous-phase and the concentrations of these species in the first haf of the fog life.

In the present model aerosol or fog droplet size-dependent processes such as aerosol nucleation, condensation and coagulation, droplet growth, evaporation and settling have either been described in terms of overall properties of the fog or have been omitted. The next level of detail in the modelling of acid deposition due to fog episodes requires the coupling of the this model with one describing aerosol and fog-droplet microphysics.

Acknowledgements

We would like to thank Prof. W. G. Zdunkowski and Dr. A. Bott, Institut für Meteorologie, Johannes Gutenberg Universität, Mainz, for providing us with the code for the radiation scheme and for their helpful comments. We would like also to thank Dr. W. P. L. Carter, University of California, Riverside, for providing us with his software for the gas-phase mechanism preparation and emissions processing. This work was supported by the State of California Air Resources Board under Agreement A732-043.

References

Aerovironment Inc., AVKERN Application Report AV-FR-83/501R2, Pasadena, Calif., 1984.

Brown R., A numerical study of radiation fog with an explicit formulation of the microphysics, *Quart. J. Roy. Met. Soc.*, 106, 781-802, 1980.

Brown R. and Roach W. T., The physics of radiation fog: II - a numerical study, *Quart. J. Roy. Met. Soc.*, 102, 335-354, 1976.

Carter W. P. L., Lurmann F. W., Atkinson R., and Lloyd A. C, Development and testing of a surrogate species chemical reaction mechanism, EPA-600/3-86-031, 1986.

Carter W. P. L. and Atkinson R., Development and implementation of an up-to-date photochemical mechanism for use in airshed modeling, Summary final report to California Air Resources Board, 1988.

Chameides, W. L., The photochemistry of a marine stratiform cloud, *J. Geophys. Res.*, 89, 4739-4755, 1984.

Eagleman, J. R., Meteorology. The atmosphere in action, Wadsworth Publishing Company, Belmont CA, 1985.

Environmental Protection Agency, Development of the 1980 NAPAP emissions inventory, report EPA/600/7-86/057a, 1986.

Fisher, E. L. and Caplan, P., An experiment in the numerical prediction of fog and stratus, *J. Atmos. Sci.*, 20, 425-537, 1963.

Forkel, R., Sievers, U. and Zdunkowski, W., Fog modelling with a new treatment of the chemical equilibrium condition, *Beitr. Phys. Atmosph.*, 60, 340-360, 1987.

Forkel, R., Panhans, W.-G., Welch, R., Zdunkowski, W., A one-dimensional nu-

merical study to simulate the influence of soil moisture, pollution and vertical exchange on the evolution of radiation fog, *Beitr. Phys. Atmosph.*, 57, 72-91, 1983.

Graedel, T. E. and Goldberg K. I., Kinetic studies of raindrop chemistry, 1. Inorganic and organic processes, *J. Geophys. Res.*, 88, 10865-10882, 1983.

Heikes B. G., Kok G. L., Walega J. G., and Lazrus A. L., H_2O_2, O_3, and SO_2 measurements in the lower troposhere over the eastern United States during the fall, *J. Geophys. Res.*, 92, 915-931, 1987.

Jacob D. J., Chemistry of OH in remote clouds and its role in the production of formic acid and peroxymonosulfonate, *J. Geophys. Res.*, 91, 9807-9826, 1986.

Jacob D. J., The origins of inorganic acidity in fogs, Ph.D. Thesis, California Institute of Technology, Pasadena, CA, 1985.

Jacob D. J., Waldman J. M., Munger J. W. and Hoffmann M. R., Chemical composition of fogwater collected along the California Coast, *Environ. Sci. Technol.*, 19, 730-736, 1985.

Jacob D. J. and Hoffmann M. R., A dynamic model for the production of H^+, NO_3 and SO_4^{2-} in urban fog, *J. Geophys. Res.*, 88, 6611-6621, 1983.

Jacob D. J., Shair F. H., Waldman J. M., Munger J. W. and Hoffmann M. R., Transport and oxidation of SO_2 in a stagnant foggy valey, *Atmos. Environ.*, 21, 1305-1314, 1987.

Kelly, T. G., Daum, P. H., Scwartz, S. E., Measurements of peroxides in cloudwater and rain, *J. Geophys. Res.*, 90, 7861-7871, 1985.

Lala, G. G., Mandel, E. and Jiusto, J. E., A numerical evaluation of radiation fog variables, *J. Atmos. Sci*, 32, 720-728, 1975.

Lee, Y-N and Schwartz, S. E., Kinetics of oxidation of aqueous sulfur(IV) by nitro-

gen dioxide in Precipitation Scavenging, Dry Deposition, and Resuspension, Volume I, H. R. Pruppacher, R. G. Semonin, and W. G. N. Slinn, eds., Elsevier, New York, 1983.

McDonald, J. E., The saturation adjustment in numerical modelling of fog, *J. Atmos. Sci.*, 20, 476-478, 1963.

McRae G. J., Goodin W. R. and Seinfeld J. H., Development of a second generation mathematical model for urban air pollution, I. Model formulation. *Atmospheric Environment*, 16, 679-696, 1982.

Munger J. W., Jacob D. J., Waldman J. M., Hoffmann M. R., Fogwater chemistry in an urban atmosphere, *J. Geophys. Res.*, 88, 5109-5121, 1983.

Munger J. W., Collett J., Daube B., Hoffmann M. R., Fogwater chemistry at Riverside California, *Atmos. Environ.*, (submitted), 1989.

Pruppacher H. R. and Klett J. D., Microphysics of Clouds and Precipitation, Reidel Pub. Comp., 1980.

Pandis S. N. and Seinfeld J. H., Sensitivity analysis of a chemical mechanism for aqueous-phase atmospheric chemistry, *J. Geophys. Res.*, 94, 1105-1126, 1989.

Schwartz, S. E., Gas- and aqueous-phase chemistry of HO_2 in liquid water clouds, *J. Geophys. Res.*, 89, 11589-11598, 1984.

Seigneur C. and Saxena P., A theoritical investigation of sulfate formation in clouds, *Atmos. Environ.*, 22, 101-115, 1988.

Seigneur C. and Saxena P., A study of atmospheric acid formation in different environments, *Atmos. Environ.*, 18, 2109-2124, 1984.

Shir C. C., A preliminary numerical study of atmospheric turbulent flows in the idealised planetary boundary layer, *J. Atmos. Sci.*, 30, 1327-1339, 1973.

Ten Brink, H. M., Schwartz, S. E. and Daum, P. H., Efficient scacenging of aerosol

sulfate by liquid water clouds, *Atmos. Environ.*, 21, 9, 2035-2052, 1987.

Tremblay A. and Leighton H., The influence of cloud dynamics upon the redistribution and transformation of atmospheric SO_2 - a numerical simulation, *Atmos. Environ.*, 18, 1885-1894, 1984.

Tremblay A. and Leighton H., A three-dimensional cloud chemistry model, *J. Climate appl. Met.*, 25, 652-671, 1986.

Turton, J. D. and Brown R., A comparison of a numerical method of radiation fog with detailed observations, *Quart. J. Roy. Meteor. Soc.*, 113, 37-54, 1987.

Waldman, J. M., Depositional aspects of pollutant bahavior in fog, Ph.D. thesis, California Institute of Technology, 1986.

Walcek, C. J. and Taylor G. R., A theoritical method for computing vertical distributions of acidity and sulfate production within cumulus clouds, *J. atmos. Sci.*, 43, 339-355, 1986.

Waldman, J. M., Munger J. W., Jacob D. J., Flagan R. C., Morgan J. J. and Hoffmann M. R., Chemical composition of acid fog, *Science*, 218, 677-680, 1982.

Zdunkowski, W. G. and Nielsen, B. C., A preliminary prediction analysis of radiation fog, *Pure and Appl. Geophys.*, 75, 278-299, 1969.

Zdunkowski, W. G., Welch, R. M. and Paegle, J., One-dimensional numerical simulation of the effects of air pollution on the planetary boundary layer, *J. Atmos. Sci.*, 33, 2399-2414, 1976.

Zdunkowski W. G., Panhans W-G., Welch R. M. and Korb G. J., A radiation scheme for circulation and climate models, *Beitr. Phys. Atmosph.*, 55, 215-238, 1982.

CHAPTER 4

ON THE RELATION BETWEEN THE SIZE AND COMPOSITION OF FOG AND CLOUD DROPLETS AND THE SIZE AND COMPOSITION OF ATMOSPHERIC AEROSOL

Chemical Composition Differences in Fog and Cloud Droplets of Different Sizes

Spyros N. Pandis, John H. Seinfeld

Department of Chemical Engineering and Environmental Quality Laboratory, California Institute of Technology, Pasadena, CA 91125, USA

and

Christodoulos Pilinis

AeroVironment Inc., 825 Myrtle Ave., Monrovia, CA 91016, USA

Abstract

The distribution of acidity and solute concentration among the various droplet sizes in a fog or cloud and the effect of the evaporation-condensation cycle on the composition and size distribution of atmospheric aerosol is studied. Significant total solute concentration differences can occur in aqueous droplets inside a fog or cloud. For the fog simulated here, during the period of dense fog, the solute concentration in droplets larger than 10 μm diameter increased with size, in such a way that droplets of diameter 20 μm attain a solute concentration that is a factor of 3.6 larger than that in the 10 μm droplets. Droplets on which most of the liquid water condenses have access to most of the reacting medium for in situ S(IV) oxidation and are therefore preferentially enriched in sulfate. The gas and aqueous-phase chemical processes result in an increase of the total solute mass concentration nonuniform over the droplet spectrum for a mature fog. These chemical processes tend to decrease the total solute mass concentration differences among the various droplet sizes. Low cooling rates of the system also tend to decrease these concentration differences while high cooling rates have exactly the opposite effect. The mass/size distribution of the condensation nuclei influences quantitatively, but not qualitatively, the above concentration differences.

Introduction

Atmospheric aerosols are multicomponent particles with sizes ranging roughly from 0.01 to 10 μm in diameter. It is well known now that the chemical composition of these aerosol particles varies significantly with size. At a specific relative humidity, which for most soluble components in the atmosphere is well below 100%, aerosol particles that are not already liquid deliquesce into aqueous solution drops. As the relative humidity keeps increasing, the droplets increase their size in accordance with water vapor equilibrium. If the relative humidity of the air parcel reaches a critical humidity, the value of which depends on the size and chemical composition of the aerosol present, the droplets become activated, grow freely by water vapor diffusion, and a cloud or fog forms. In addition to having solute concentration differences that arise from differences in the composition of the condensation nuclei, fog and cloud droplets scavenge soluble gases like nitric acid and ammonia and act as a medium for various aqueous-phase reactions, including the oxidation of absorbed SO_2 to sulfate.

Despite the fact that cloud microphysics suggests that diffusional growth of aqueous droplets could result in size dependent concentration and composition, the concentration/size distribution of cloud or fog droplets has not been quantitatively modeled. The main available experimental information on chemical composition differences in cloud droplets was reported by Noone et al. (1988) who sampled droplets from a marine stratus cloud and calculated that the volumetric mean solute concentration of the 9- to 18-μm droplets was a factor of 2.7 smaller than that in the 18- to 23-μm droplets. The concentration/size dependence of cloud or fog droplets has been addressed as a secondary problem in a few theoretical studies with inconclusive results. A study of Flossmann et al. (1985), using an entraining air parcel cloud model, suggested that the mass mixing ratio of the aerosol that served as condensation nuclei or was scavenged by the aqueous droplets is larger inside smaller drops than inside larger drops when

condensation and collision-coalescence are the dominant processes. Other theoretical studies (Hegg and Hobbs, 1979; Jensen and Charlson, 1984) have implied that the opposite is true, namely that the total solute mass concentration is smaller inside the smaller drops when nucleation scavenging is the controlling process.

The investigation of the possible chemical heterogeneities among fog or cloud droplets is of primary importance for both the modeling of acid deposition processes and the design of cloud or fog sampling. Measured droplet spectra in clouds and fogs of various types are usually far from monodisperse (Pruppacher and Klett, 1980). A major assumption common to virtually all atmospheric aqueous-phase chemistry models developed to this point, however, (Graedel and Goldberg, 1983; Chameides, 1984; Schwartz, 1984; Jacob, 1986; Seigneur and Saxena, 1988; Pandis and Seinfeld, 1989) is that the cloudwater or fogwater consists of a monodisperse, chemically homogeneous distribution of droplets.

Each of the theoretical studies attempting to address the concentration/size dependence of fog or cloud droplets has focused on cloud microphysics, neglecting chemical processes associated with the gas and aqueous phases. This study combines for the first time a detailed description of the gas and aqueous-phase atmospheric chemistry occurring in a cloud or fog with the microphysics of the condensational growth of an aqueous droplet distribution. The thermodynamics and dynamics of multicomponent aerosols are described explicitly for the period before the fog (or cloud) formation and that after the aqueous phase dissipates. The coupling of the descriptions of all the above physical and chemical processes enables us to simulate the concentration/size dependence of fog and cloud droplets under a variety of conditions and during the various stages of fog (or cloud) development.

We begin with separate descriptions of the gas-phase chemistry, aerosol dynamics and thermodynamics, aqueous-phase chemistry, and droplet microphysics and then

describe the complete model used in this study. Model predictions are then presented together with an analysis of the importance of the gas- and aqueous-phase chemical processes. The sensitivity of the results to the initial aerosol size/composition distribution and to the temperature change are also addressed.

Model Description

The mathematical model employed in this study describes the physicochemical processes of gas-phase chemistry, aerosol dynamics and thermodynamics, aqueous-phase chemistry and droplet microphysics, in a closed volume of air in which a fog or a cloud is formed and dissipated. The primary input to the model is the temperature of the system.

The life cycle of a fog or a cloud can be divided into three periods, namely the conditioning period (relative humidity, RH, rises from the initial value to saturation), the rapid growth period (RH exceeds 100%), and the dissipation period (RH drops under 100%). In the first and the last periods the aqueous droplets can exist in equilibrium with the surrounding air and the amount of the aqueous-phase (liquid water content) is small, while in the rapid growth period droplets grow unstably resulting in the creation of a fog or cloud with considerable liquid water content. Therefore, the physics of the problem suggest strongly that the numerical simulation itself should be divided into three stages corresponding to the three different periods of the fog or cloud life cycle. These three stages can be defined by choosing an appropriate relative humidity threshold value, RH_c, so that the first stage lasts until the system's relative humidity reaches RH_c, the rapid growth period is defined by $RH \geq RH_c$, and the dissipation period starts when the relative humidity drops again under RH_c.

Several factors should be considered in selecting RH_c. The value of RH_c should be low enough so that the available amount of liquid water remains small during the first

and third simulation stage, and aqueous-phase reactions can be neglected during these periods. Additionally, the higher the RH_c value, the larger the size of the water drops at this relative humidity, the larger their corresponding relaxation time to equilibrium, and thus the larger the errors introduced by the water equilibrium assumption. At the same time, the lower the RH_c value, the longer the rapid growth period lasts, the longer the complete system of differential equations has to be solved, resulting in excessive computing requirements and numerical problems associated with the inherent stiffness of the differential equations. Several numerical tests showed that the choice of $RH_c = 99\%$ represents a reasonable compromise, preserving the accuracy of the computation while minimizing the computing time requirements.

1. Conditioning period

During this stage as the RH is increasing but still is below RH_c the model simulates the gas-phase chemistry and the aerosol behavior. Aqueous-phase chemical reactions are neglected because of the relatively small amount of liquid water present, and the water is assumed to be in equilibrium between the gas and aerosol phase. For computational purposes the continuous aerosol size distribution is discretized into n uniform sections (Warren and Seinfeld, 1985). The dependent variable vector $F^{(t)}$, whose evolution in time is calculated by the model during this period, contains the gas-phase concentrations of 62 species arising from the gas-phase chemical mechanism used and the concentrations of 18 particulate-phase species in each of the aerosol sections. The numerical solution of the evolution of the aerosol size spectrum and gas-phase concentrations is accomplished by using an operator splitting technique, in which one divides the full problem into various subproblems that are solved sequentially. The scheme used to calculate the value of the variable vector F at time $t + h$ is in operator notation:

$$F^{(t+h)} = A_{int}(h)A_{th}(h)A_d(h)A_{gch}(h)F^{(t)} \quad (1)$$

where $A_{gch}(h)$ indicates advancing the gas-phase chemistry over a time step of length h, and A_{int}, A_{th}, A_d indicate similar advancements for the intersectional movement of aerosol particles, the aerosol thermodynamics and aerosol dynamics, respectively (Pilinis and Seinfeld, 1988). These operators will now be explained.

Gas-phase chemistry operator

The gas-phase chemistry operator describes the gas-phase atmospheric chemical reactions occuring inside a homogeneous air parcel. The evolution of the concentration of the i^{th} gaseous species, C_i, is governed by the spatially homogeneous chemical reaction rate equations,

$$\frac{dC_i}{dt} = R_i^g(C_1, C_2, ..., C_n) \quad (2)$$

where R_i^g is the rate of change of species i via gas-phase chemical reactions. To calculate R_i^g the detailed SAPRC/ERT gas-phase chemical reaction mechanism (Carter et al., 1986) with the modifications and extensions of Carter and Atkinson (1988) is used. This gas-phase chemical mechanism is a state-of-the-art description the complex chemical reactions of hydrocarbon/NO_x/SO_2 mixtures in a polluted atmosphere, using 154 reactions and 62 species (39 active, 7 accumulating and 16 steady state species). The photochemical mechanism preparation and emissions processing software of Carter and Atkinson (1988) has been used to prepare the gas-phase mechanism dependent portion of the code.

Aerosol operators

The size and composition of aerosol particles undergoing nucleation, condensation, and coagulation are described by the aerosol general dynamic equation (Seinfeld,

1986). Using the sectional approximation, in which the continuous size distribution is approximated by a series of step functions (Warren and Seinfeld, 1985; Pilinis et al., 1987), the evolution of the mass concentration of species i in the l^{th} size section, Q_{il}, is described by:

$$\frac{dQ_{il}}{dt} = \left[\frac{\partial Q_{il}}{\partial t}\right]_{cond./evap.} + \left[\frac{\partial Q_{il}}{\partial t}\right]_{coag.} + \left[\frac{\partial Q_{il}}{\partial t}\right]_{sources/sinks} \tag{3}$$

where $\left[\frac{\partial Q_{il}}{\partial t}\right]_{cond./evap.}$ and $\left[\frac{\partial Q_{il}}{\partial t}\right]_{coag.}$ are the rates of change of species i in the l^{th} section due to condensation or evaporation and coagulation, respectively, (Gelbard and Seinfeld, 1980; Gelbard et al., 1980; Warren and Seinfeld, 1985; Pilinis et al., 1987) and $\left[\frac{\partial Q_{il}}{\partial t}\right]_{source/sinks}$ is the rate of change due to nucleation, primary aerosol injection and removal. The three aerosol operators, A_{int}, A_{th}, and A_d, applied successively to the variable vector F represent a method for the solution of equation (3).

Typical components in the aqueous aerosol phase are H_2O, NH_4^+, SO_4^{2-}, NO_3^-, H^+, Na^+, Cl^-, HSO_4^- and H_2SO_4 and possible components in the solid phase are Na_2SO_4, $NaHSO_4$, NaCl, $NaNO_3$, NH_4Cl, NH_4NO_3, $(NH_4)_2SO_4$, NH_4HSO_4 and $(NH_4)_3H(SO_4)_2$ (Pilinis and Seinfeld, 1987). The aerosol thermodynamics operator computes the chemical equilibrium of volatile species such as H_2O, NH_3, HCl, and HNO_3 between the gas and aerosol phases while the aerosol dynamics operator describes explicitly the diffusion controlled gas-to-particle conversion of non-volatile species such as sulfuric acid (Pilinis and Seinfeld, 1987). During aerosol evaporation or condensation the operator for the intersectional movement, A_{int}, decribes the movement of the aerosol particles from each constant size section to its neighboring sections (Warren and Seinfeld, 1985; Pilinis et al., 1987).

2. Rapid Growth Period

When the relative humidity of the system reaches the threshold value RH_c ma-

jor changes take place. The aqueous droplets approach the region of unstable growth and their liquid water content increases considerably. Important processes during this period include gas-phase chemistry, aqueous-phase chemistry, and microphysics of aqueous droplets. The droplet size distribution is discretized as before into n individual size sections but because of the magnitude of the size changes occuring each droplet size section is now allowed to move in the time-diameter space increasing its diameter when water condensation is taking place and decreasing its size in case of evaporation.

Let d_l and d_{l+1} denote the boundaries of each fixed size section during the conditioning period. We represent the droplets in each section during the rapid growth period by the mass mean diameter of that section, D_l. In other words, we replace the N_l particles of total mass M_l evenly distributed between diameters from d_l to d_{l+1} from the conditioning period with N_l particles of the same total mass M_l but with the single diameter D_l, where D_l is calculated by:

$$D_l = \left[\frac{2d_l^2 d_{l+1}^2}{d_l + d_{l+1}}\right]^{1/3} \tag{4}$$

A new dependent variable vector Y is defined that contains the concentartions of all 62 gas-phase species, the concentrations of 49 aqueous-phase species in each of the n sections and the n diameters D_l (one for each section). The gas-phase chemistry is decoupled from the aqueous-phase chemistry and droplet microphysics by using the following operator splitting scheme:

$$Y^{(t+h)} = A_{ach}(h) A_{gch}(h) Y^{(t)} \tag{5}$$

with A_{ach} being the aqueous-phase chemistry and droplet microphysics operator.

Aqueous-phase chemistry and droplet microphysics operator

In previous cloud or fog modelling studies, droplets have been defined as aerosol particles that have been activated, with the non-activated particles considered as the

interstitial aerosol (Flossman et al., 1985). Here, in the aqueous-phase chemistry and droplet microphysics operator, there need be no explicit difference in the treatment of the interstitial aerosol particles and the aqueous droplets and, for reasons of simplicity, both will be referred to as droplets from now on. The change of the mass concentration of species i in moving section l, q_{il}, is calculated by:

$$\frac{dq_{il}}{dt} = \left[\frac{\partial q_{il}}{\partial t}\right]_{cond./evap.} + R_i^a(q_{1l}, q_{2l}, ..., q_{nl}) \tag{5}$$

where $\left[\frac{\partial q_{il}}{\partial t}\right]_{cond./evap.}$ is the mass transfer rate of species i from the gas phase to the aqueous droplets in moving section l. For water the detailed growth equation derived by Pruppacher and Klett (1980) is used and for the remainder of the volatile species the expression used by Pandis and Seinfeld (1989) is applied. The reaction rates R_i^a are derived from the aqueous-phase chemical mechanism presented by Pandis and Seinfeld (1989), which includes 49 individual aqueous-phase species, 17 aqueous-phase ionic equilibria and 109 aqueous-phase reactions.

The change in section diameter is calculated by:

$$\frac{dD_l}{dt} = \frac{2}{N_l \rho_l \pi D_l^2} \sum_{i=1}^{Nv} \left[\frac{\partial q_{il}}{\partial t}\right]_{cond./evap.} \tag{6}$$

where N_l is the number, and ρ_l the density of droplets in section l, respectively, and Nv is the number of volatile species. The number of droplets, N_l, is assumed constant with time since droplet coagulation is neglected and since the section moves in such a way that particles do not grow out of a section.

3. Dissipation period

When the relative humidity becomes less than the critical relative humidity (RH_c) the system passes to the third stage, where the aerosol operators are reactivated and all the calculations are performed exactly as in the conditioning period.

Representative Cases for Evaluation

There has been conflicting opinions in the literature concerning the nature of the solute concentration/size dependence of cloud or fog droplets. At the same time there is no available information concerning the possible differences in chemical composition of the various droplet sizes, e.g. differences in sulfate concentration, etc. To investigate these phenomena, the model described above has been applied under representative conditions to elucidate differences in chemical composition of droplets of different sizes inside a fog or a cloud. Unfortunately, a data set including the size/composition distribution of atmospheric aerosol and aqueous-phase droplets before, during, and after fog or cloud development is not available for the model's evaluation. Therefore, a representative set of initial conditions together with a temporal temperature variation have been chosen. We will henceforth refer to this as Case 1, the parameters of which are given in Table I. The sensitivity of the results to the temperature variation profile used has been studied by performing two additional simulations (Cases 2 and 3). Finally the effects of the aerosol size distribution before the fog development on the concentration differences in fog and cloud droplets of different sizes have been investigated in the simulation for Case 4.

Case 1 (base case).

In this case a winter maritime urban fog is simulated. The concentrations of ammonia, nitric acid, hydrochloric acid, sulfate and sodium are based on the measurements of Russell and Cass (1984) for Long Beach, California. Due to lack of specific data, an initial hydrogen peroxide concentration of 2 ppb is assumed after Heikes et al. (1987). The remainder of the gas-phase concentrations are derived from Seigneur and Saxena (1984) characteristic of an urban fog in the Los Angeles area.

The system temperature is assumed to vary with time as shown in Figure 1. This

Table I. Base case parameters and initial conditions.

Model Parameter	*Value*
Latitude	34.5
Solar declination	0°
Time at start	7 : 00 PST
Relative humidity at start	95%

Gas – phase species	*Initial concentration (ppb)*
SO_2	20.0
NH_3	3.17
HNO_3	2.21
HCl	0.55
O_3	20.0
NO	35.0
NO_2	70.0
H_2O_2	2.0
HCHO	20.0
PAN	1.0
ETHE	85.0
Parafins	700.0
Olefins	45.0
Aromatics	150.0

Aerosol species	*Initial concentration* ($\mu g/m^3$)
Sulfate	3.72
Sodium	1.8

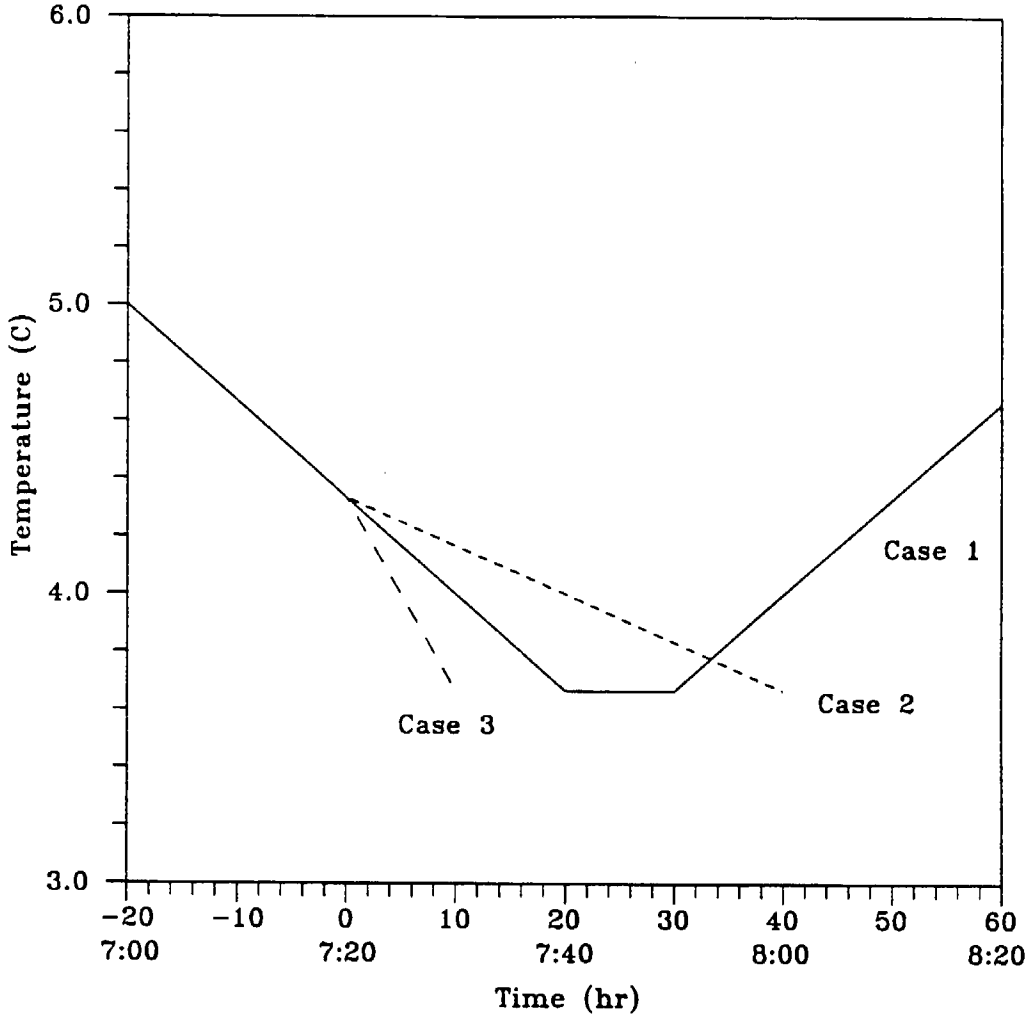

Figure 1. Temperature variation profiles used in the various simulations. The profile used in Case 4 is the same as in Case 1.

temperature variation corresponds to that reported for an early morning winter fog development episode (Roach et al., 1976).

The model has been applied with 7 logarithmically spaced sections covering initially the diameter range from 0.2-8 μm. The size (diameter) sections used are (1) 0.2-0.34 μm, (2) 0.34-0.57 μm, (3) 0.57-0.97 μm, (4) 0.97-1.65 μm, (5) 1.65-2.79 μm, (6) 2.79-4.72 μm, (7) 4.72-8.0 μm. The initial sulfate and sodium have been distributed over these sections based on the measurements of Wall et al. (Wall et al., 1988) for wet maritime air. The initial aerosol mass concentration distribution calculated assuming thermodynamic equilibrium between the gas and aerosol phases for the sulfate, nitrate, chloride, sodium, ammonium, water system (Pilinis and Seinfeld, 1987), is shown in Figure 2a.

Case 2

The conditions used were the same as in Case 1, except for the assumed temperature profile (Figure 1). A cooling rate of 1 ^{o}C hr^{-1} was assumed during the growth period compared to the 2 ^{o}C hr^{-1} used in Case 1.

Case 3

All the conditions were the same as in the two previous cases but a cooling rate of 4 ^{o}C hr^{-1} was assumed during the growth period (Figure 1) resulting in a much faster development of the aqueous phase. This cooling rate corresponds to a vertical velocity of the air parcel around 10 cm s^{-1}, and this simulation is applicable to the initial stages of formation of a stratus cloud (Hänel, 1987).

Case 4

The temperature of the system varied as in Case 1. The initial aerosol size/composition was changed by increasing the amount of sulfate from 3.72 μg m^{-3} (Case 1) to 8 μg m^{-3}

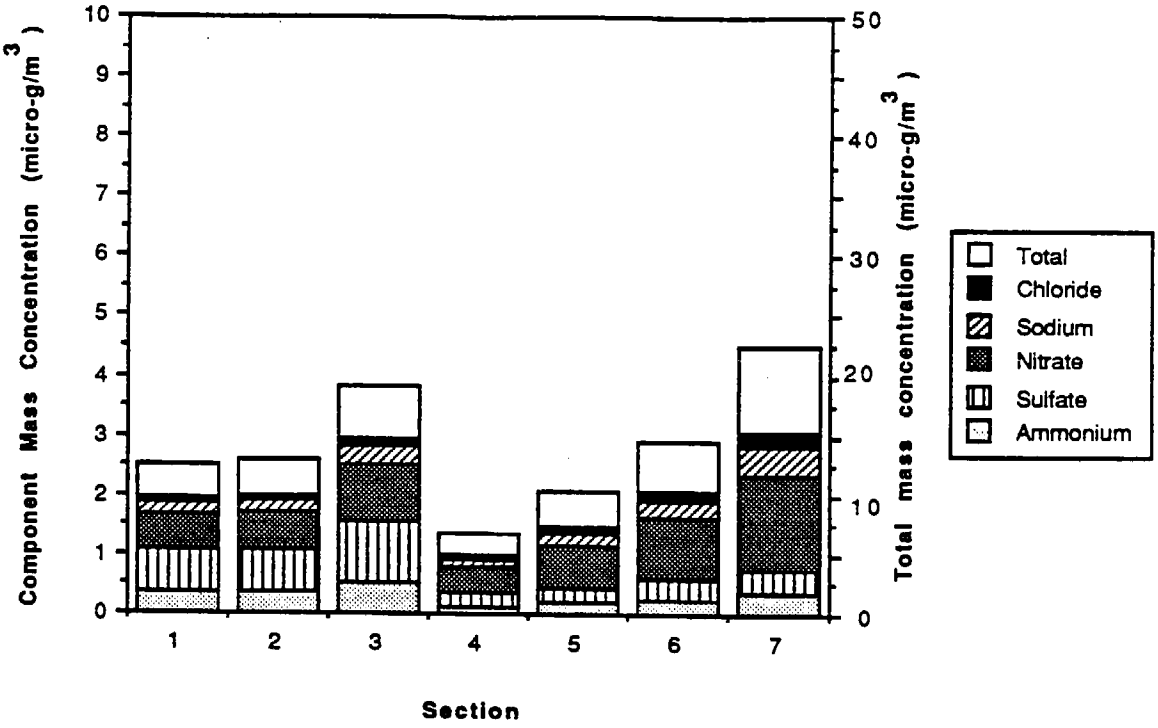

Figure 2a. Calculated aerosol size/composition distribution at the beginning of the Case 1 simulation, 7:00 ($t = -20$ min), assuming thermodynamic equilibrium for the sulfate, nitrate, sodium, ammonium, and water system.

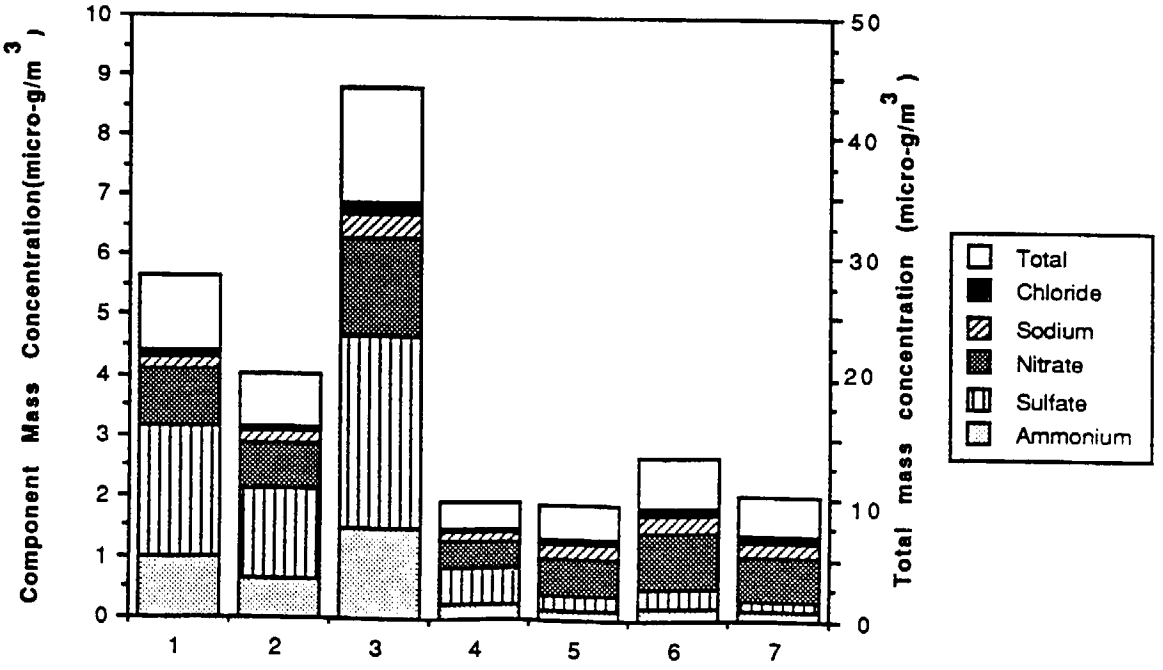

Figure 2b. Calculated aerosol size/composition distribution at the beginning of the Case 4 simulation, 7:00 ($t = -20$ min), assuming thermodynamic equilibrium for the sulfate, nitrate, sodium, ammonium, and water system.

and the available NH_3 to 6 ppb. The initial aerosol distribution calculated assuming thermodynamic equilibrium for the system at 95% relative humidity is shown in Figure 2b. The main feature of this aerosol distribution compared to that used in Case 1 is the enrichment in solute mass of the three smallest sections covering the range from 0.2 to 1 μm in diameter.

Results and Discussion

Size/Composition Distribution of Fog and Cloud Droplets (Base Case)

In all cases, after 20 minutes the relative humidity of the system reaches 99% (RH_c) and the rapid growth period begins (see Figure 1). We define this time as $t = 0$, at which all the seven size sections are growing. In the base case, by $t = 6$ min, the smallest droplet section reaches a maximum diameter of 0.52 μm and starts evaporating slowly, following the decreasing relative humidity, with the second smallest section soon following. These two smallest sections represent the interstitial aerosol particles. At $t = 6$ min the system supersaturation has reached its maximum value of 0.11% (Figure 3). This maximum is a result of two competing processes, the tendency of the supersaturation to increase due to the system's cooling and the tendency of the supersaturation to decrease due to the transfer of water vapour to the aqueous-phase. The fog has fully developed at $t = 20$ min reaching a liquid water content of 0.23 g m^{-3} (Figure 3). At this time the two smallest non-activated droplet sections are evaporating because the system's relative humidity remains below their corresponding equilibrium vapor pressures, while the remainder of the size sections are growing. This observation is in agreement with that of Hänel (1987) that after the supersaturation in a cloud has reached its maximum there are three types of droplets, small non-activated particles shrinking slowly, activated droplets growing unstably, and large droplets growing slowly. The third droplet section starts evaporating slowly at $t = 21$ min and the fog starts

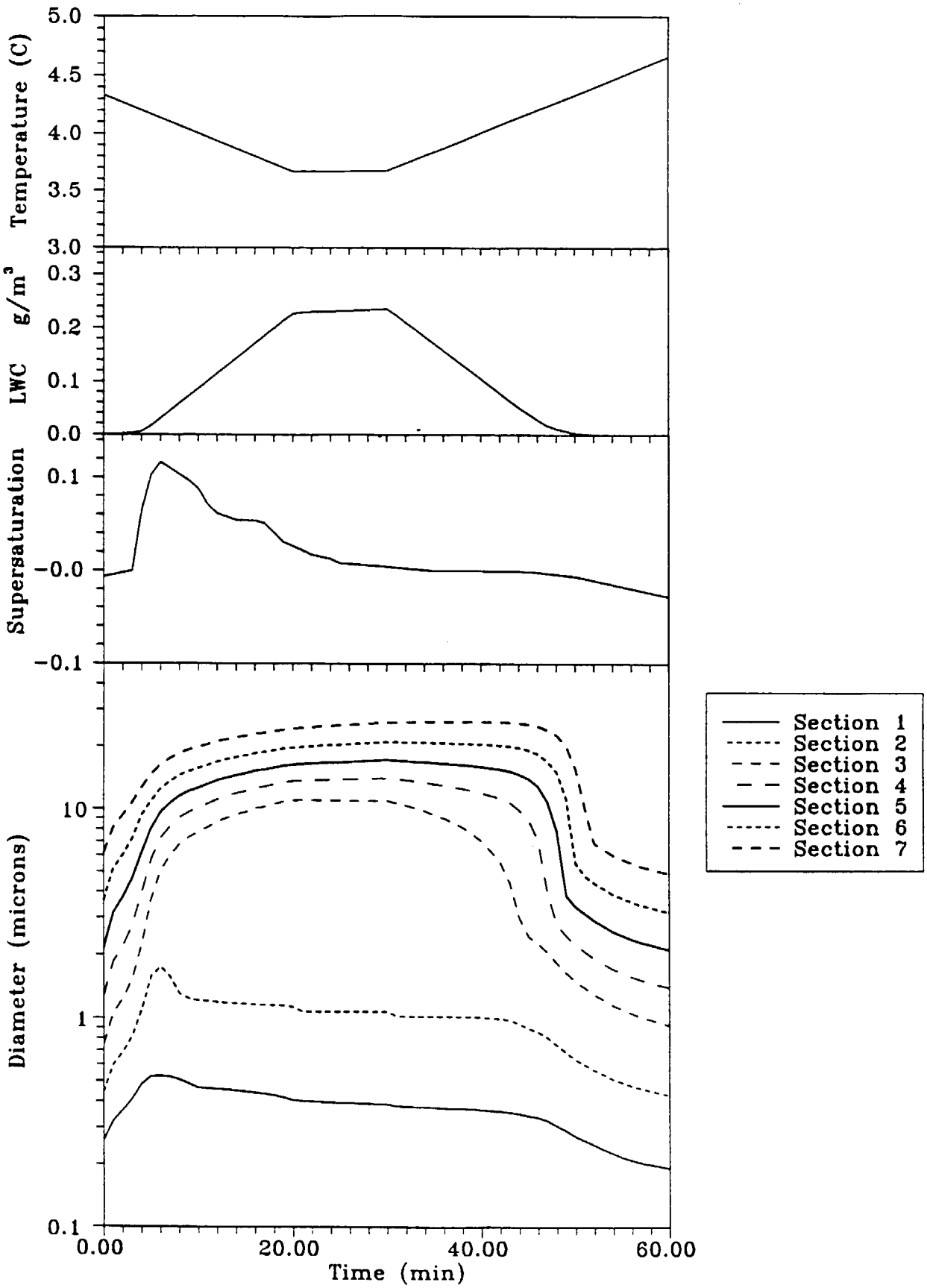

Figure 3. Calculated variation of the mass mean diameter of the 7 sections, the system's supersaturation, the liquid water content and the temperature with time. $t = 0$ corresponds to 7:20.

dissipating at $t = 31$ min due to the temperature increase. Noticeably, the droplets in the largest section, characterized by a large relaxation time (defined as the time required for the adaptation of the droplets to the changing conditions of their environment), continue to grow slowly for 8 more minutes before commencing to evaporate (Figure 3).

A significant portion of the fogwater is concentrated over a relatively short range of droplet diameters, with a peak at 14 μm at the time of maximum liquid water content (Figure 4). This mass distribution is in qualitative agreement with the measurements of Waldman (1986). The distribution of the dissolved compounds over this water droplet spectrum exhibits very interesting behavior. Initially ($t = 0$) all droplets are quite concentrated with solute concentrations of the order of 2×10^4 mg/liter water with the larger droplets being more dilute than the smaller ones. For example, the droplets in section 3 ($D_3(0) = 0.8\mu$m) are 15% more concentrated than the droplets of section 4 ($D_4(0) = 1.2\mu$m). This monotonic concentration variation changes drastically during the droplet growth period (Figure 5a). The droplets in the 3rd section, that are the smallest activated droplets, are able to grow much faster than the larger droplets. Therefore the resulting dilution rate for the droplets in the 3rd section is much higher than for those in the 4th etc. and these droplets become more dilute than the larger ones. For example at $t = 20$ the droplets in section 3 ($D_3 = 11\mu$m) have a total solute concentration (volatile and non-volatile) of 93 μg/liter water while droplets in section 4 ($D_4 = 13.6\mu$m) have a concentration of 125 μg/liter, in 5 ($D_5 = 16.3\mu$m) 197 μg/liter, in 6 ($D_6 = 19.7\mu$m) 340 μg/liter and finally in 7 ($D_7 = 24.3\mu$m) 610μg/liter. During the fog evaporation stage the concentration variation over the droplet distribution returns again to the initial monotonic shape (Figure 5b). The reason for this behavior is that the smaller droplets evaporate faster than the larger ones. The above results are in essential agreement with the measurements of Noone et al. (1988).

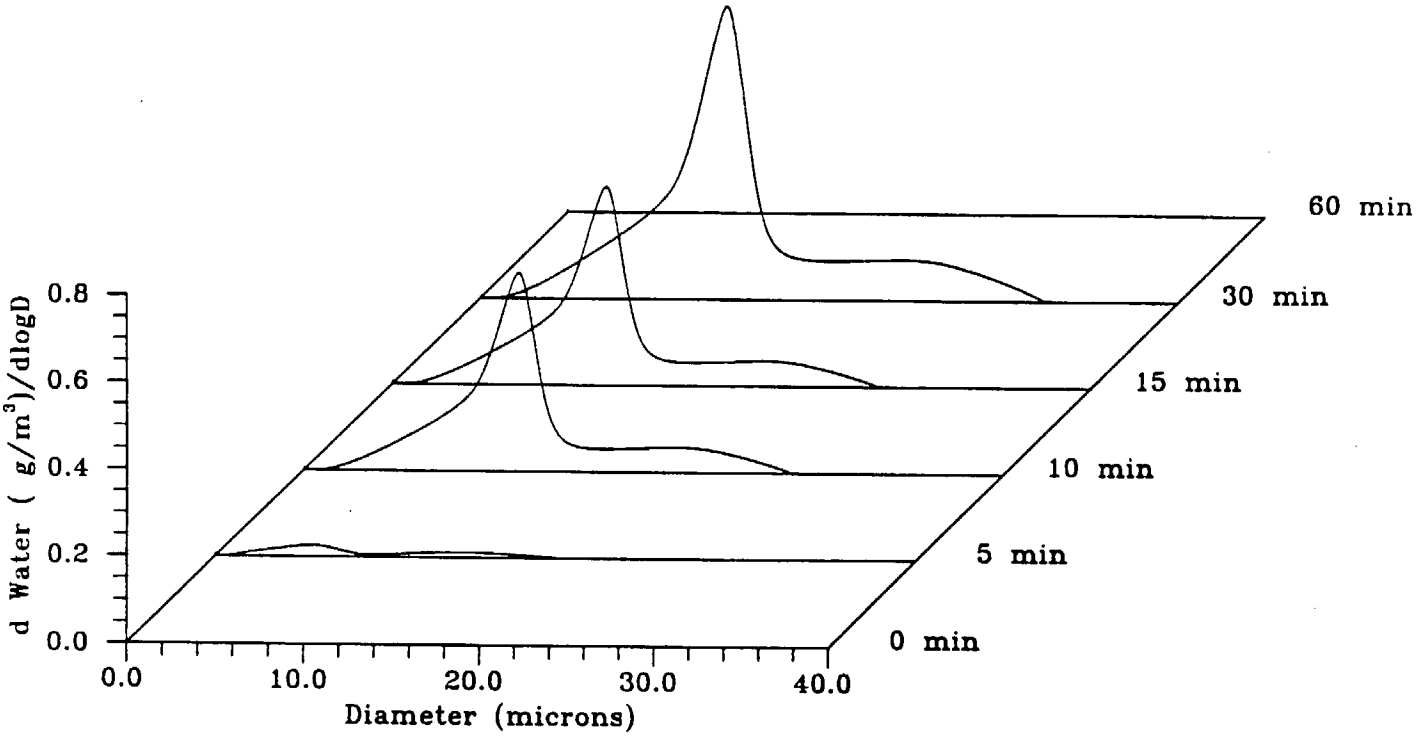

Figure 4. Calculated time evolution of the droplet mass distribution as a function of the droplet diameter.

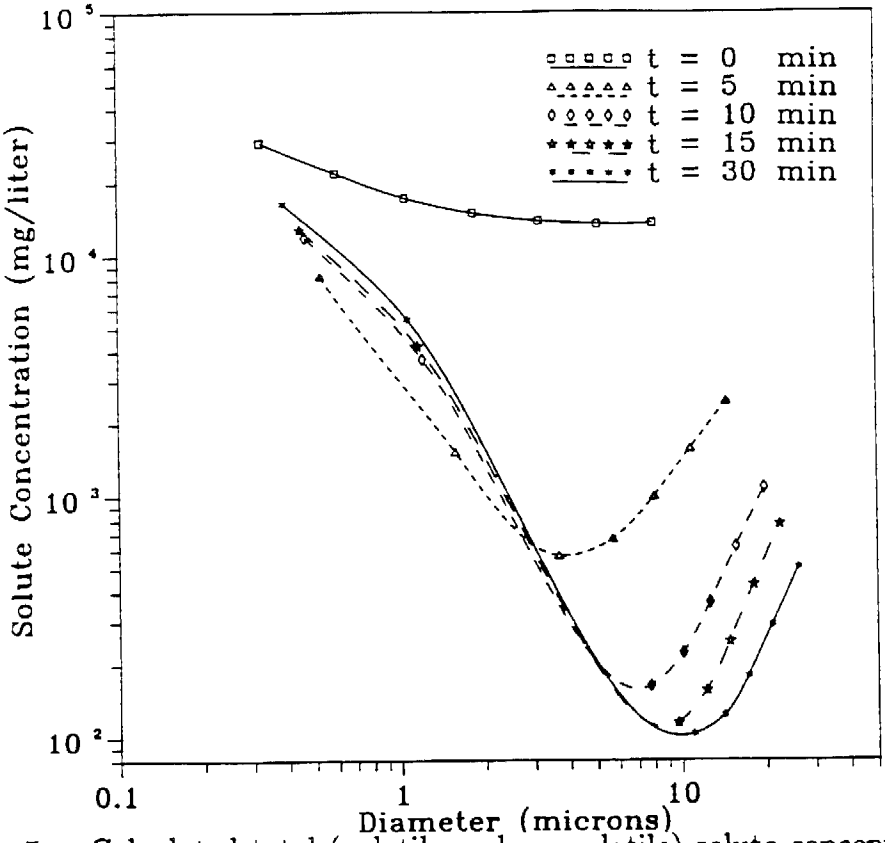

Figure 5a. Calculated total (volatile and nonvolatile) solute concentration as a function of droplet diameter for five different times during the growth period

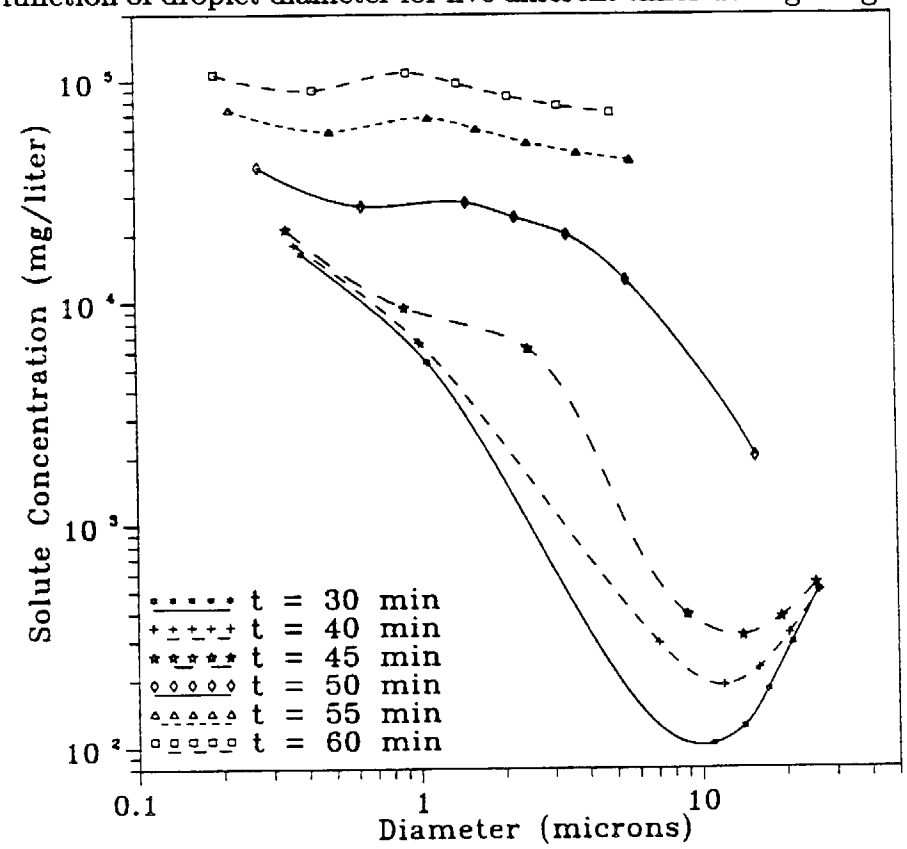

Figure 5b. Calculated total (volatile and nonvolatile) solute concentration as a function of droplet diameter for five different times during the fog dissipation.

These observations of the solute concentration size distribution are a direct result of the fact that droplets of different sizes grow and consequently dilute at different rates, that is smaller droplets grow faster and therefore dilute faster than the larger ones. This can be shown quantitatively using the following simple argument (a similar argument was presented also by Noone et al. (1988)). Assume that the dry aerosol particle size distribution is divided into discrete intervals i with diameters D_s^i. Let the dry particles of diameter D_s^i grow and become aqueous droplets of diameter D_d^i. Assuming for simplicity that the density of the dry particles is 1 g/cm^3, the mass mixing ratio of droplets in section i is $W_i = (D_s^i/D_d^i)^3$. Defining the dilution rate of section i as $DR_i = -(1/W_i)(dW_i/dt)$ and assuming that the mass of scavenged aerosol in droplets in section i remains constant with time (that is neglecting processes like scavenging of gas-species, coagulation etc) one gets for sections 1 and 2 with $D_d^1 > D_d^2$ that $(DR_1/DR_2) = (D_d^2/D_d^1)[(dD_d^1/dt)/(dD_d^2/dt)]$. Assuming that the droplets are sufficiently large that $(dD_d^i/dt) = K/D_d^i$ where K a constant depending on the system's conditions and not on D_d^i (of course K defined by the growth equation is a weak function of D_d^i) then $(DR_1/DR_2) = (D_d^2/D_d^1)^2 > 1$ and the smaller droplets are diluted at a faster rate than the larger ones if growth by water diffusion is the only process occurring.

Interesting changes in the size/composition spectrum of the droplets take place because of the simultaneous fogwater chemistry and the transfer of species between the gas and the aqueous phases. The amount of sulfate in the aqueous phase increases considerably from 4.0 μg m^{-3} at $t = 0$ min to 12.6 μg m^{-3} at $t = 30$ min and 12.8 μg m^{-3} an hour later. The main pathway for this sulfate production is the aqueous-phase oxidation of S(IV) by hydrogen peroxide. The other chemical pathways for sulfate formation do not contribute significantly because the pH of the aqueous phase remains under 4 at which and these reactions are very slow. Therefore after the hydrogen peroxide depletion at $t = 20$ the sulfate production is slowed down considerably. The

distribution of the produced sulfate is nonuniform over the size spectrum (Figure 6). The peak that is developed can be explained by the fact that most of the liquid water during the fog is in this droplet size regime, that is the 3rd section. These droplets have access to most of the reacting medium for S(IV) oxidation and therefore are preferentially enriched in sulfate. Despite this enrichment the condensational growth effects dominate in this case and these droplets are the most dilute. After the fog dissipation the produced sulfate remains in the aerosol phase resulting in a peak around 1 μm at $t = 60$ min.

The same enrichment as in the case of sulfate is observed with nitrate (Figure 7). Nitric acid produced in the gas phase is most efficiently scavenged by the droplets that carry most of the fog liquid water content. During the droplet evaporation stage some of the nitrate returns back to the gas phase as nitric acid. Ammonia is assumed to exist in limited quantities in this base case. During the initial period (before $t = 0$), where thermodynamic equilibrium is assumed, most of the ammonia resides in the aerosol phase. The small quantities of ammonia that are left in the gas-phase are again preferentially scavenged by the droplets that carry most of the water causing a relatively small change of the distribution. During the latter stages of fog development no dramatic changes in the ammonium distribution over the droplet size spectrum occur because the available ammonia remains in the acidic aerosol phase and no emissions have been included in this simulation. The small change in the ammonium distribution can be seen by comparing the distributions at $t = 0$ and $t = 60$ min.

Influence of gas- and aqueous-phase chemistry

The importance of the chemical processes in both the gas and aqueous phases for the phenomena described above has been investigated by performing an additional simulation. The base case scenario has been reexamined but with no gas or aqueous-

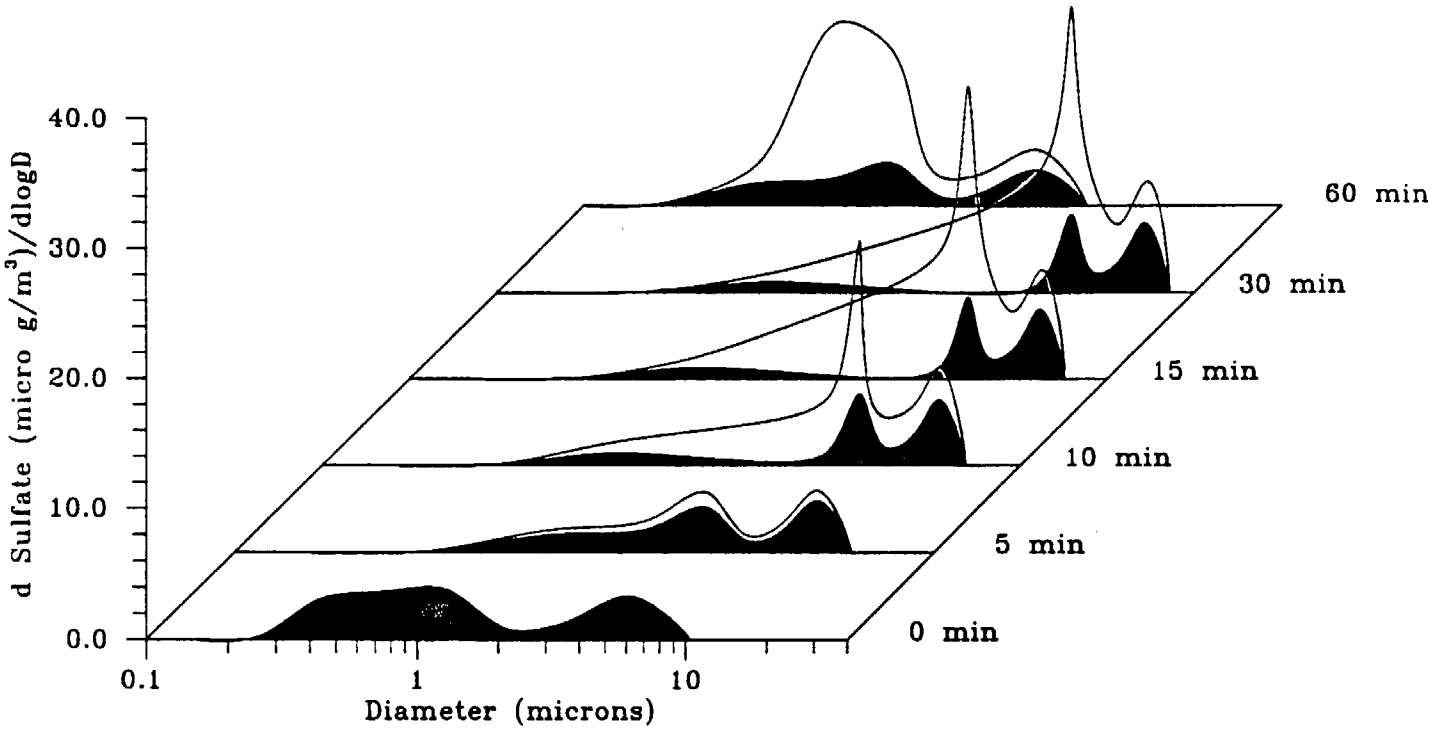

Figure 6. Calculated time evolution of the sulfate mass distribution as a function of the droplet diameter. The shaded area corresponds to the sulfate that initially exists in the aerosol particles and the rest is the sulfate produced during the fog evolution.

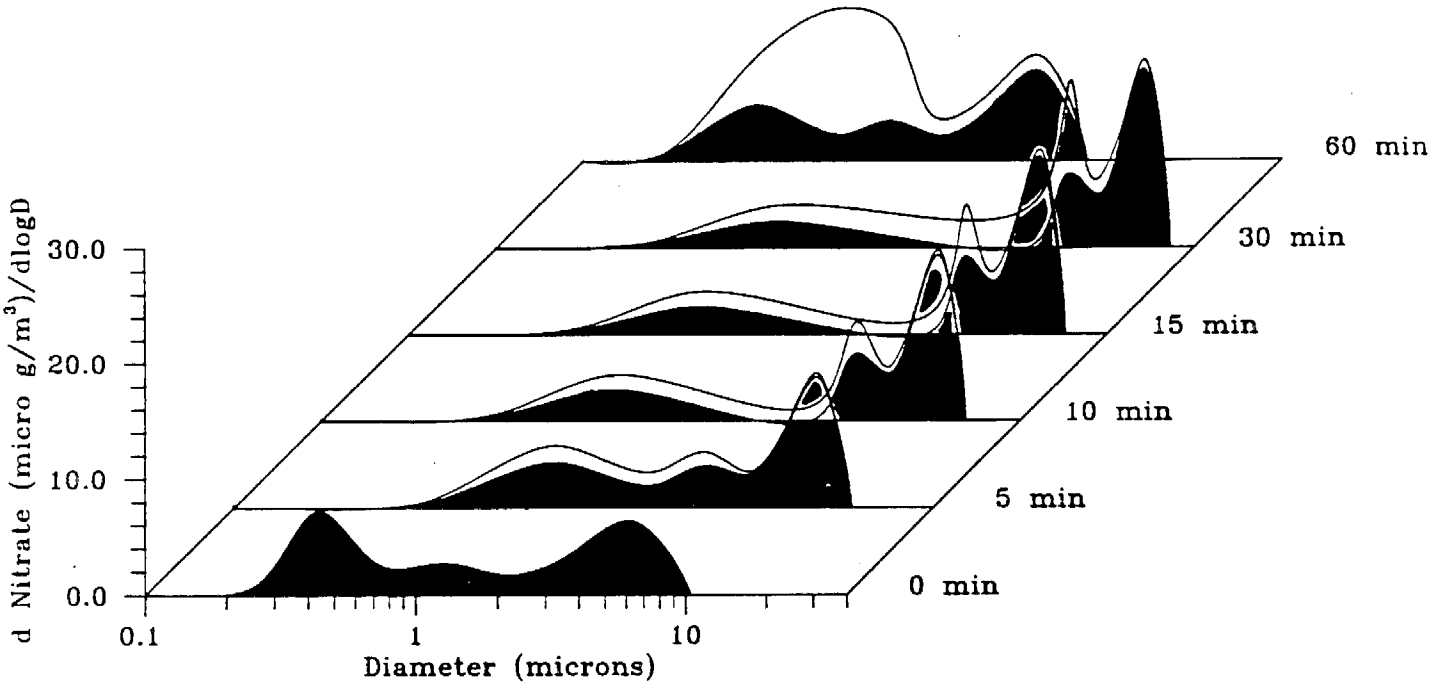

Figure 7. Calculated time evolution of the nitrate mass distribution as a function of the droplet diameter.

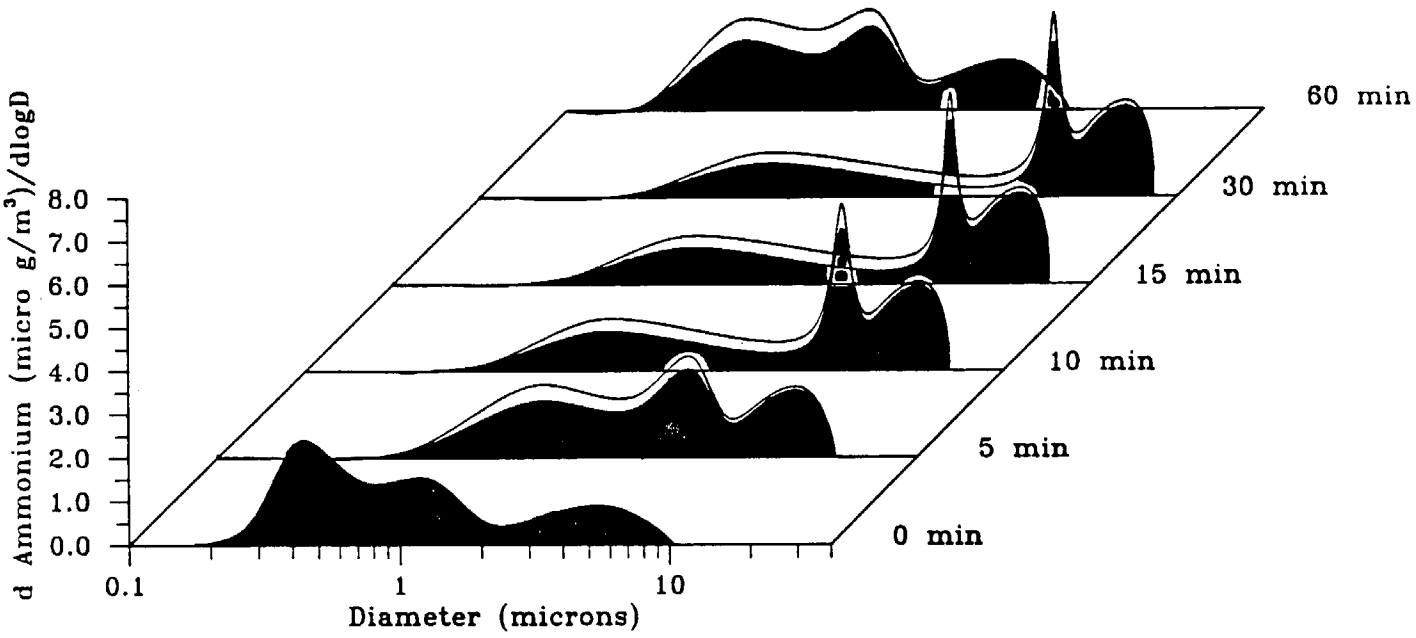

Figure 8. Calculated time evolution of the NH_4^+ mass distribution as a function of the droplet diameter.

phase chemistry and without scavenging of species from the gas phase from $t = 0$ to $t = 60$ min. Hence, the liquid water is simply allowed to condense on the pre-existing multicomponent aerosol particles as they become activated to form cloud droplets.

The maximum liquid water content attained was again 0.23 g/m^3 and the drop size distribution did not change significantly from the base case suggesting that the liquid water formed is not influenced by the chemical reactions as long as no new condensation nuclei are formed. On the contrary, the solute concentration inside the droplets changes dramatically with the aqueous solutions being much more dilute than the corresponding droplets in the base case. The solute concentration inside the droplets of diameter 11 μm is, at $t = 30$ min, 24 mg/liter compared to 103 mg/liter when the gas and aqueous-phase chemical processes are included. The ratios of the total solute mass concentrations of the two cases are shown in Figure 9 for $t = 30$, the point when the liquid water content attains its maximum value. The effect of the gas and aqueous-phase chemical reactions is therefore to enrich droplets of diameters 10 to 15 μm with dissolved species. Bearing in mind that these droplets are more dilute than the others, one concludes that the chemical processes tend to smooth out the minimum solute concentration in the size/concentration distribution (Figure 5) and therefore tend to decrease the concentration differences between the various droplet sizes.

Influence of Cooling Rate

The temperature change is the direct or indirect driving force of the whole series of processes desribed above. Therefore it is reasonable to expect that in the dynamic framework of the current model, changes are going to occur based on the cooling rate of the system and the ability of the droplets or particles to follow these changes. To investigate these possible changes two additional simulations have been performed, referred above as Cases 2 and 3.

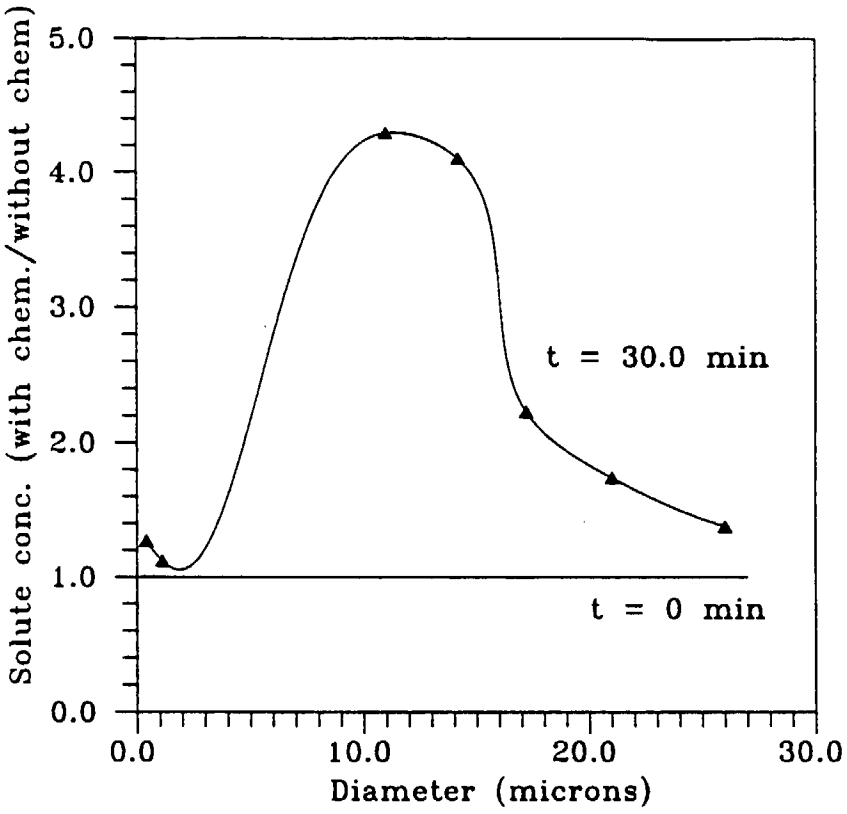

Figure 9. The ratio of the total solute concentration calculated by considering gas and aqueous phase chemistry over the total solute concentration calculated by neglecting chemical processes versus droplet diameter at $t = 30$.

In Case 2 a cooling rate slower than that used in the base case has been used. The relatively slow rate of change enables the larger droplets to follow more closely the ambient relative humidity. The maximum amount of liquid water that is formed ($t = 40$) is 0.24 g m^{-3}, that is just 5% higher than the liquid water for the base case at $t = 20$ min. The change in the liquid water size distribution is more profound. The distribution is shifted towards the larger droplet sizes proving that the slow cooling rate enables the larger droplets to attract larger quantities of water from the competing small droplets (Figure 10). The attraction of more water to the larger droplets results in the further dilution of these droplets and therefore decreases the solute concentration differences between small and large droplets (Figure 11). For example, the solute concentration of the 10 μm droplets is almost 50% larger than the concentration of the 20 μm droplets, while in the base case it was 250%. Interesting changes are also observed in the distribution of the total solute mass over the droplet size spectrum (Figure 12). The total solute mass increases from 34.5 μg m^{-3} (base case, $t = 20$ min) to 38.6 μg m^{-3} ($t = 40$ min), an increase that is attributable mainly to the time difference and the subsequent production of more nitrate in the gas phase and secondarily to the increase of the fog liquid water content. Most of this additional solute mass is found in the droplets of diameter larger than 20 μm ($t = 40$).

In Case 3 a relatively rapid cooling of the system has been assumed. In contrast with Case 2 the larger droplets are not able to compete succesfully with the smaller ones for the available liquid water. The maximum supersaturation increases to about 0.13% resulting in the activation of the particles in Section 2, leaving only the particles in Section 1 as the interstitial aerosol. The activation of these extra particles has interesting consequences because the number of growing droplets in the system increases significantly. The maximum liquid water ($t = 10$ min) decreases slightly compared to the previous cases to 0.22 g m^{-3}, evidence of the difficulty of the droplets to follow

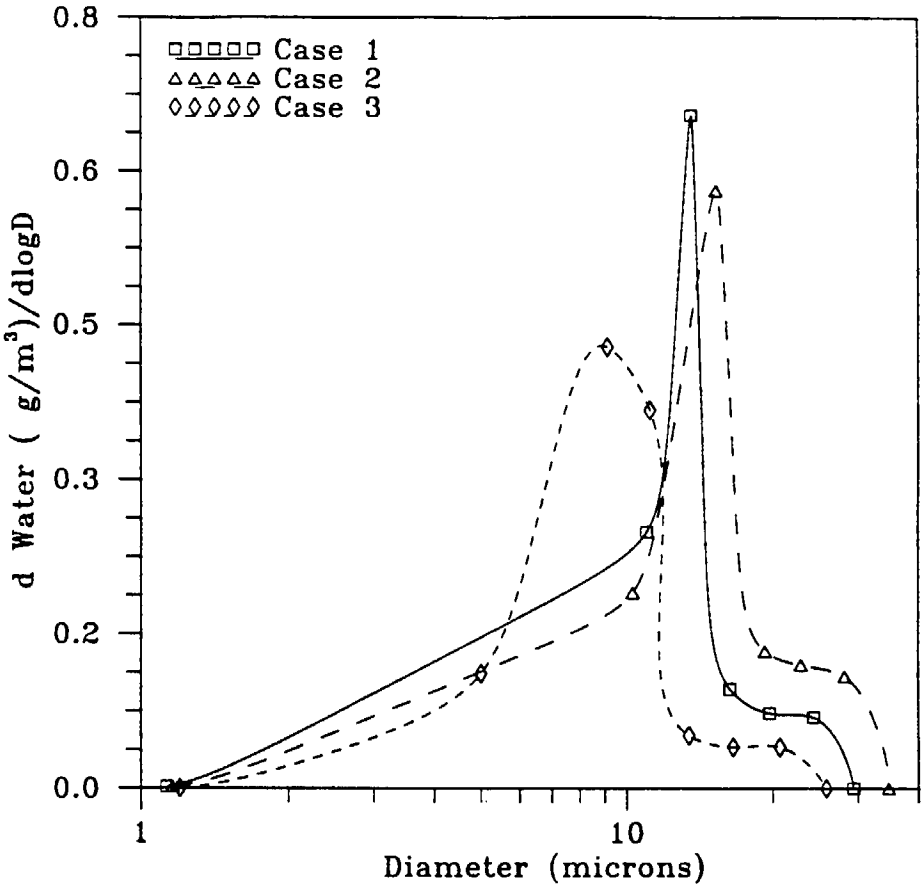

Figure 10. Comparison of the calculated liquid water mass distributions as a function of droplet diameter for Case 1 (base case, t = 20 min), Case 2 (small cooling rate, t = 40 min) and Case 3 (large cooling rate, t = 10 min).

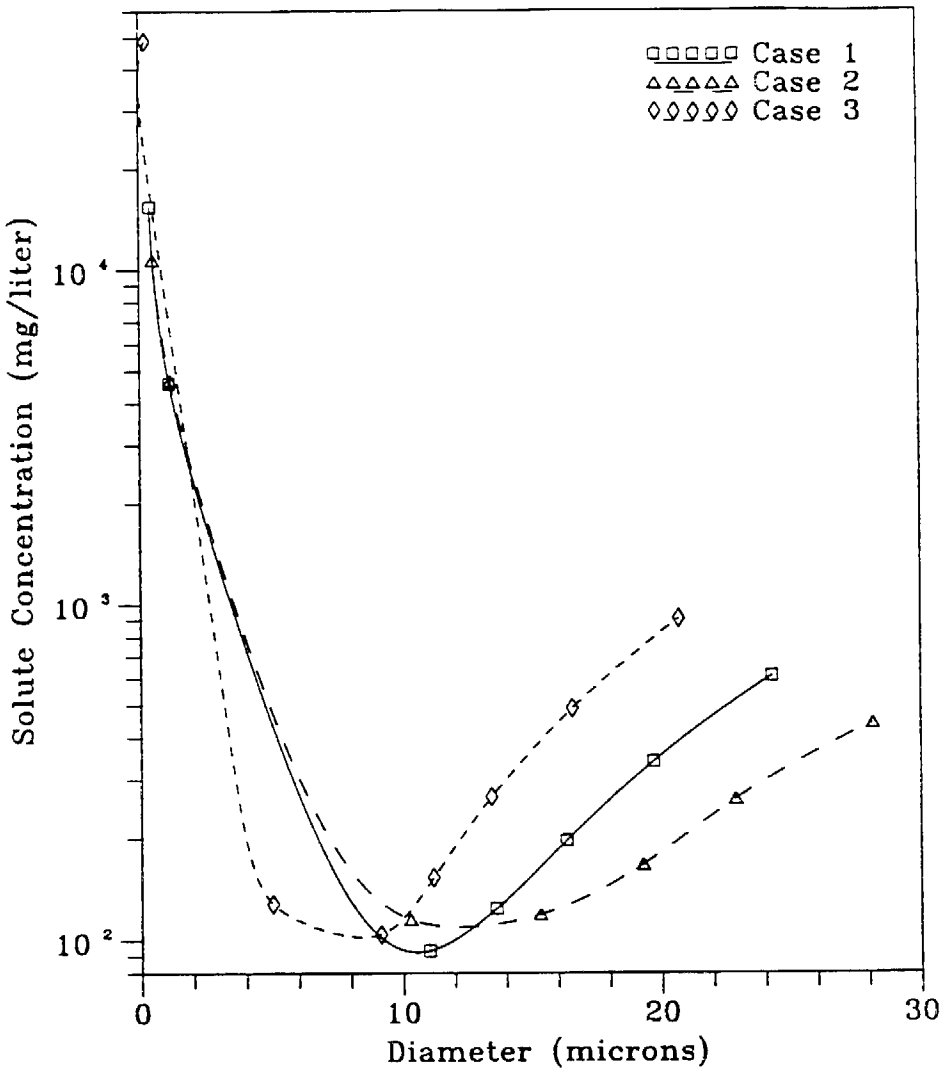

Figure 11. Comparison of the calculated total (volatile and nonvolatile) solute concentration as a function of droplet diameter for Case 1 (base case, $t = 20$ min), Case 2 (small cooling rate, $t = 40$ min) and Case 3 (large cooling rate, $t = 10$ min).

tha rapid change of the ambient relative humidity. The liquid water distribution is shifted towards the smaller droplet diameters and at the same time the peak of the distribution is smaller and less sharp due to the fact that more droplets in a wider range are activated (Figure 10). The large droplets attract only small quantities of the condensing water and their solute concentration increases considerably, resulting in an increase of the solute concentration differences among the different droplet sizes (Figure 11). The total solute concentration of the 20 μm droplets is in this case almost 7.5 times larger than the corresponding concentration of the 10 μm droplets at $t = 10$ min. For the same reasons as in Case 2 (small time period) the total solute mass decreases to 32.7 μg m^{-3} and is shifted towards the smaller droplet diameters (Figure 12).

Influence of Initial Aerosol Distribution (Case 4)

The aerosol distribution before the fog development is a major factor in the all the above processes not only because it usually represents a large percentage of the solute mass (more than 30% in Case 1 at $t = 30$ min) but because it also affects the water distribution. The solute concentration distribution, for the aerosol shown in Figure 4 (at 95% relative humidity), is depicted in Figure 13. The two distributions generally exhibit the same behavior with a minimum around 10 μm even if most of the droplets in Case 1 are more dilute. The concentration differences are smaller, with the 20 μm droplets 2.4 times more concentrated than the 10 μm ones.

The above findings suggest that the quantitative results depend on the aerosol mass/size distribution that serve as condensation nuclei. This dependence is not strong enough, under most conditions, to change qualitatively the conclusions reached above.

Conclusions

A model has been developed to study the interactions between the chemical processes in the gas and aqueous phases and the growth of aerosol particles to fog or cloud

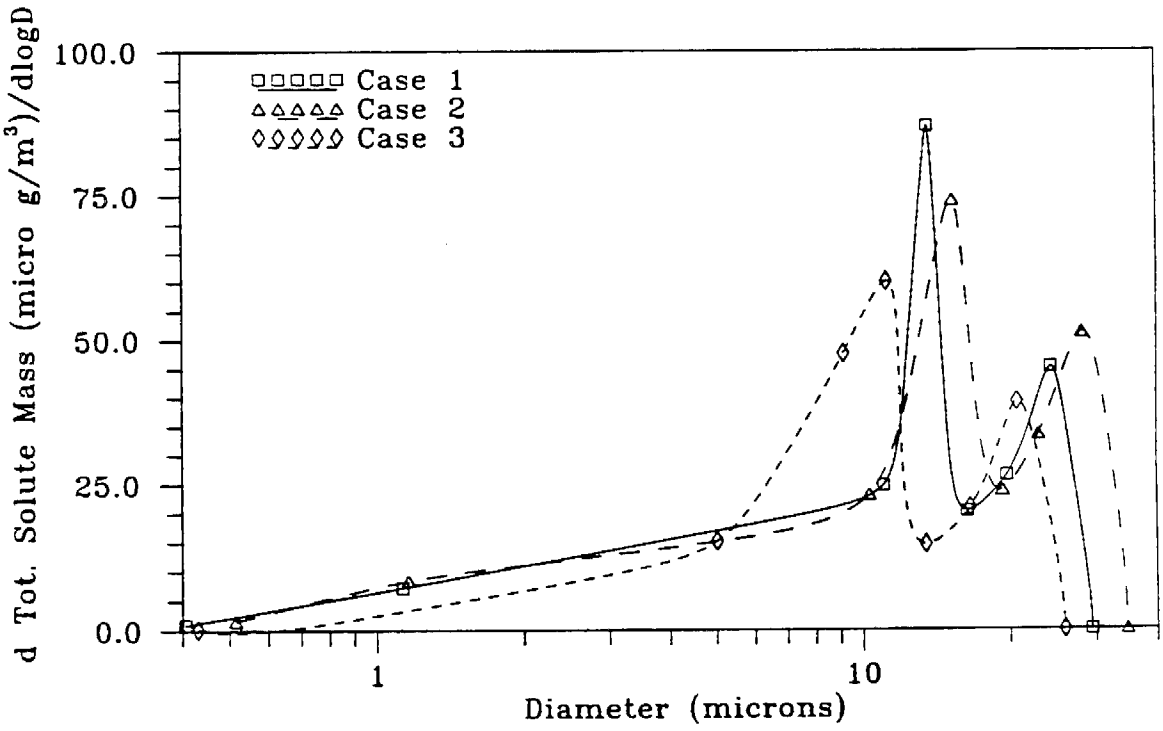

Figure 12. Comparison of the calculated total (volatile and nonvolatile) solute mass distribution as a function of droplet diameter for Case 1 (base case, t = 20 min), Case 2 (small cooling rate, t = 40 min) and Case 3 (large cooling rate, t = 10 min).

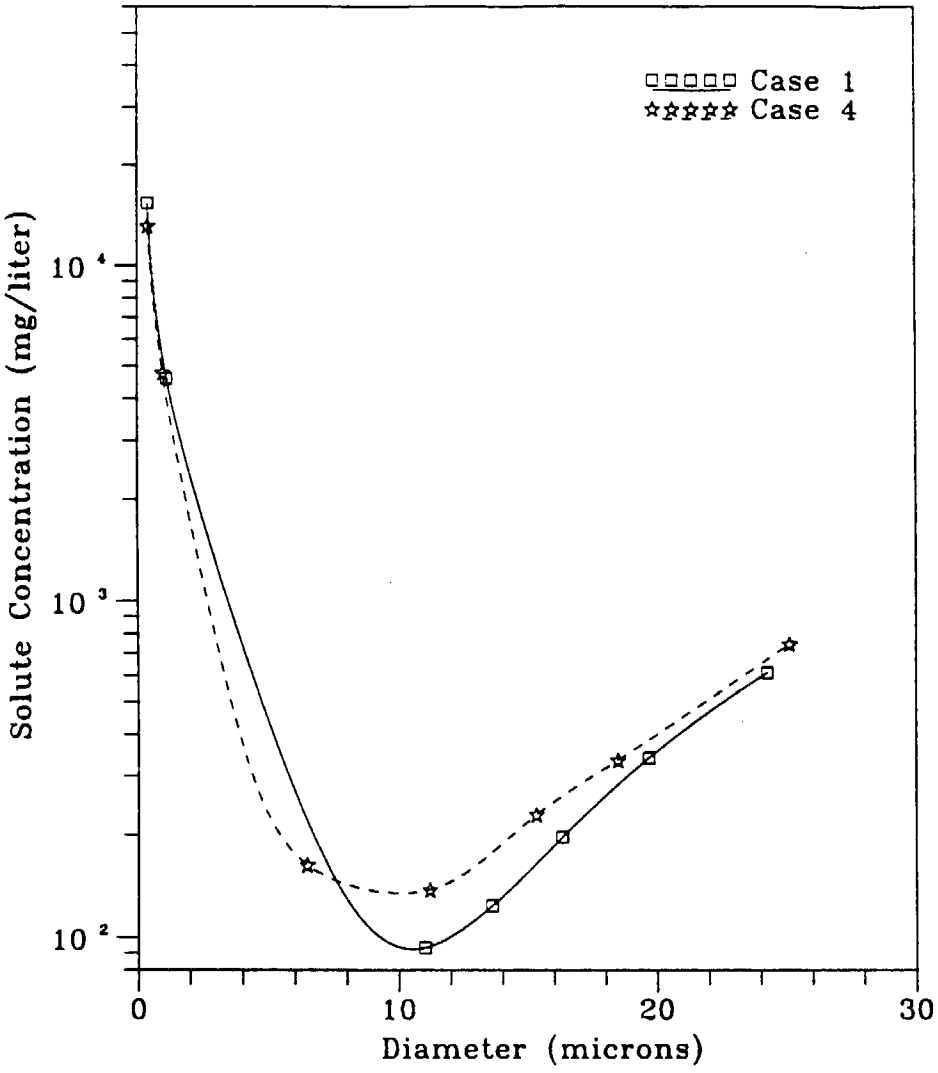

Figure 13. Comparison of the calculated total (volatile and nonvolatile) solute concentration as a function of droplet diameter for Case 1 ($t = 20$ min) and Case 4 ($t = 20$ min).

droplets. The model assumes thermodynamic equilibrium for volatile components such as NH_3, HCl, HNO_3 and water between gas and aerosol phases, and diffusion controlled gas-to-particle conversion of H_2SO_4 when the system's relative humidity is less than a critical value (e.g 99%). When the relative humidity exceeds this critical value, the growth equation for water is solved for the entire particle spectrum, and the mass transfer of all species between gas and aqueous-phases and the aqueous-phase chemical reactions are described in detail.

We have investigated possible differences in chemical composition of droplets of different sizes in a fog or cloud. The results suggest that significant total solute mass concentration differences can occur in such aqueous droplets. For the fog studied as a base case, during its full development stage, the mass solute concentration in droplets larger than 10 μm diameter increased with size in agreement with the findings of Noone et al. (1988), such that droplets of diameter 20 μm are found to have a solute concentration that is a factor of 3.6 larger than that in the 10 μm droplets. These total mass concentration differences reach a maximum during the fog liquid water peak and decrease during the fog development and dissipation stages.

Significant differences are suggested for the chemical composition of droplets of various sizes. Droplets on which most of the fog liquid water condenses are found to be enriched disproportionally in sulfate, and a peak in the sulfate mass is developed coincident with the peak of the liquid water distribution. This peak continues to exist after the fog dissipates and is due to the aqueous-phase conversion of S(IV) to S(VI). A similar behavior is exhibited by nitrate with the difference that nitric acid is produced in the gas-phase and scavenged by the droplets that have most of the liquid water.

The gas- and aqueous-phase chemical processes result in an increase of the solute total mass concentration for a mature fog over that if only aerosol scavenging is accounted for. This enrichment of fogwater due to gas- and aqueous-phase chemistry

is nonuniform over the droplet spectrum, reaching a maximum value of around 4 for the droplets with most of the liquid water. Thus gas- and aqueous-phase chemical processes tend to decrease the total solute mass concentration differences between the various droplet sizes.

The cooling rate of the system is found to have a major impact on the process as it affects directly the distribution of the available water over the droplet size spectrum. High cooling rates favor the smaller droplets that have small relaxation times as far as liquid condensation is concerned, while low cooling rates favor the larger slowly relaxing droplets. The higher the cooling rates the larger the solute concentration differences between the droplets of different sizes.

The mass/size distribution of the aerosol particles that serve as condensation nuclei affects in a quantitative, but not a qualitative way the concentration differences among droplets of different sizes.

Physical processes like droplet deposition and coagulation have not been included in the present model. A further step is the addition of descriptions of droplet coagulation and gravitational settling and the determination of their effects on the concentration differences between droplets of different sizes.

Acknowledgements

We would like to thank Dr. W. P. L. Carter, University of California, Riverside, for providing us with software for the gas-phase mechanism preparation and emissions processing. This work was supported by State of California Air Resources Board Agreement A732-043.

References

Carter W. P. L., Lurmann F. W., Atkinson R. and Lloyd A. C. (1986) Development

and testing of a surrogate species chemical reaction mechanism. EPA-600/3-86-031.

Carter W. P. L. and Atkinson R. (1988) Development and implementation of an up-to-date photochemical mechanism for use in airshed modeling. Summary final report to California Air Resources Board.

Chameides W. L. (1984) The photochemistry of a marine stratiform cloud. *J. Geophys. Res.* **89**, 4739-4755.

Flossman A. I., Hall W. D. and Pruppacher H. R. (1985) A theoretical study of the wet removal of atmospheric pollutants, I, The redistribution of aerosol particles captured through nucleation and impaction scavenging by growing cloud drops. *J. Atmos. Sci.* **42**, 583-606.

Gelbard F. and Seinfeld J. H. (1980) Simulation of multicomponent aerosol dynamics. *J. Colloid Interface Sci.* **78**, 485-501.

Gelbard F., Tambour Y. and Seinfeld J. H. (1980) Sectional representation for simulating aerosol dynamics *J. Colloid Interface Sci.* **76**, 541-556.

Graedel T. E. and Goldberg K. I. (1983) Kinetic studies of raindrop chemistry, 1. Inorganic and organic processes *J. Geophys. Res.* **88**, 10865-10882.

Hänel G. (1987) The role of aerosol properties during the condensational stage of cloud; a reinvestigation of numerics and microphysics *Beitr. Phys. Atmos.* **60**, 321-339.

Hegg D. A. and Hobbs P. V. (1979) The homogeneous oxidation of sulfur dioxide in cloud droplets. *Atmos. Environ.* **13**, 981-987.

Heikes B. G., Kok L. G., Walega J. G. and Lazrus A. L. (1987) H_2O_2, O_3 and SO_2 measurements in the lower troposphere over the eastern United States during the fall. *J. Geophys. Res.* **92**, 915-931.

Jacob D. J. (1986) Chemistry of OH in remote clouds and its role in the production

of formic acid and peroxymonosulfate *J. Geophys. Res.* **91**, 9807-9826.

Jensen J. B. and Charlson R. J. (1984) On the efficiency of nucleation scavenging. *Tellus* **36B**, 367-375.

Noone K. J., Charlson R. J., Covert D. S., Ogren J. A. and Heintzenberg J. (1988) Cloud droplets : solute concentration is size dependent. *J. Geophys. Res.* **93**, 9477-9482.

Pandis S. N. and Seinfeld J. H. (1989a) Sensitivity analysis of a chemical mechanism for aqueous-phase atmospheric chemistry. *J. Geophys. Res.* **94**, 1105-1126.

Pandis S. N. and Seinfeld J. H. (1989b) Mathematical modelling of acid deposition due to radiation fog- evaluation of a Lagrangian model. *J. Geophys. Res.*, (in press).

Pilinis C. and Seinfeld J. H. (1987) Continued development of a general equilibrium model for inorganic multicomponent atmospheric aerosols. *Atmos. Environ.* **21**, 2453-2466.

Pilinis C., Seinfeld J. H. and Seigneur C. (1987) Mathematical modeling of the dynamics of multicomponent atmospheric aerosols. *Atmos. Environ.* **21**, 943-955.

Pilinis C. and Seinfeld J. H. (1988) Development and evaluation of an Eulerian photochemical gas-aerosol model. *Atmos. Environ.* **22**, 1985-2001.

Pruppacher H. R. and Klett J. D. (1980), *Microphysics of Clouds and Precipitation*, Reidel Pub. Co., The Netherlands.

Roach W. T., Brown R., Caughey S. J., Garland J. A. and Readings C. J. (1976) The physics of radiation fog:I - A field study *Quart. J. R. Met. Soc.* **102**, 313-333.

Russel A. G. and Cass G. R. (1984) Aquisition of regional air quality model valida-

tion data for nitrate, sulfate, ammonium ion and their precursors. *Atmos. Environ.* **18**, 1815-1827.

Schwartz S. E. (1984) Gas- and aqueous-phase chemistry of HO_2 in liquid water clouds. *J. Geophys. Res.* **89**, 11589-11598.

Seigneur C. and Saxena P. (1984) A study of atmospheric acid formation in different enviroments. *Atmos. Environ.* **18** 2109-2124.

Seigneur C. and Saxena P. (1988) A theoretical investigation of sulfate formation in clouds. *Atmos. Environ.* **22** 101-115.

Seinfeld J. H. (1986) *Atmospheric Chemistry and Physics of Air Pollution*, John Wiley, New York.

Waldman J. M. (1986) Depositional aspects of pollutant behavior in fog. *Ph.D. thesis* California Institute of Technology.

Wall S. M., John W. and Ondo J. L. (1988) Measurement of aerosol size distributions for nitrate and major ionic species. *Atmos. Environ.* **22**, 1649-1656.

Warren D. R. and Seinfeld J. H. (1985) Simulation of aerosol size-distribution evolution in systems with simultaneous nucleation, condensation and coagulation. *Aerosol Sci. Technol.*, **4**, 31-43.

APPENDIX

BRIEF DOCUMENTATION OF ACID DEPOSITION MODULES 1-3

Appendix

Brief Documentation for Acid Deposition Modules 1-3

The three acid deposition modules have been developed to answer some specific fundamental questions concerning acid deposition. A user-friendly interface will be added later on together with the full three dimensional model. At this stage we would recommend that anyone intending to use the codes to contact the authors.

The computational requirements of the three modules developed are compared against the CIT gas and aerosol trajectory models in Table I. It has been found that the CPU time required for any simulation is strongly dependent on the initial and boundary conditions and can be in extreme cases even an order of magnitude different from the CPU times indicated in Table I. All the three modules (AQDRIVER, FOGMOD, DROPCHEM) have not yet been optimized for minimum computing time requirements and there is undoubtedly room for improvement.

A short description of the computer programs necessary for the three modules, as well as of the input and output files is given below.

Table I. CPU time and computer time requirements for several CIT models

Model	*Computational Cells*	*Simulation Period (hr)*	*Memory (Kbytes)*	*CPU$^{\alpha}$(min)*	*Relative CPU$^{\beta}$*
AQDRIVER	1	2	86	2.1	0.52
FOGMOD	12	24	573	258	64.5
DROPCHEM	1	1	1092	540	135
CIT – GAS	10	17	198	4.0	1
CIT – AEROSOL	5	5	5805	225	56.2

$^{\alpha}$ CPU time for a micro-VAX III. This time is just indicative of the computing requirements of the model and it generally depends strongly on the simulation conditions.

$^{\beta}$ CPU time relative to the CIT trajectory model for gas-phase chemistry only.

Module 1

Purpose

Simulation of aqueous-phase chemistry in a homogeneous parcel of air containing water droplets (fog or cloud).

Reference

S. N. Pandis and J. H. Seinfeld, Sensitivity analysis of a chemical mechanism for aqueous-phase atmospheric chemistry, *J. Geophys. Res.*, **94** 1105-1126, 1989.

Main Input Variables

- Liquid Water Content
- Droplet Radius
- Temperature
- Initial gas and aqueous-phase concentrations.

Main Output Variables

- Gas-phase species concentrations.
- Aqueous-phase species concentrations.

List of Programs

1. AQDRIVER.COM

Command File used for the test problem.

2. AQDRIVER.FOR

The driver used for the test program. It contains all the necessary input data.

3. AQCHEM.FOR

The main code for Module 1. It simulates the aqueous-phase chemistry for any number of computational cells for a prescribed period of time. Therefore it can be used as a box

model (1 computational cell), included in a n level trajectory model (n computational cells), or in an three dimensional eulerian model.

4. VARIABL.FOR

Fortran code that is 'INCLUDE'd in several subroutines. It contains the number of computational cells for which the simulation will be performed.

5. AQSUB.FOR

Collection of subroutines called by the main code.

6. INTEGRB.FOR

The hybrid integrator used for the integration of the stiff ODEs of the model.

This module requires the use of subroutines from the IMSL library.

Input Files

All the input variables are included in the driving program AQDRIVER.FOR.

Output Files

AQRES.DAT

Contains all the gas-phase concentrations, aqueous-phase concentrations of main species (eg S(IV), S(VI), N(V), N(III) etc) and the concentrations of ionic species (eg H^+, HSO_3^-, SO_3^{2-}, NO_2^- etc).

Module 2

Purpose

Simulation of acid deposition due to radiation fog using parametrized droplet microphysics.

Reference

S. N. Pandis and J. H. Seinfeld, Mathematical modeling of acid deposition due to radiation fog, it J. Geophys. Res., (in press), 1989.

Main Input Variables

- Initial temperature vertical profile.
- Initial relative humidity vertical profile.
- Initial gas concentrations vertical profile.
- Initial aerosol concentration profile.
- Average droplet diameter.
- Emission Inventory for NO_x, HC, SO_2, NH_3 etc.
- Wind speed.

Main Output Variables

- Liquid water content vertical profile for radiation fog.
- Relative humidity vertical profile.
- Temperature vertical profile.
- Fog height.
- Gas-phase concentrations vertical profiles.
- Aqueous-phase concentrations vertical profiles.
- Deposition rates of all ionic species.

List of Programs

1. FOGMOD.COM

Command File used for the test problem.

2. FOGMOD.FOR

Main program.

3. GASOPER.FOR

The operator for gas-phase chemistry (see reference for description).

4. AQOPER.FOR

The operator for aqueous-phase chemistry (see reference for description).

5. FOGOPER.FOR

The operator for the fog development and dissipation (see reference for description).

6. VARIABL.FOR

Fortran code that is 'INCLUDE'd in several subroutines.

7. MODLSPC.FOR

Fortran code that is 'INCLUDE'd in several subroutines.

8. RADCOM.FOR

Fortran code that is 'INCLUDE'd in the radiation subroutines.

9. FOGSUB1.FOR

Collection of subroutines called by the gas-phase operator.

10. FOGSUB2.FOR

Collection of subroutines called by the aqueous-phase operator.

11. FOGSUB3.FOR

Collection of subroutines called by the fog operator.

12. INTEGRB.FOR

Subroutine for the integration of stiff ODEs.

This module requires the use of subroutines from the IMSL library.

Input Files

1. ACIDE221.MOD

Standard file with the parameters of the gas-phase mechanism.

2. ACIDE221.RXP

Standard file with the parameters for the lumped species of the gas-phase mechanism.

3. INCON.DAT

Initial aqueous-phase concentration profiles.

4. INDAT.DAT

Initial conditions for the radiation fog.

5. INGAS.DAT

Initial values for gas species that are not treated by the gas-phase operator.

6. INMET.DAT

Concentrations of Fe^{3+}, Mn^{2+}, Na^{+}.

7. INSPEC.DAT

Initial gas-phase concentrations, emission inventory and wind speed.

8. OPTIN.DAT

Standard data file for atmospheric radiation calculations (it should never be changed).

Output Files

SJV.DAT

Contains all the output information.

Module 3

Purpose

Simulation of the changes in the size-composition distribution of aqueous droplets as a result of water condensation on the aerosol particles and of chemical changes in the gas and aqueous-phases inside a spatially homogeneous air parcel (fog or cloud).

References

1. S. N. Pandis, J. H. Seinfeld and C. Pilinis, On the relation between the size and composition of fog and cloud droplets and the size and composition of atmospheric aerosol, (to be presented at the *82nd APCA Annual Meeting*, Anaheim, California, June 1989)

2. S. N. Pandis, J. H. Seinfeld and C. Pilinis, Chemical composition differences in fog and cloud droplets of different sizes, (submitted for publication in *Atmospheric Environment* April 1989)

Main Input Variables

- Temperature as a function of time.
- Initial relative humidity.
- Initial gas concentrations.
- Initial size distribution of the aerosol sulfate and sodium.

Main Output Variables

- Liquid water content of fog or cloud.
- Relative humidity.
- Water droplet and aerosol size-composition distributions.
- Gas phase concentrations.

List of Programs

1. DROPCHEM.COM

Command File used for the test problem.

2. DROPLET.FOR

Main program.

3. DGASOPER.FOR

The operator for gas-phase chemistry.

4. CLOUD2.FOR

Part of the aerosol dynamics and thermodynamics operators (see references for description).

5. CLOUD3.FOR

Part of the aerosol dynamics and thermodynamics operators (see references for description).

6. CLOUD4.FOR

Part of the aerosol dynamics and thermodynamics operators (see references for description).

7. CLOUD5.FOR

Part of the aerosol dynamics and thermodynamics operators (see references for description).

8. VARIABL.FOR

Fortran code that is 'INCLUDE'd in several subroutines.

9. DROPVAR.FOR

Fortran code that is 'INCLUDE'd in several subroutines.

10. DROPVAR1.FOR

Fortran code that is 'INCLUDE'd in several subroutines.

11. DROPVAR2.FOR

Fortran code that is 'INCLUDE'd in several subroutines.

12. MODLSPC.FOR

Fortran code that is 'INCLUDE'd in several subroutines.

13. DROPSUB1.FOR

Collection of subroutines called by the gas-phase operator (see references for description).

14. DROPSUB2.FOR

Collection of subroutines used for the aqueous phase chemistry calculations

15. RATES.FOR

Subroutine for the calculation of rates of change of droplet diameters and aqueous-phase concentrations.

16. TRANS.FOR

Subroutine that performs the necessary changes for the activation of the aqueous-phase operator.

17. SPRINT.FOR

Subroutines for the output of information.

This module requires the use of subroutines from the IMSL library.

Input Files

1. DINSPEC.DAT

Contains the initial gas phase concentrations.

2. ACIDE221.MOD

Standard file with the parameters of the gas-phase mechanism.

3. ACIDE221.RXP

Standard file with the parameters for the lumped species of the gas-phase mechanism.

4. The rest of the necessary input (temperature variation, initial relative humidity and initial aerosol sulfate and sodium distributions) are included in DROPLET.FOR and RATES.FOR.

Output Files

1. DATGAS.DAT

Contains all the gas phase concentrations. Used for Plotting.

2. H2O2.DAT

Contains the aqueous-phase concentration of H_2O_2. Used for Plotting.

3. HCHO.DAT

Contains the aqueous-phase concentration of HCHO. Used for Plotting.

4. HCl.DAT

Contains the aqueous-phase concentration of HCl. Used for Plotting.

5. HCOOH.DAT

Contains the aqueous-phase concentration of HCOOH. Used for Plotting.

6. HSO5.DAT

Contains the aqueous-phase concentration of HSO_5^-. Used for Plotting.

7. MASSEC.DAT

Contains the total solute mass in every size section. Used for Plotting.

8. MGAS.DAT

Contains the main gas phase concentrations. Used for Plotting.

9. NH3.DAT

Contains the aqueous-phase concentration of NH_3. Used for Plotting.

10. NIII.DAT

Contains the aqueous-phase concentration of HNO_2. Used for Plotting.

11. NV.DAT

Contains the aqueous-phase concentration of HNO_3. Used for Plotting.

12. RATSEC.DAT

Contains the total solute concentration in every size section. Used for Plotting.

13. SEC7-60.DAT

Contains the mass of every species in every section. Used for debugging purposes.

14. SEC7-70.DAT

Contains the aqueous-phase concentrations of every species in every section. Used for debugging purposes.

15. SIV.DAT

Contains the aqueous-phase concentration of S(IV). Used for Plotting.

16. SVI.DAT

Contains the aqueous-phase concentration of S(VI). Used for Plotting.

17. ACIDE221.DOC

Optional documentation of the gas-phase mechanism used in the module.

00001323
ASSET